Reliability and Availability

Introduction:

The changing size of projects and designs has caused an increased adoption of reliability and availability determinations. These activities have been in place for many years but generally fell into a select few design areas. The increased interest in these methods has been driven by several factors. If a design proves to be unreliable, a significant cost can be incurred to repair the devices. As scientific detectors become larger and more complicated, repairing tens of thousands of circuit boards would have a severe cost impact and has the potential to cause the experiment to be canceled after a great deal of money and effort has been invested.

The following article is reprinted with permission from Prenscia HBK (Reliasoft). HBMPrenscia.com

It does not represent an endorsement of the company or its products but rather it is an example of a methodology for Reliability and Availability calculation methods.

MIL-217, Bellcore/Telcordia and Other Reliability Prediction Methods for Electronic Products - ReliaSoft

The article discusses both Reliability and Availability.

MIL-217, Bellcore/Telcordia and Other Reliability Prediction Methods for Electronic Products

[Please note that the following article — while it has been updated from our newsletter archives — may not reflect the latest software interface and plot graphics, but the original methodology and analysis steps remain applicable.]

Software Used: Lambda Predict, Weibull++, ALTA

In today's competitive electronic products market, having higher reliability than competitors is one of the key factors for success. To obtain high product reliability, consideration of reliability issues should be integrated from the very beginning of the design phase. This leads to the concept of *reliability prediction*. Historically, this term has been used to denote the process of applying mathematical models and component data for the purpose of estimating the field reliability of a system before failure data are available for the system. However, the objective of reliability prediction is not limited to predicting whether reliability goals, such as MTBF, can be reached. It can also be used for:

- Identifying potential design weaknesses
- Evaluating the feasibility of a design
- Comparing different designs and life-cycle costs
- Providing models for system reliability/availability analysis
- Establishing goals for reliability tests
- Aiding in business decisions such as budget allocation and scheduling

Once the prototype of a product is available, lab tests can be utilized to obtain more accurate reliability predictions. Accurate prediction of the reliability of electronic products requires knowledge of the components, the design, the manufacturing process and the expected operating conditions. Several different approaches have been developed to achieve the reliability prediction of electronic systems and components. Each approach has its unique advantages and disadvantages. Among these approaches, three main categories are often used within government and industry: empirical (standards based), physics of failure and life testing. In this article, we will provide an overview of all three approaches.

First, we will discuss empirical prediction methods, which are based on the experiences of engineers and on historical data. Standards, such as MIL-HDBK-217 and Bellcore/Telcordia, are widely used for reliability prediction of electronic products. Next, we will discuss physics of failure methods, which are based on root-cause analysis of failure mechanisms, failure modes and stresses. This approach is based upon an understanding of the physical properties of the materials, operation processes and technologies used in the design. Finally, we will discuss life testing methods, which are used to determine reliability by testing a relatively large number of samples at their specified operation stresses or higher stresses and using statistical models to analyze the data.

Empirical (or Standards Based) Prediction Methods

Empirical prediction methods are based on models developed from statistical curve fitting of historical failure data, which may have been collected in the field, in-house or from manufacturers. These methods tend to present good estimates of reliability for similar or slightly modified parts. Some parameters in the curve function can be modified by integrating engineering knowledge. The assumption is made that system or equipment failure causes are inherently linked to components whose failures are independent of each other. There are many different empirical methods that have been created for specific applications. Some have gained popularity within industry in the past three decades. The table below lists some of the available prediction standards and the following sections describe two of the most commonly used methods in a bit more detail.

Prediction Method	Applied Industry	Last Update
MIL-HDBK-217F and Notice 1 and 2	Military	1995
Bellcore/Telcordia	Telecom	2011
NSWC	Mechanical	2011
FIDES	Commercial/French Military	2009

MIL-HDBK-217 Predictive Method

MIL-HDBK-217 is very well known in military and commercial industries. It is probably the most internationally recognized empirical prediction method, by far. The latest version is MIL-HDBK-217F, which was released in 1991 and had two revisions: Notice 1 in 1992 and Notice 2 in 1995.

The MIL-HDBK-217 predictive method consists of two parts; one is known as the *parts count* method and the other is called the *part stress* method [1]. The parts count method assumes typical operating conditions of part complexity, ambient temperature, various electrical stresses, operation mode and environment (called *reference conditions*). The failure rate for a part under the reference conditions is calculated as:

$$\lambda_{b,i} = \sum_{i=1}^{n} (\lambda_{ref})_i$$

where:

- λ_{ref} is the failure rate under the reference conditions
- i is the number of parts

Since the parts may not operate under the reference conditions, the real operating conditions will result in failure rates that are different from those given by the "parts count" method. Therefore, the part stress method requires the specific part's complexity, application stresses, environmental factors, etc. (called *Pi factors*). For example, MIL-HDBK-217 provides many environmental conditions (expressed as π_E) ranging from "ground benign" to "cannon launch." The standard also provides multi-level quality specifications (expressed as π_Q). The failure rate for parts under specific operating conditions can be calculated as:

$$\lambda = \sum_{i=1}^{n} (\lambda_{ref,i} \times \pi_S \times \pi_T \times \pi_E \times \pi_Q \times \pi_A)$$

where:

- π_S is the stress factor
- π_T is the temperature factor
- π_E is the environment factor
- π_Q is the quality factor
- π_A is the adjustment factor

Figure 1 shows an example using the MIL-HDBK-217 method (in ReliaSoft Lambda Predict software) to predict the failure rate of a ceramic capacitor. According to the handbook,

the failure rate of a commercial ceramic capacitor of 0.00068 μF capacitance with 80% operation voltage, working under 30 degrees ambient temperature and "ground benign" environment is 0.0217 / 10^6 hours. The corresponding MTBF (mean time before failure) or MTTF (mean time to failure) is estimated to be 4.6140 / 10^7 hours.

Folio1

2 of 2 System Hierarchy

Name	Failure Rate (t=INF)	MTBF
MIL-HDBK-217F	0.0217 FPMH	4.6140E+07 hrs
Capacitor	0.0217	4.6140E+07

Properties Derating Publishing

Properties	Values
Identifiers	
General	
Application	
Environment	Ground, benign
Ambient Temperature (°C)	30
Applied Voltage (V)	0
Voltage Stress	0.8
Connection Type	Reflow Solder
Circuit Resistance (Ω/V)	0.6
Adjustment Factor	1
Physical	
Capacitor Style	Ceramic, Temp Com, NER
Capacitance (μF)	0.00068
Number of Pins	2
Rated Voltage (V)	0
Quality, Capacitors	Commercial or Unknown
History	

Component

Figure 1: MIL-HDBK-217 capacitor failure rate example

Bellcore/Telcordia Predictive Method

Bellcore was a telecommunications research and development company that provided joint R&D and standards setting for AT&T and its co-owners. Because of dissatisfaction with military handbook methods for their commercial products, Bellcore designed its own reliability prediction standard for commercial telecommunication products. In 1997, the company was acquired by Science Applications International Corporation (SAIC) and the company's name was changed to Telcordia. Telcordia continues to revise and update the standard. The latest two updates are SR-332 Issue 2 (September 2006) and SR-332 Issue 3 (January 2011), both called "Reliability Prediction Procedure for Electronic Equipment."

The Bellcore/Telcordia standard assumes a serial model for electronic parts and it addresses failure rates at the infant mortality stage and at the steady-state stage with Methods I, II and III [2-3]. Method I is similar to the MIL-HDBK-217F parts count and part stress methods. The

standard provides the generic failure rates and three part stress factors: device quality factor (π_Q), electrical stress factor (π_S) and temperature stress factor ($_T$). Method II is based on combining Method I predictions with data from laboratory tests performed in accordance with specific SR-332 criteria. Method III is a statistical prediction of failure rate based on field tracking data collected in accordance with specific SR-332 criteria. In Method III, the predicted failure rate is a weighted average of the generic steady-state failure rate and the field failure rate.

Figure 2 shows an example in Lambda Predict using SR-332 Issue 3 to predict the failure rate of the same capacitor in the previous MIL-HDBK-217 example (shown in Figure 1). The failure rate is 9.655 Fits, which is 9.655 / 10^9 hours. In order to compare the predicted results from MIL-HBK-217 and Bellcore SR-332, we must convert the failure rate to the same units. 9.655 Fits is 0.0009655 / 10^6 hours. So the result of 0.0217 / 10^6 hours in MIL-HDBK-217 is much higher than the result in Bellcore/Telcordia SR-332. There are reasons for this variation. First, MIL-HDBK-217 is a standard used in the military so it is more conservative than the commercial standard. Second, the underlying methods are different and more factors that may affect the failure rate are considered in MIL-HDBK-217.

Folio1

2 of 2 System Hierarchy

Name	Failure Rate (t=INF)	MTBF
Telcordia SR-332 Issue 3	0.9655 FITs	1.0358E+09 hrs
Capacitor	0.9655	1.0358E+09

Properties Derating Publishing

Properties	Values
Identifiers	
General	
Application	
Temperature (°C)	30
Applied Voltage (V)	0
Voltage Stress	0.8
Confidence Level for Upper Bound (%)	90
Adjustment Factor	1
Physical	
Type	Fixed, Ceramic
Rated Voltage (V)	0
Quality	Level I
Method	
Early Life Data	
Lab Test Data	
Field Data	
History	

Component

Figure 2: Bellcore capacitor failure rate example

Discussion of Empirical Methods

Although empirical prediction standards have been used for many years, it is always wise to use them with caution. The advantages and disadvantages of empirical methods have been discussed a lot in the past three decades. A brief summary from the publications in industry, military and academia is presented next [5-9].

Advantages of empirical methods:

1. Easy to use, and a lot of component models exist
2. Relatively good performance as indicators of inherent reliability
3. Provide an approximation of field failure rates

Disadvantages of empirical methods:

1. A large part of the data used by the traditional models is out-of-date
2. Failure of the components is not always due to component-intrinsic mechanisms but can be caused by the system design
3. The reliability prediction models are based on industry-average values of failure rate, which are neither vendor-specific nor device-specific
4. It is hard to collect good quality field and manufacturing data, which are needed to define the adjustment factors, such as the Pi factors in MIL-HDBK-217

Physics of Failure Methods

In contrast to empirical reliability prediction methods, which are based on the statistical analysis of historical failure data, a physics of failure approach is based on the understanding of the failure mechanism and applying the physics of failure model to the data. Several popularly used models are discussed next.

Arrhenius's Law

One of the earliest and most successful acceleration models predicts how the time-to-failure of a system varies with temperature. This empirically based model is known as the *Arrhenius equation*. Generally, chemical reactions can be accelerated by increasing the system temperature. Since it is a chemical process, the aging of a capacitor (such as an electrolytic capacitor) is accelerated by increasing the operating temperature. The model takes the following form.

$$L(T) = A \exp\left(\frac{E_a}{kT}\right)$$

where:

- $L(T)$ is the life characteristic related to temperature
- A is the scaling factor
- E_a is the activation energy
- k is the Boltzmann constant
- T is the temperature.

Eyring and Other Models

While the Arrhenius model emphasizes the dependency of reactions on temperature, the Eyring model is commonly used for demonstrating the dependency of reactions on stress factors other than temperature, such as mechanical stress, humidity or voltage.

The standard equation for the Eyring model [10] is as follows:

$$L(T,S) = AT^{\alpha}\exp\left[\frac{E_a}{kT} + \left(B + \frac{C}{T}\right)S\right]$$

where:

- $L(T,S)$ is the life characteristic related to temperature and another stress
- A, α, B and C are constants
- S is a stress factor other than temperature
- T is absolute temperature

According to different physics of failure mechanisms, one more term (i.e., stress) can be either removed or added to the above standard Eyring model. Several models are similar to the standard Eyring model. They are:

Two Temperature/Voltage Model:

$$L(T,V) = Ae^{\frac{E_a}{kT}}V^{-\beta}$$

Three Stress Model (Temperature-Voltage-Humidity):

$$L(T,V,H) = Ae^{\frac{\Delta H}{kT}}V^{-\beta}RH^{-\tau}$$

Corrosion Model:

Electronic devices with aluminum or aluminum alloy with small percentages of copper and silicon metallization are subject to corrosion failures and therefore can be described with the following model [11]:

$$L(RH, V, T) = B_0 \exp[(-a)RH] f(V) \exp\left(\frac{E_a}{kT}\right)$$

where:

- B_0 is an arbitrary scale factor
- α is equal to 0.1 to 0.15 per % RH
- $f(V)$ is an unknown function of applied voltage, with empirical value of 0.12 to 0.15

Hot Carrier Injection Model:

Hot carrier injection describes the phenomena observed in MOSFETs by which the carrier gains sufficient energy to be injected into the gate oxide, generate interface or bulk oxide defects and degrade MOSFETs characteristics such as threshold voltage, transconductance, etc. [11]:

For n-channel devices, the model is given by:

$$L(I, T) = B(I_{sub})^{-N} \exp\left(\frac{E_a}{kT}\right)$$

where:

- B is an arbitrary scale factor
- I_{sub} is the peak substrate current during stressing
- N is equal to a value from 2 to 4, typically 3
- E_a is equal to -0.1eV to -0.2eV

For p-channel devices, the model is given by:

$$L(I, T) = B(I_{gate})^{-M} \exp\left(\frac{E_a}{kT}\right)$$

where:

- B is an arbitrary scale factor
- I_{gate} is the peak gate current during stressing
- M is equal to a value from 2 to 4
- E_a is equal to -0.1eV to -0.2eV

Since electronic products usually have a long time period of useful life (i.e., the constant line of the bathtub curve) and can often be modeled using an exponential distribution, the life characteristics in the above physics of failure models can be replaced by MTBF (i.e., the life characteristic in the exponential distribution). However, if you think your products do not exhibit a constant failure rate and therefore cannot be described by an exponential distribution, the life characteristic usually will not be the MTBF. For example, for the Weibull distribution, the life characteristic is the scale parameter *eta* and for the lognormal distribution, it is the *log mean*.

Black Model for Electromigration

Electromigration is a failure mechanism that results from the transfer of momentum from the electrons, which move in the applied electric field, to the ions, which make up the lattice of the interconnect material. The most common failure mode is "conductor open." With the decreased structure of Integrated Circuits (ICs), the increased current density makes this failure mechanism very important in IC reliability.

At the end of the 1960s, J. R. Black developed an empirical model to estimate the MTTF of a wire, taking electromigration into consideration, which is now generally known as the *Black model*. The Black model employs external heating and increased current density and is given by:

$$MTTF = A_0 (J - J_{threshold})^{-N} \exp\left(\frac{E_a}{kT}\right)$$

where:

- A_0 is a constant based on the cross-sectional area of the interconnect
- J is the current density
- $J_{threshold}$ is the threshold current density
- E_a is the activation energy
- k is the Boltzmann constant
- T is the temperature
- N is a scaling factor

The current density (J) and temperature (T) are factors in the design process that affect electromigration. Numerous experiments with different stress conditions have been reported in the literature, where the values have been reported in the range between 2 and 3.3 for N, and 0.5 to 1.1eV for E_a. Usually, the lower the values, the more conservative the estimation.

Coffin-Manson Model for Fatigue

Fatigue failures can occur in electronic devices due to temperature cycling and thermal shock. Permanent damage accumulates each time the device experiences a normal power-up and power-down cycle. These switch cycles can induce cyclical stress that tends to weaken materials and may cause several different types of failures, such as dielectric/thin-film cracking, lifted bonds,

solder fatigue, etc. A model known as the (modified) *Coffin-Manson model* has been used successfully to model crack growth in solder due to repeated temperature cycling as the device is switched on and off. This model takes the form [9]:

$$N_f = A f^{-\alpha} \Delta T^{-\beta} G(T_{max})$$

where:

- N_f is the number of cycles to failure
- *A* is a coefficient
- *f* is the cycling frequency
- ΔT is the temperature range during a cycle
- *A* is the cycling frequency exponent
- *A* is the temperature exponent
- $G(T_{max})$ is equal to:

$$\exp\left(\frac{E_a}{k} \times \frac{1}{T_{max}}\right)$$

which is an Arrhenius term evaluated at the maximum temperature in each cycle.
Three factors are usually considered for testing: maximum temperature (T_{max}), temperature range (ΔT) and cycling frequency (*f*). The activation energy is usually related to certain failure mechanisms and failure modes, and can be determined by correlating thermal cycling test data and the Coffin-Manson model.

Discussion of Physics of Failure Methods

A given electronic component will have multiple failure modes and the component's failure rate is equal to the sum of the failure rates of all modes (i.e., humidity, voltage, temperature, thermal cycling and so on). The system's failure rate is equal to the sum of the failure rates of the components involved. In using the above models, the model parameters can be determined from the design specifications or operating conditions. If the parameters cannot be determined without conducting a test, the failure data obtained from the test can be used to get the model parameters. Software products such as ReliaSoft ALTA can help you analyze the failure data.

We will give an example of using ALTA to analyze the Arrhenius model. For this example, the life of an electronic component is considered to be affected by temperature. The component is tested under temperatures of 406, 416 and 426 Kelvin. The usage temperature level is 400 Kelvin. The Arrhenius model and the Weibull distribution are used to analyze the failure data in ALTA. Figure 4 shows the data and calculated parameters. Figure 5 shows the reliability plot and the estimated B10 life at the usage temperature level.

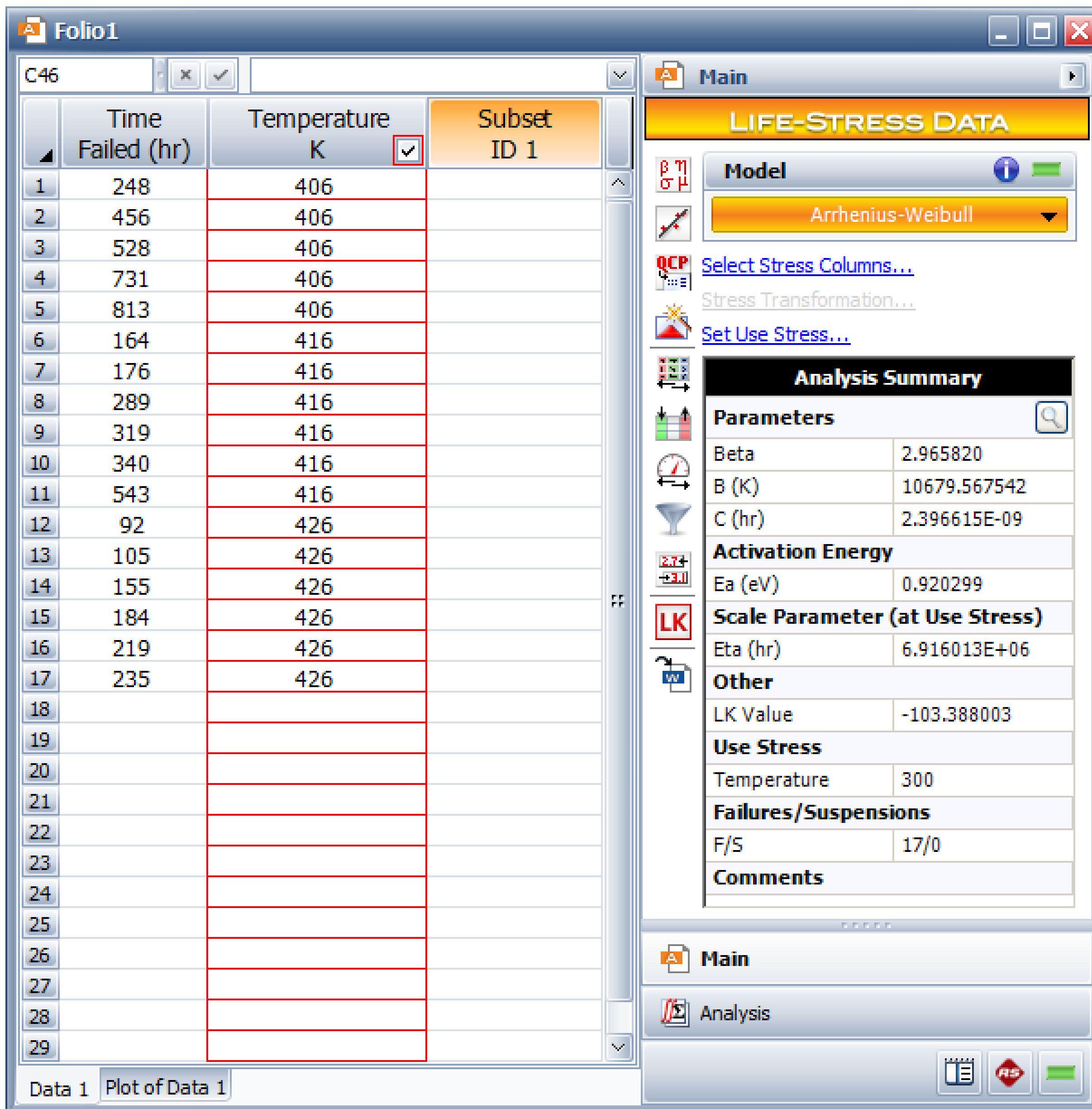

Figure 4: Data and analysis results in ALTA with the Arrhenius-Weibull model

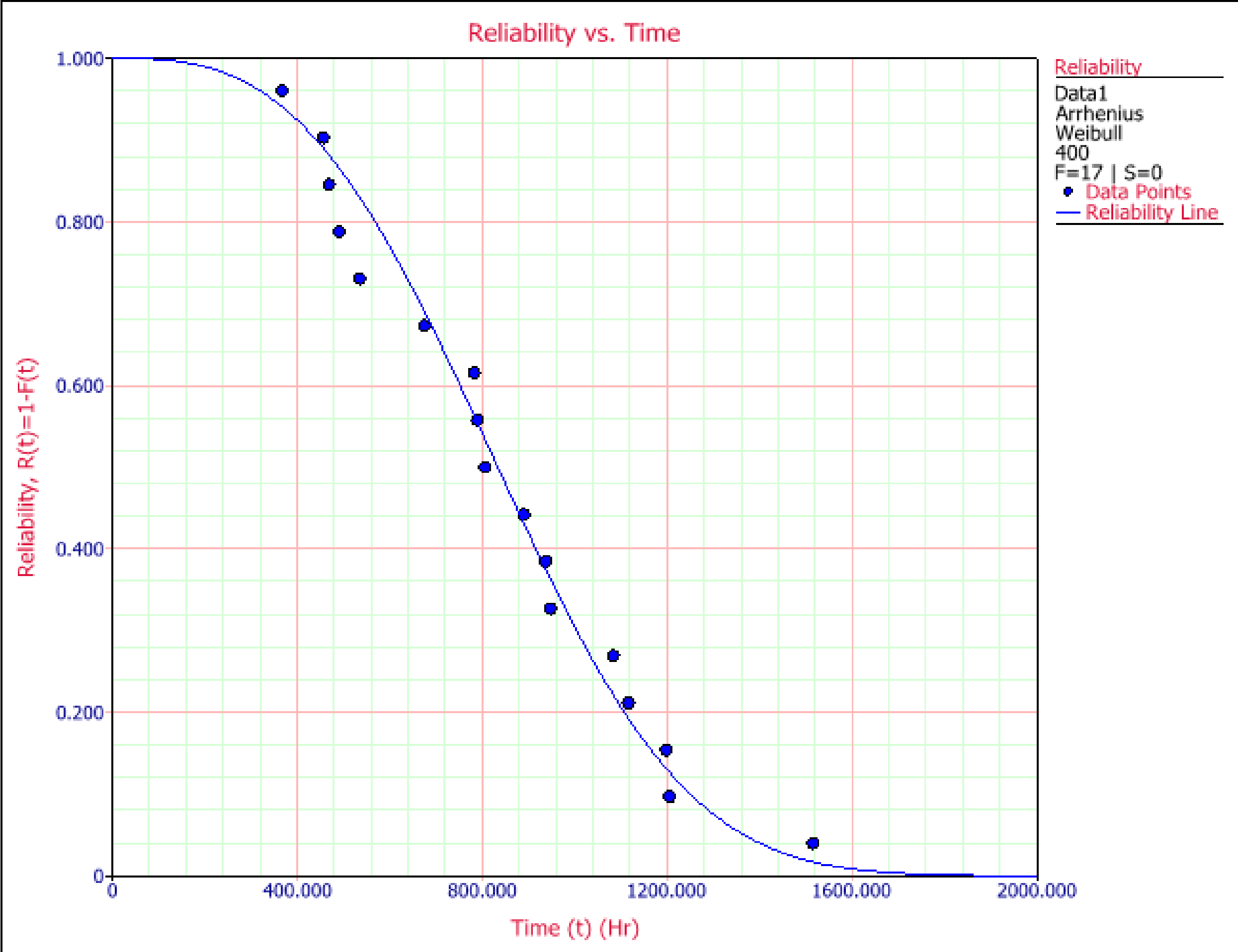
Reliability vs. Time
Reliability, R(t)=1-F(t)
1.000
0.800
0.600
0.400
0.200
0
400.000
800.000
1200.000
1600.000
2000.000
Time (t) (Hr)
Reliability
Data1
Arrhenius
Weibull
400
F=17 | S=0
Data Points
Reliability Line

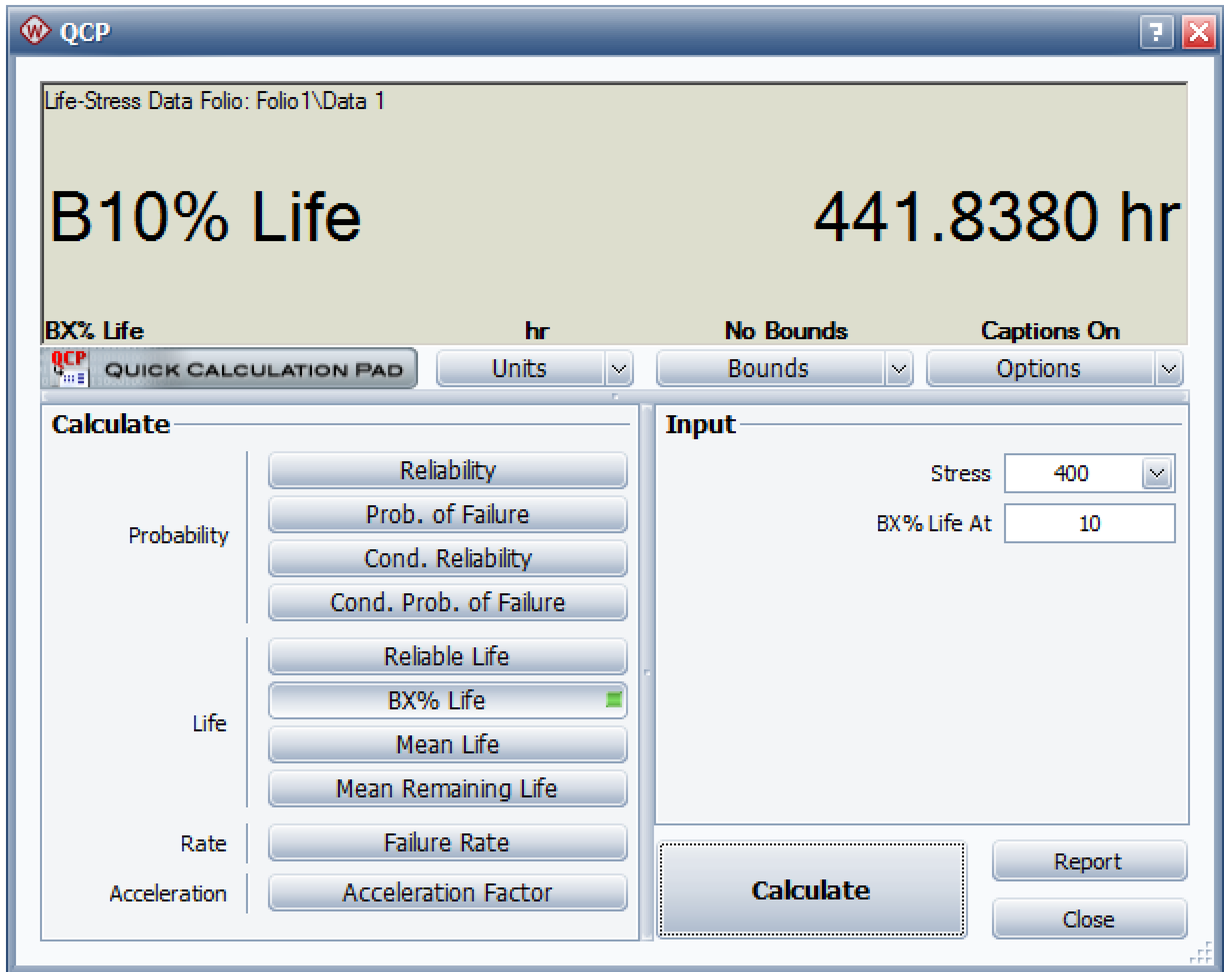

Figure 5: Reliability vs. Time plot and calculated B10 life

From Figure 4, we can see that the estimated activation energy in the Arrhenius model is 0.92. Note that, in ALTA, the Arrhenius model is simplified to a form of:

$$LT = C \exp\left(\frac{B}{T}\right)$$

Using this equation, the parameters *B* and *C* calculated by ALTA can easily be transformed to the parameters described above for the Arrhenius relationship.

Advantages of physics of failure methods:

1. Accurate prediction of wearout using known failure mechanisms
2. Modeling of potential failure mechanisms based on the physics of failure
3. During the design process, the variability of each design parameter can be determined

Disadvantages of physics of failure methods:

1. Need detailed component manufacturing information (such as material, process and design data)
2. Analysis is complex and could be costly to apply
3. It is difficult to assess the entire system

Life Testing Method

As mentioned above, time-to-failure data from life testing may be incorporated into some of the empirical prediction standards (i.e., Bellcore/Telcordia Method II) and may also be necessary to estimate the parameters for some of the physics of failure models. However, in this section of the article, we are using the term *life testing method* to refer specifically to a third type of approach for predicting the reliability of electronic products. With this method, a test is conducted on a sufficiently large sample of units operating under normal usage conditions. Times-to-failure are recorded and then analyzed with an appropriate statistical distribution in order to estimate reliability metrics such as the B10 life. This type of analysis is often referred to as *Life Data Analysis* or *Weibull Analysis*.

ReliaSoft Weibull++ software is a tool for conducting life data analysis. As an example, suppose that an IC board is tested in the lab and the failure data are recorded. Figure 6 shows the data entered into Weibull++ and analyzed with the 2-parameter Weibull lifetime distribution, while Figure 7 shows the Reliability vs. Time plot and the calculated B10 life for the analysis.

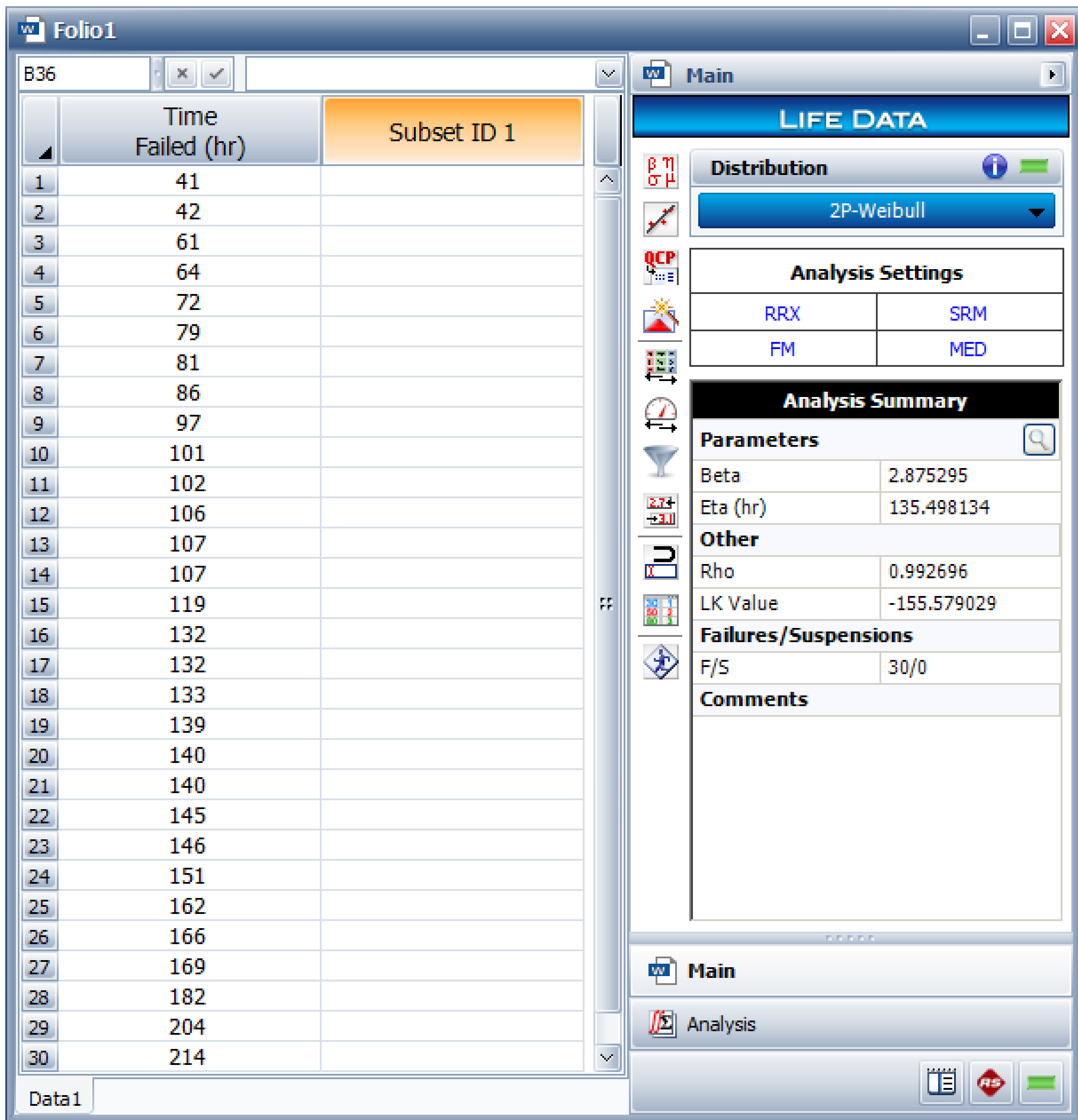

Figure 6: Data and analysis results in Weibull++ with the Weibull distribution

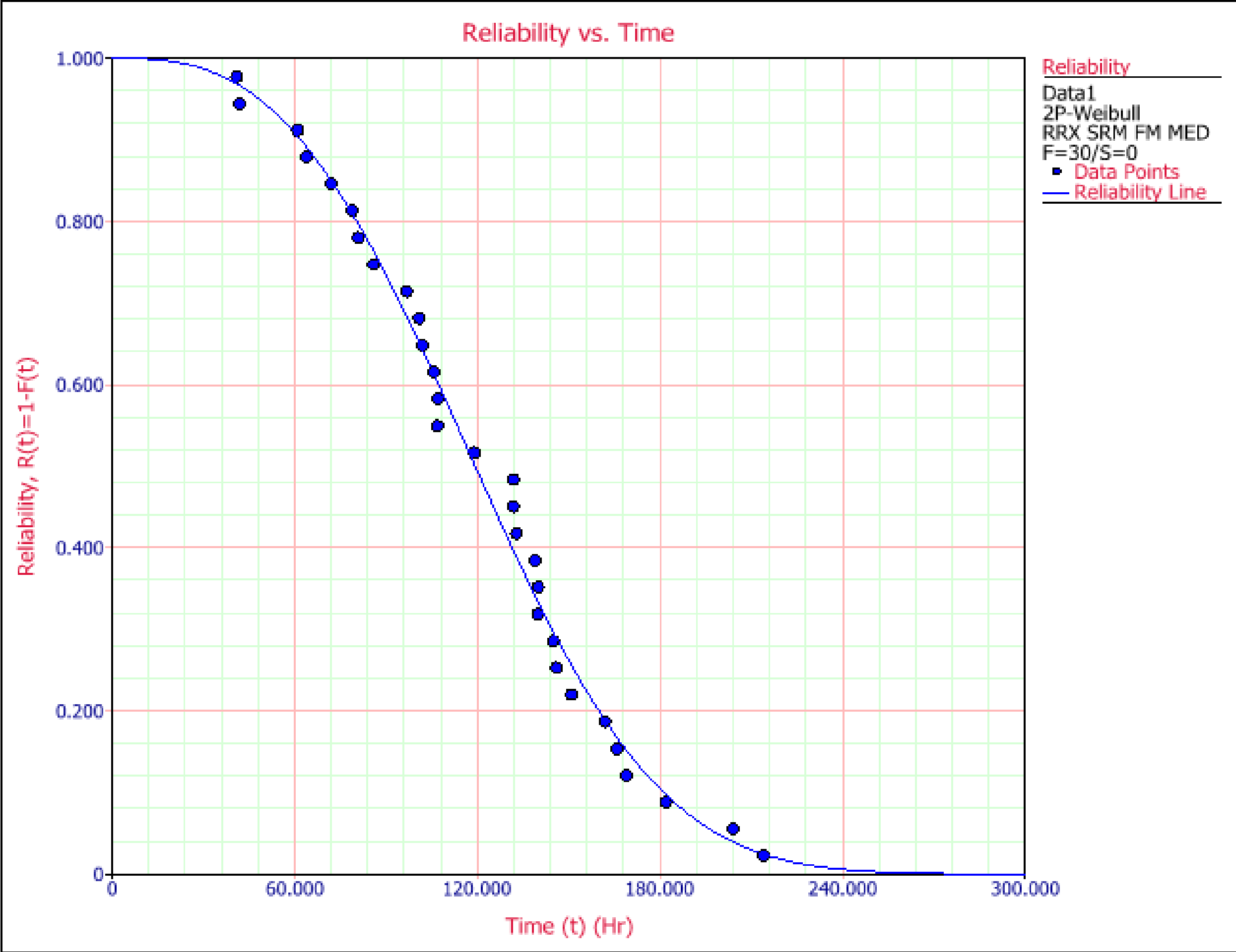

Reliability vs. Time
Reliability
Data1
2P-Weibull
RRX SRM FM MED
F=30/S=0
Data Points
Reliability Line
Reliability, R(t)=1-F(t)
1.000
0.800
0.600
0.400
0.200
0
60.000
120.000
180.000
240.000
300.000
Time (t) (Hr)

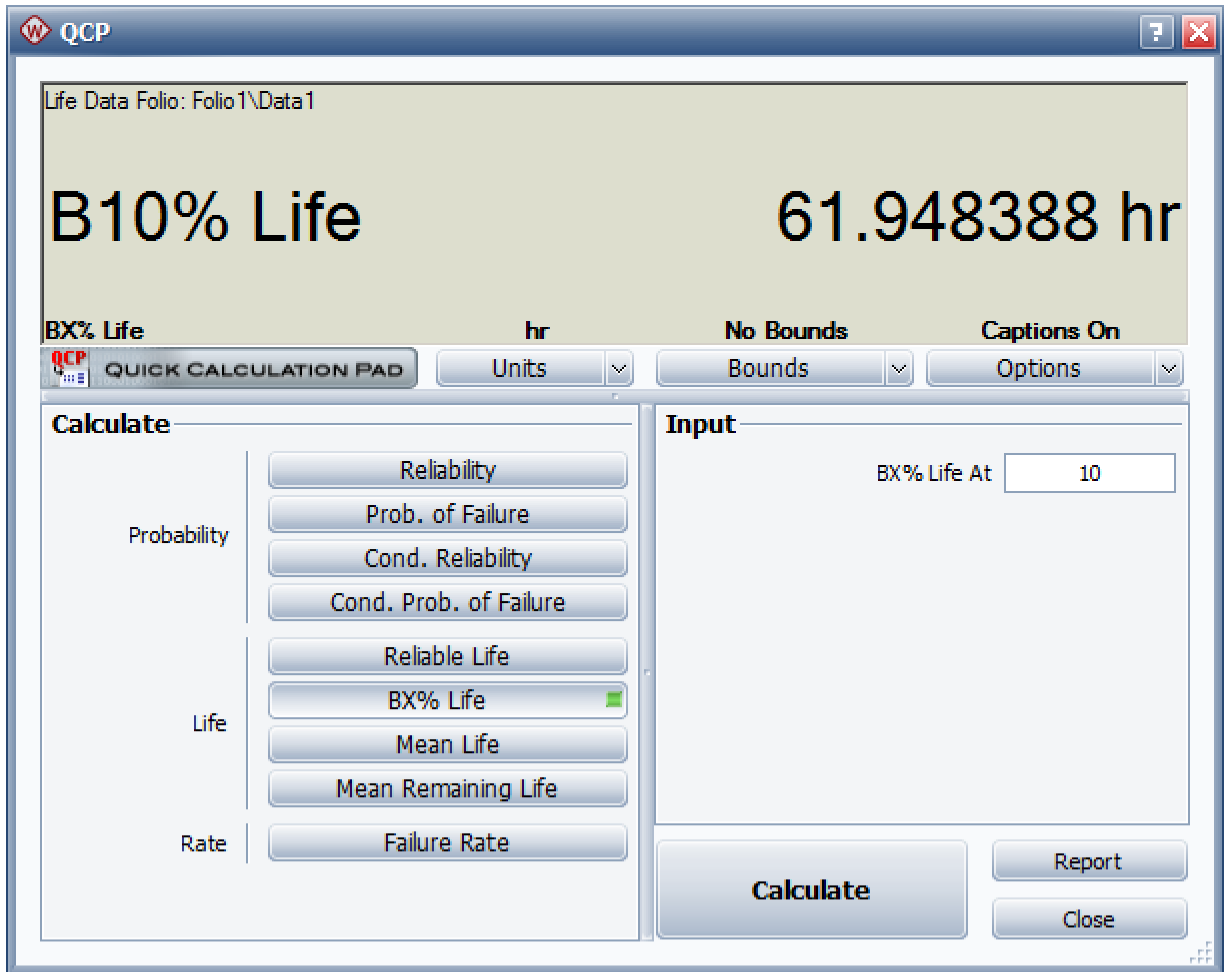

Figure 7: Reliability vs. Time plot and calculated B10 life for the analysis

Discussion of the Life Testing Method

The life testing method can provide more information about the product than the empirical prediction standards. Therefore, the prediction is usually more accurate, given that enough samples are used in the testing.

The life testing method may also be preferred over both the empirical and physics of failure methods when it is necessary to obtain realistic predictions at the system (rather than component) level. This is because the empirical and physics of failure methods calculate the system failure rate based on the predictions for the components (e.g., using the sum of the component failure rates if the system is considered to be a serial configuration). This assumes that there are no interaction failures between the components but, in reality, due to the design or manufacturing, components are not independent. (For example, if the fan is broken in your laptop, the CPU will fail faster because of the high temperature.) Therefore, in order to consider the complexity of the entire system, life tests can be conducted at the system level, treating the system as a "black box," and the system reliability can be predicted based on the obtained failure data.

Conclusions

In this article, we discussed three approaches for electronic reliability prediction. The empirical (or standards based) methods can be used in the design stage to quickly obtain a rough estimation of product reliability. The physics of failure and life testing methods can be used in both design and production stages. In physics of failure approaches, the model parameters can be determined from design specs or from test data. On the other hand, with the life testing method, since the failure data from your own particular products are obtained, the prediction results usually are more accurate than those from a general standard or model.

References

[1] MIL-HDBK-217F, *Reliability Prediction of Electronic Equipment*, 1991. Notice 1 (1992) and Notice 2 (1995).

[2] SR-332, Issue 1, Reliability Prediction Procedure for Electronic Equipment, Telcordia, May 2001.

[3] SR-332, Issue 2, Reliability Prediction Procedure for Electronic Equipment, Telcordia, September 2006.

[4] ITEM Software and ReliaSoft, *D490 Course Notes: Introduction to Standards Based Reliability Prediction and Lambda Predict*, 2015.

[5] B. Foucher, J. Boullie, B. Meslet and D. Das, "A Review of Reliability Prediction Methods for Electronic Devices," *Microelectron. Wearout*., vol. 42, no. 8, August 2002, pp. 1155-1162.

[6] M. Pecht, D. Das and A. Ramarkrishnan, "The IEEE Standards on Reliability Program and Reliability Prediction Methods for Electronic Equipment," *Microelectron. Wearout*., vol. 42, 2002, pp. 1259-1266.

[7] M. Talmor and S. Arueti, "Reliability Prediction: The Turnover Point," 1997 *Proc. Ann. Reliability and Maintainability Symp*., 1997, pp. 254-262.

[8] W. Denson, "The History of Reliability Prediction," *IEEE Trans. On Reliability*, vol. 47, no. 3-SP, September 1998.

[9] D. Hirschmann, D. Tissen, S. Schroder and R.W. de Doncker, "Reliability Prediction for Inverters in Hybrid Electrical Vehicles," *IEEE Trans. on Power Electronics*, vol. 22, no. 6, November 2007, pp. 2511-2517.

[10] NIST Information Technology Library. [Online document] Available HTTP: www.itl.nist.gov

[11] Semiconductor Device Reliability Failure Models. [Online document] Available HTTP: www.sematech.org/docubase/document/3955axfr.pdf

Reliability links:
A Guide to Reliability Prediction Standards & Failure Rate | Relyence
How to Perform Reliability Predictions Easily and Efficiently (relyence.com)

- FMEA (Failure Mode and Effects Analysis) identifies potential failures, provides a way to assess the criticality of those failures, and then tracks ways to eliminate or mitigate them.
- FRACAS (Failure, Reporting, Analysis and Corrective Action System) and its related CAPA (Corrective and Preventive Action) enable you to effectively track and manage your corrective action process.
- FTA (Fault Tree Analysis) assesses the risk of catastrophic events.
- Reliability Prediction computes MTBF metrics and provides a platform for "designing-in" reliability.
- RBD (Reliability Block Diagram) offers full scale system modeling and analysis of complex designs including those that use redundancy.
- Maintainability Prediction provides the ability to ensure repair and maintenance procedures are effective and efficient.
- Weibull analysis is a versatile tool for predictive analytics using life data.
- ALT (Accelerated Life Testing) allows you to take accelerated life data and extrapolate real world system performance.

FMEA, or Failure Mode and Effects Analysis, is an organized, systematic approach for assessing potential system failures and the resulting consequences of those failures. The objective of a FMEA is to evaluate the risk associated with the identified failure effects and come up with a plan to detect, prevent, or mitigate those deemed most critical.
Fault Tree Analysis (FTA) uses a top-down deductive approach to assess the likelihood of occurrence of an undesired, often catastrophic, event. FTA provides an important measured-based approach for risk analysis.
RAMS analysis is a well-established approach for evaluating four critical factors related to system performance: ***reliability***, ***availability***, ***maintainability***, and ***safety***. Widely used in engineering disciplines, RAMS analysis ensures that systems meet operational requirements throughout the lifecycle. The objective of RAMS analysis is to assess reliability, availability, maintainability, and safety in an organized way, identify areas of concern, and facilitate improvements to ensure that program goals are met.
Reliability is defined as the probability, or likelihood, that an item will perform a desired function without failure under stated conditions for a stated period of time. In general, reliability is an indicator of the likelihood a product will operate without failure.
Availability is defined as the probability that a repairable system is in a working state when it is required to be operational
Maintainability is defined in MIL-STD-721 as "the measure of the ability of an item to be retained in or restored to a specified condition when maintenance is performed by personnel having specified skill levels, using prescribed procedures and resources, at each prescribed level of maintenance and repair."
Safety is a term with a much clearer definition! When used in reference to RAMS analysis, safety analysis is performed in order evaluate ways to prevent harm to people and the environment.

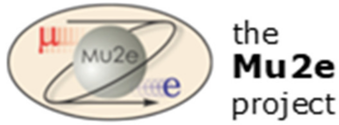

A Reliability Analysis
of the
Mu2e Calorimeter Front End Amplifier Board

By Gary Drake[1], Giovanni Corradi[2]

Mar. 19, 2020
Version 1.0

[1]Fermi National Accelerator Laboratory, Batavia, IL, USA
[2]INFN, Inst. Nazionale Di Fisica Nucleare, Frascati, Italy

Abstract

This note describes the estimation process and the calculation results in performing a reliability analysis for the ***Mu2e Calorimeter Front End Amplifier Board***. The analysis is based upon the procedures set forth in the military handbook, "Reliability Prediction of Electronic Equipment," also known as MIL-HDBK-217F. The analysis shows that the value of ***the Mean Time to Failure for this board is estimated to be 1.92 x 10⁶ hours.*** Estimates of the probability of failure and a prediction of the number of board failures as a function of time are presented.

Table of Contents

1. Introduction 3
   1.1. Scope 3
   1.2. Description of the Board 4
   1.3. Limits of Scope 7
2. Methodology 9
   2.1. Overview of the Analysis Process 9
   2.2. Resistors 11
   2.3. Capacitors 15
   2.4. Low Frequency Diodes 19
      2.4.1. Temperature Factor for General Purpose Diodes 19
      2.4.2. Temperature Factor for Voltage Regulator Diodes 20
      2.4.3. Stress, Contact Construction, Quality, and Environmental Factors 21
   2.5. Low-Frequency, Silicon MOSFETS 24
   2.6. Low-Frequency Bipolar Transistors 27
   2.7. Linear Integrated Circuits 32
      2.7.1. Temperature Factor for Linear ICs 32
      2.7.2. Environmental Factor for Linear ICs 34
      2.7.3. Quality and Learning Factors for Linear ICs 35
   2.8. Connectors 37
3. Analysis Results 40
   3.1. Analysis Results 1 – No Harsh Environment Factors 40
   3.2. Analysis Results 2 – With Harsh Environment Factors 45
   3.3. Discussion 49
   3.4. Interpretation of this Analysis 51
4. Appendix I – Overview of Reliability Analysis Methodology 53
5. References 59

1. Introduction

1.1. Scope

This note describes an analysis of the reliability of the ***Mu2e Calorimeter Front End Electronics Board***. The analysis is based upon the methodology described in the military handbook, "Reliability Prediction of Electronic Equipment," also known as MIL-HDBK-217F [1] (hereafter referred to as "the handbook,") which was developed by the Dept. of Defense for analyzing the reliability of military and aerospace systems. The results from this reliability analysis provide a prediction of the average failure rate for this board in the Mu2e Calorimeter instrumentation system. The analysis is limited to the evaluation of the components on the board, using the guidance set forth in the handbook, which uses specific weighting or acceleration factors in the calculation of the failure rate for each individual part on the board. These factors are functions of certain aspects of the application and parts choices, including temperature, voltage, power, packaging, complexity, fabrication technology, environment, and quality of manufacturing. Once the failure rate for each part is calculated, they are then combined to obtain the overall failure rate for the board. From this calculation, the "Mean Time to Failure," or MTTF, can be calculated. This is the standard quantity used in reliability analysis. From the MTTF, estimates of the probability of failure and expected number of failures as functions of time for the system can be obtained.

1.2. Description of the Board

The Mu2e Calorimeter [2-3] is comprised of two disks, each constructed as an array of cesium iodide (CsI) crystals. A rendering of the detector is shown in Fig. 1.2.1. There are a total of 1348 crystals in the detector, split evenly between the two disks. Each crystal is configured with four sets of three silicon photo-multipliers (SiPMs) across the face of the crystal as shown in Fig. 1.2.2. Each set of three SiPMs is connected in series. The signals from two such groups are summed together and instrumented with a Front End Board connected to the back side of the SiPM holder as shown. Thus, each crystal is read out using two Front End Boards. ***This yields a total of 2,696 Front End Boards in the system.***

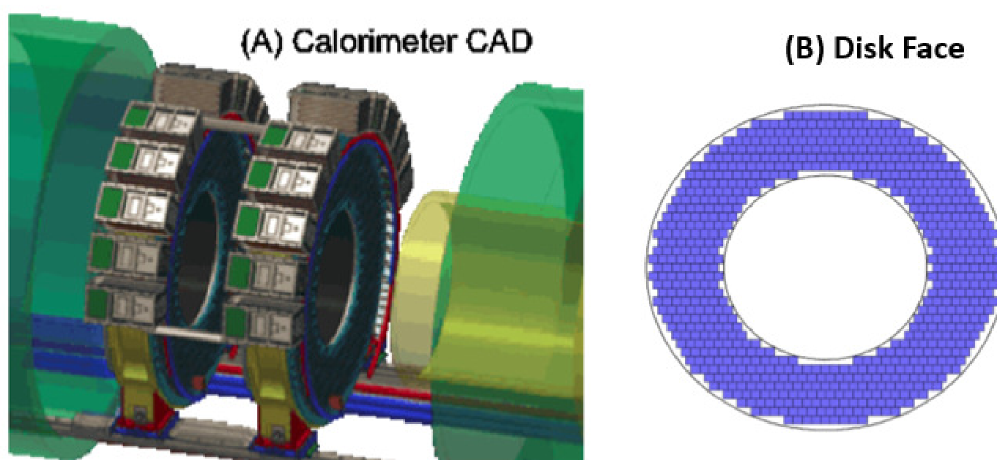

Fig. 1.2.1. (A) Configuration of two Calorimeter Disks in the Mu2e detector
(B) Configuration of CsI Crystals Looking into the Face of a Disk

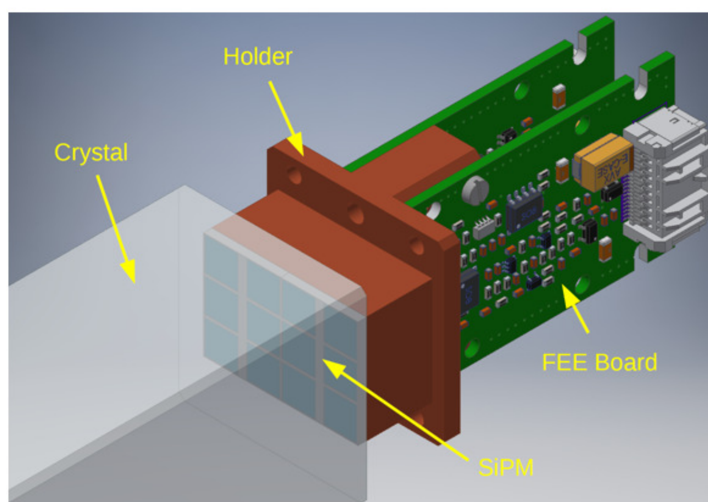

Fig. 1.2.2. Configuration of SiPMs and Associated Front End Boards on a CsI Crystal

A diagram of the readout electronics is shown in Figure 1.2.3. The Front End Boards process the charge signals from the SiPMs, and send analog voltages off-board differentially to be digitized. The analog signals are passed through a Mezzanine Board, and on to the waveform digitizer board, which is call the DIRAC. These boards reside a short distance away from the Front End Boards in crates located on the outer ring of the Calorimeter Disks, as sown in Fig. 1.2.1. Each DIRAC digitizes signals from 20 Front End Boards, and sends the digitized data off-detector to the back-end data acquisition system over optical data cables.

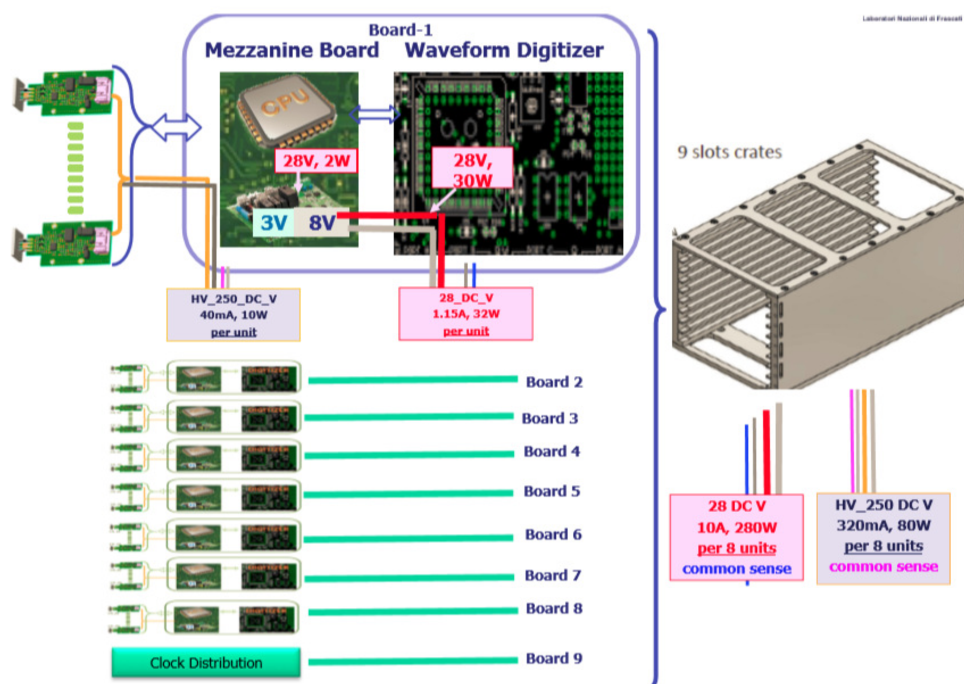

Fig. 1.2.3. Diagram of the On-Detector Readout for the Calorimeter

A block diagram of a Front End Board is shown in Fig. 1.2.4. The board has two main functions. One is to process the charge signals from the SiPMs as described previously. The second is to control and monitor the bias voltage that is needed by the SiPMs. To achieve this, the board contains an analog-to-digitize converter (ADC) for digitizing the bias voltage, and a digital-to-analog converter (DAC) for producing an analog voltage that controls the bias voltage value. The overall control of the bias circuit is implemented using an ARM microprocessor that resides on the Mezzanine Board. The microprocessor distributes the bias voltage reference values to the DACs on the Front End Boards, and then reads back the digitized values from the ADCs, adjusting the DAC values as needed to achieve the desired bias voltage. The bias control and monitor data are also read out through the DIRAC and then passed to the back-end Detector Control System (DCS) over the optical data cable. Groups of 20 Front End Boards are controlled by each Mezzanine Board. The Front End Board also contains a regulator section for regulating the voltages needed by the board, as shown in the figure. Design notes and performance reports for the Front End Board can be found in [4-12].

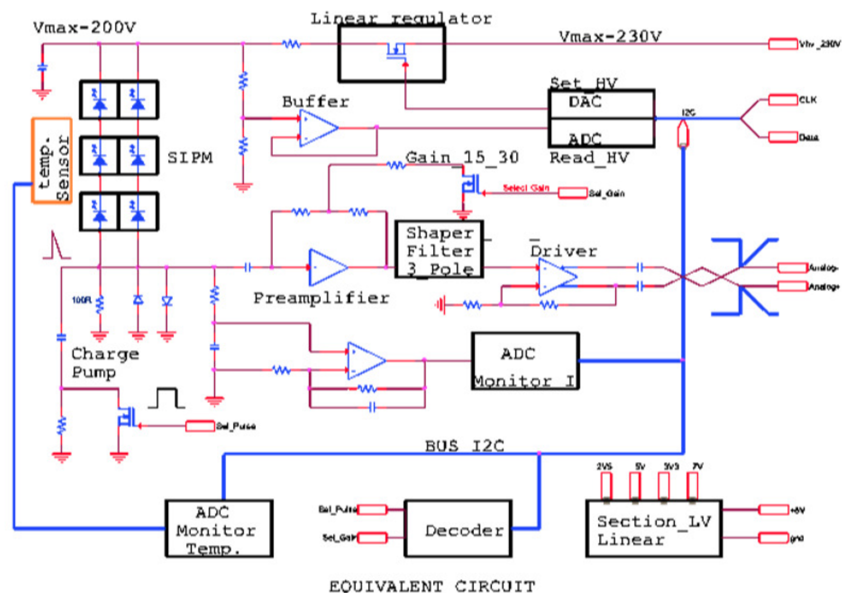

Fig. 1.2.4. Block Diagram of a Front End Board

Pictures of the Front End Board are shown in Fig. 1.2.5. The top side contains circuitry for the amplifier section, while the back side contains circuitry for the bias control and voltage regulators. There is a total of 86 different parts, some having multiple instances that yield 176 parts total. All of the parts have surface mount packaging (SMT), including resistors and capacitors with several different package sizes, diodes, discrete transistors, integrated circuits (ICs), and connectors.

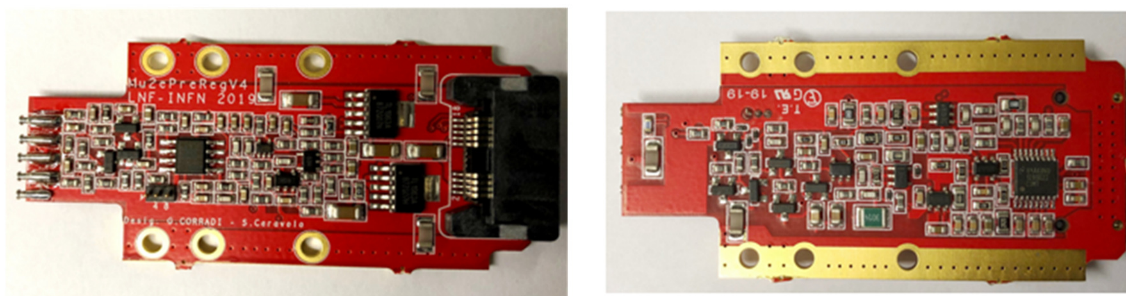

Fig. 1.2.5. Picture of a Front End Board
Left is the Top (AMP) Side; Right is the Bottom (HV) Side

In the reliability analysis described in this note, the parts are categorized according to the types defined in the handbook. The handbook then defines acceleration factors for each part type and prescribes how to calculate them based upon operating conditions, packaging, etc. The details of these calculations are presented in Section 2 for each part type. Note that this analysis only pertains to the Front End Boards. The reliability of the DIRAC and Mezzanine Boards will be covered separately.

1.3. Limits of Scope

This analysis does not include consideration of the quality or reliability of the printed circuit board itself, neither the fabrication nor the assembly. These aspects are more difficult to assess and require intimate knowledge of the practices and materials used by individual vendors, which may be a function of time. Fortunately, experience in designing and supporting large High Energy Physics (HEP) detector instrumentation systems [13-21] has shown that the dominate failure mode of electronics tends to be due component failures, provided that care is taken to select printed circuit board fabrication and assembly vendors who have been qualified, such as ISO900x certification.

This analysis does not include consideration of radiation damage. Indeed, for HEP applications, this can be a significant aspect in reliability analysis, and this is true for the Mu2e experiment. Specifications for radiation tolerance have been developed for the different subsystems in the experiment [22], and radiation tolerance measurement campaigns are either in progress or have been completed. However, at the time of this report, results for the Calorimeter Front End Board were not available in a form that lend themselves to the framework of this analysis, i.e. the multiplicative acceleration factors that modify base failure rates for individual parts. Radiation damage aspects that affect the reliability of these electronics will therefore not be addressed here, and instead will be reported separately.

In lieu of formal consideration of radiation damage, the handbook does provide the means for considering aspects that affect reliability related to the nature of the environment that the equipment operates in. Not surprisingly, since the handbook was developed by the Dept. of Defense, the environments defined in the handbook tend to be related to military applications, such as ground-based military, naval, aerospace, missile launch, etc. One of these environments, A_{UC}, *Airborne, Uninhabited Cargo*, has similarities to a HEP experiment, where human access is limited, and with somewhat harsh environmental conditions. The analysis performed for the Calorimeter Front End Board includes consideration of the impact on the MTTF if this environmental factor is applied. Even for the military applications, these environmental factors are estimates or approximations, providing a means to evaluate the trend in decreased reliability that various harsh conditions can cause, albeit with factors that likely have large uncertainties. To the extent that the A_{UC} environment has similarities to an HEP experiment, this analysis serves to illustrate how the reliability of this board can degrade by extreme environmental conditions, albeit with the caveat concerning uncertainties. This effect will be described in the discussion of the results in Section 3.

This analysis also does not include any part-specific reliability information from manufacturers or vendors. In general, it has proved to be very difficult to obtain reliability information for non-mil-spec, commercial off-the-shelf (COTS) parts. If manufacturers have this information at all, it is often not published in data sheets. Sometimes it can be obtained through private inquiry, but this is rare, and it is often difficult to find the right contact person. From a manufacturer perspective, performing reliability measurements and adhering to advertised limits on a production line certainly adds cost, in a competitive

environment where cost is often weighted more highly than reliability. Indeed, COTS parts are generally not manufactured with the same quality regimen as high-reliability parts, so publishing reliability information can have a negative marketing effect. Lastly, potential liability concerns are also factors that disfavor publishing reliability data. The MIL-HDBK-217F handbook provides a means for electronics design teams to evaluate system reliability as a function of different parts choices, quality level choices, testing levels, etc., when information from the component vendors is not available. This has inherent limitations, which are discussed further in Section 3.

2. Methodology

2.1. Overview of the Analysis Process

The following is a short summary of the mathematical concepts and relationships that form the basis for this analysis, primarily derived from [32], although there have been many good textbooks published on the subject. A more detailed treatment is provided in the Appendix.

In the general case, a system may be thought of as being composed of a number of units. Each unit can have a number of components. The goal in a reliability analysis is to determine the failure rate of the units in the system. This in turn involves the analysis of the failure rate of the individual components within a unit. In the simplest type of reliability analysis, the failure of any component in a unit represents a failure of that unit.

In general, the probability of failure of electronic components and systems during their useful lifetime tends to have an exponential distribution [33-34]. The quantity F(t), called the *Cumulative Distribution Function* (CDF), is defined as the accumulated number of failures as a function of time, normalized as a fraction of the total number of a given units in a system. For the case where the probability of failure is exponential in nature, F(t) has the form:

$$F(t) = 1 - e^{-\lambda t}, \quad 0 \leq t \leq \infty \qquad (2.1.1)$$

where λ is a constant, called the hazard rate or the average failure rate. The units of λ are in "number of failures per unit time." In the electronics industry, this is often expressed as the number of failures in 1E9 hours of operation, and is called "Failures in Time," or FITs.

The quantity R(t), called the Reliability function or the Survival function, is defined as the number of units that survive at time t, again normalized as a fraction of the total number of a given component type. R(t) is related to F(t) as:

$$R(t) = 1 - F(t), \quad 0 \leq t \leq \infty \qquad (2.1.2)$$

For the case where the probability of failure is exponential in nature, R(t) has the form:

$$R(t) = 1 - F(t) = e^{-\lambda t}, \quad 0 \leq t \leq \infty \qquad (2.1.3)$$

For a printed circuit board containing M components, each with hazard rates λ_1, λ_2, …λ_M respectively, the hazard rates are added together to give an overall hazard rate for the board:

$$\lambda_{BD} = \sum_1^M \lambda_i \qquad (2.1.4)$$

Once the hazard rate for a board is known, the probability of having a failure in the system at a time t_i, can be calculated as:

$$Probability\ of\ Failures\ at\ time\ t_i \ = \ \left(1 - e^{-(\lambda_{BD} * \ t_i)}\right), 0 \ \leq \ t_i \ \leq \ \infty \qquad (2.1.5)$$

For a system consisting of N identical units, an estimate of the accumulated number of failures that will have occurred at time t_i, is given by:

$$\#\ Failures\ at\ time\ t_i \ = \ N * \left(1 - e^{-(\lambda_{BD} * \ t_i)}\right), 0 \ \leq \ t_i \ \leq \ \infty \qquad (2.1.6)$$

For any given component on a board, there may be several factors that contribute to the hazard rate. Examples include temperature, mechanical or electrical stress, overall quality of the part, the environment, etc. One could model this as individual hazards or failure mechanisms. The approach used in MIL-HDBK-217F is to define a base hazard rate for each type of part, λ_b, and then define multiplicative factors that are functions of a particular failure mechanism. These factors are called weighting factors or acceleration factors, or sometimes "pi factors." The resulting hazard rate for a part then has the form,

$$\lambda_p = \lambda_b * \pi_1 * \pi_2 * \ldots * \pi_K \text{ , for K failure mechanisms} \qquad (2.1.7)$$

The base rate can be thought of as the failure rate under baseline conditions when all acceleration factors equal 1.

In the subsections that follow, a description of the failure mechanisms and hazard rate factors is presented addressing specifically the components on this board, which again is based upon the approach used in MIL-HDBK-217F.

2.2. Resistors

From MIL-HDBK-217F, Section 9.1, the hazard rate for resistors is specified as the following:

$$\lambda_p = \lambda_b * \pi_T * \pi_P * \pi_S * \pi_Q * \pi_E \tag{2.2.1}$$

where:
λ_p = the overall hazard rate
λ_b = the base hazard rate
π_T = the temperature factor
π_P = the power factor
π_S = the stress factor
π_Q = the quality factor
π_E = the environment factor (2.2.2)

The handbook lists several different types of resistors, including: carbon composition, metal film, thick film, wire wound, chip, etc. Each type tends to have the acceleration factors shown above, although the values may differ from resistor type to resistor type. For this board, the resistors used are all surface mount, type ***RM, Resistor, Fixed, Film, Chip, Established Reliability***. The type RM resistor is specified to have a bas hazard rate of 3.7 failures per 1E9 hours. There is also one thermistor on the board, which is denoted as type ***RTH, Thermistor***, and has a base hazard rate of 1.9 failures per 1E9 hours of operation.

The aging of resistors is accelerated with increasing temperature, compared to operation at a reference temperature. The temperature factor, π_T, modifies the base rate as shown in equation (2.2.1). For the type RM resistor, it is modeled by the following relationship:

$$\pi_T = e^{\left(\frac{-E_a}{8.617*10^{-5}} * \left(\frac{1}{T_a+273} - \frac{1}{T_{REF}+273}\right)\right)} \tag{2.2.3}$$

where E_a is the activation energy, T_a is the ambient temperature, and T_{REF} is a reference temperature. For the type RM resistor, the temperature parameters correspond to column 2 in the handbook. The activation energy is specified as 0.08 Joules. The reference temperature is usually taken to be room temperature (25 C.) A plot of the temperature factor as a function of operating temperature for a chip resistor is shown in Fig. 2.2.1. For the type RTH thermistor, temperature is not a factor in the aging, and the temperature factor is specified to be 1.

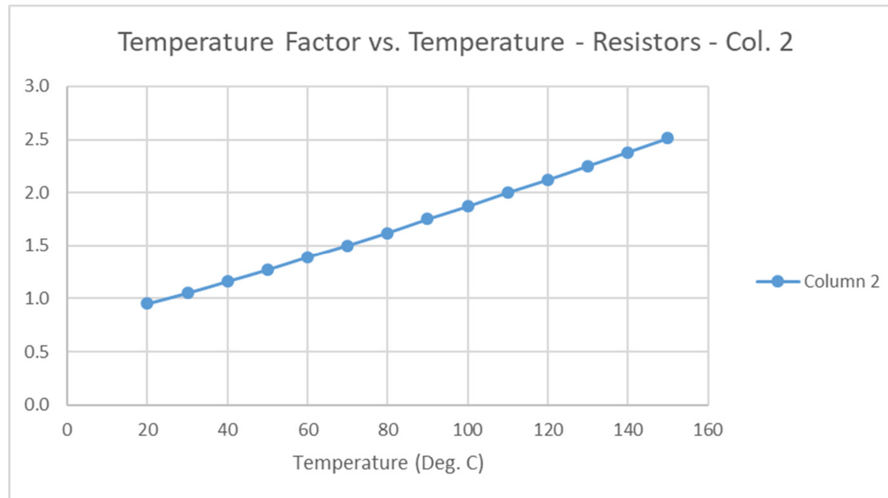

Fig. 2.2.1. Temperature Factor vs. Temperature for Chip Resistors

Power dissipation in a resistor creates heat, and therefore contributes to lifetime acceleration in a similar way as temperature. The acceleration factor for power, π_P, modifies the base rate as shown in equation (2.2.1), and is a function of the power dissipation in the resistor. For the type RM resistor, the relationship is modeled by:

$$\pi_P = (Power\ Dissipation)^{0.39} \tag{2.2.4}$$

A plot of the temperature factor as a function of operating temperature is shown in Fig. 2.2.2.

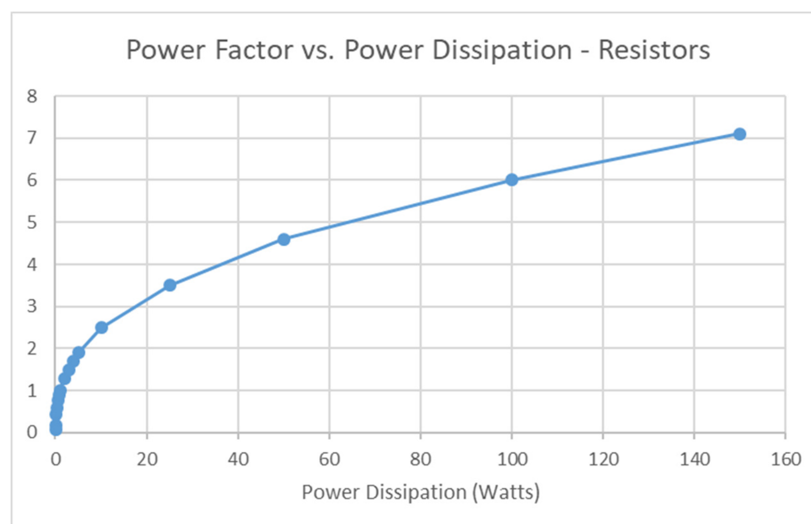

Fig. 2.2.2. Power Factor vs. Power Dissipation for Chip Resistors

Power dissipation in a resistor also creates stress, which contributes to accelerated lifetime. The acceleration factor for stress, π_S, also modifies that base rate as shown in

equation (2.2.1). For the type RM resistor, column 1 of the stress table for resistors is used. The stress is a function of the actual power compared to the rating. The relationship is modeled by:

$$\pi_S = (0.71) * e^{(1.1 * S)}, \text{ where } S = \frac{Actual\ Power}{Power\ Rating} \tag{2.2.5}$$

A plot of the stress factor is shown in Fig. 2.2.3. For the type RTH thermistor, stress is not a factor in the aging, and the stress factor is specified to be 1.

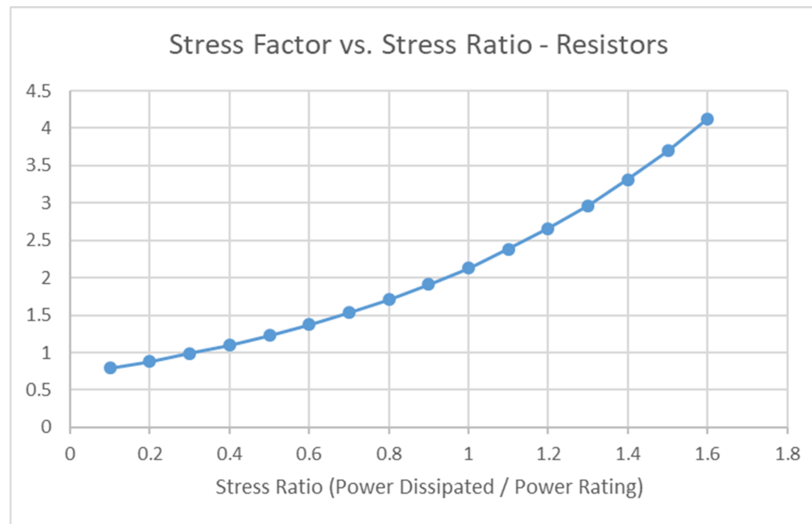

Fig. 2.2.3. Stress Factor vs. Stress Ratio for Chip Resistors

The quality factor, π_Q, is an attribute of the quality level in manufacturing from the vendor. The table from MIL-HDBK-217F for resistors is shown in Table 2.2.1. Unless specifically called out in the Bill of Materials, it will be assumed that the quality level is "Non-Established Reliability."

Designation	π_Q
S	0.03
R	0.1
P	0.3
Q	1.0
Non-Established Reliability	3.0
Commercial or Unknown	10.0

Table 2.2.1. Quality Factors for Resistors as a Function of Quality Levels

The environmental factor, π_E, is an attribute of the environment. The table from MIL-HDBK-217F for resistors is shown in Table 2.2.2. As discussed earlier, this analysis will use the "A_{UC}, Airborne, Uninhabited Cargo" for consideration of harsh conditions in HEP experiments that may accelerate failure. This will be discussed in the Section 3.

Designation	**Meaning**	π_E
G_B	Ground, benign	1.0
G_F	Ground, Fixed	4.0
G_M	Ground, Mobile	16.0
N_S	Naval, Sheltered	12.0
N_U	Naval, Unsheltered	42.0
A_{IC}	Airborne, Inhabited, Cargo	18.0
A_{IF}	Airborne, Inhabited, Fighter	23.0
A_{UC}	**Airborne, Uninhabited, Cargo**	**31.0**
A_{UF}	Airborne, Uninhabited, Fighter	43.0
A_{RW}	Airborne, Rotary, Winged	63.0
S_F	Space Flight	0.5
M_F	Missile, Flight	37.0
M_L	Missile, launch	87.1
C_L	Cannon, Launch	1728

Table 2.2.2. Environmental Factors for Resistors as a Function of Environment

2.3. Capacitors

From MIL-HDBK-217F, Section 10.1, the hazard rate for capacitors is given as the following:

$$\lambda_p = \lambda_b * \pi_T * \pi_C * \pi_V * \pi_{SR} * \pi_Q * \pi_E \qquad (2.3.1)$$

where:
λ_p = the overall hazard rate.
λ_b = the base hazard rate
π_T = the temperature factor
π_C = the capacitance factor
π_V = the voltage stress factor
π_{SR} = the series resistance factor (tantalum capacitors)
π_Q = the quality factor
π_E = the environment factor (2.3.2)

There are several different types of capacitors listed in the handbook, most notably differing by the type of dielectric, including: paper, metalized plastic, mica, ceramic, glass, electrolytic, tantalum, etc. There are many different packaging options listed as well. Each type tends to have the acceleration factors shown above, although the values may differ from type to type. For this board, the capacitors are all surface mount with ceramic dielectric, type ***CDR, Capacitor, Chip, Multiple Layer, Fixed, Ceramic Dielectric, Established Reliability.*** The base rate for the CDR capacitor is specified as 2.0 failures per 1E9 hours of operation.

The aging of capacitors is accelerated with increasing temperature, compared to operation at a reference temperature. The temperature factor, π_T, modifies the base rate as shown in equation (2.3.1). The value of π_T is modeled by the following relationship:

$$\pi_T = e^{\left(\frac{-E_a}{8.617* 10^{-5}} * \left(\frac{1}{T_a+273} - \frac{1}{T_{REF}+273}\right)\right)} \qquad (2.3.3)$$

where E_a is the activation energy, T_a is the ambient temperature, and T_{REF} is a reference temperature. For the type CDR capacitor, the temperature parameters correspond to column 2 in the handbook. The activation energy is specified as 0.35 Joules. The reference temperature is usually taken to be room temperature (25 C.) A plot of the temperature factor as a function of operating temperature for a chip capacitor is shown in Fig. 2.3.1.

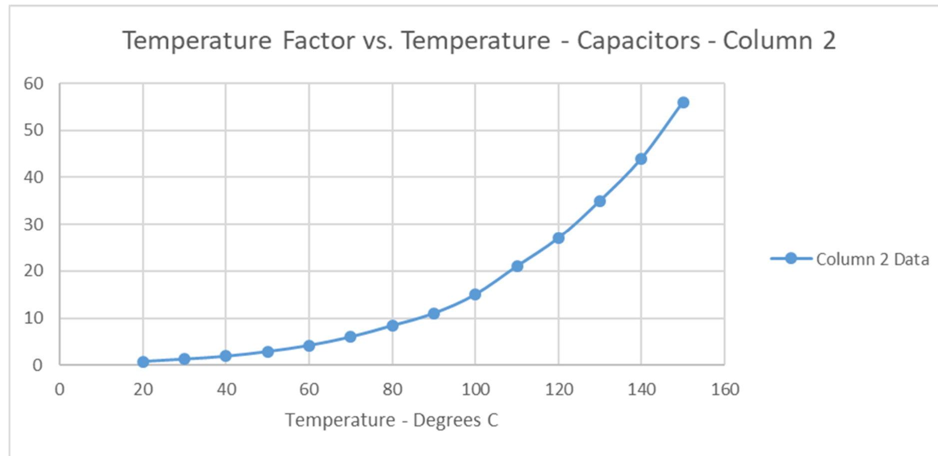

Fig. 2.3.1. Temperature Factor vs. Temperature for Chip Capacitors
(Referenced to 25Deg. C Ambient)

The acceleration factor for capacitance, π_C, modifies the base rate as shown in equation 2.3.1. Generally, the larger the capacitance, the higher the probability of failure. For the type CDR capacitor, column 1 of the capacitance factor table is used. The data is modeled by the equation:

$$\pi_C = (Capacitance\ in\ uF)^{0.09} \quad (2.3.4)$$

A plot of the capacitance factor as a function of capacitance value for a chip capacitor is shown in Fig. 2.3.2.

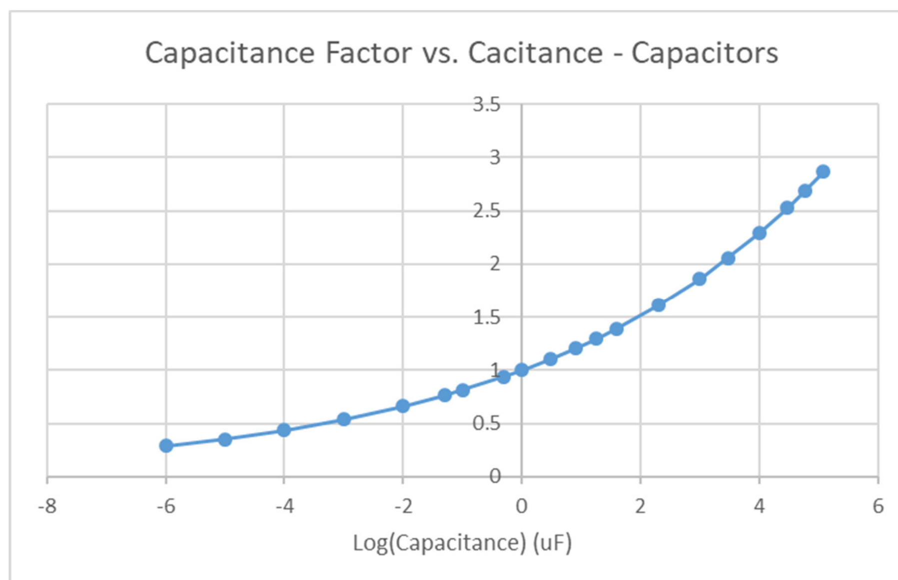

Fig. 2.3.2. Capacitance Factor vs. Capacitance for Chip Capacitors

The operating voltage applied to a capacitor also creates stress, which can lead to accelerated failures. The acceleration factor for voltage stress, π_V, also modifies that base rate as shown in equation (2.3.1). For the type CDR capacitor, column 3 of the stress table for capacitors is used. The stress is a function of the applied voltage compared to the voltage rating. The relationship is modeled by:

$$\pi_V = (S/0.6)^3 + 1, \text{ where } S = \frac{\text{Applied Voltage}}{\text{Voltage Rating}} \tag{2.3.5}$$

A plot of the voltage factor as a function of applied voltage for a chip capacitor is shown in Fig. 2.3.3.

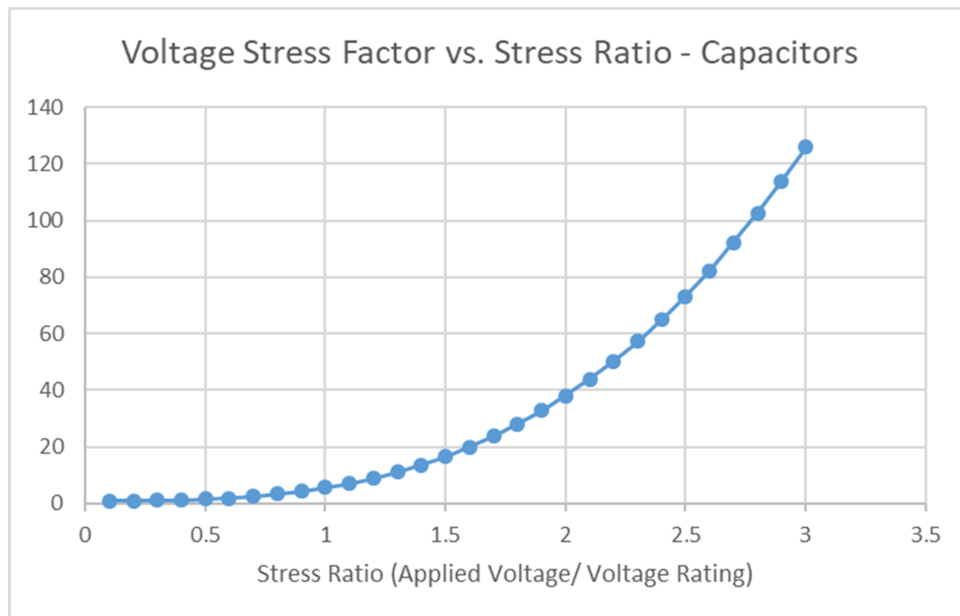

Fig. 2.3.3. Voltage Stress Factor vs. Stress Ratio for Chip Capacitors

The quality factor, π_Q, is an attribute of the quality level in manufacturing from the vendor. The table from MIL-HDBK-217F for capacitors is shown in Table 2.3.1. Unless specifically called out in the Bill of Materials, it will be assumed that the quality level is "Non-Established Reliability."

Designation	π_Q
D	0.001
C	0.01
S,B	0.03
R	0.1
P	0.3
M	1.0
L	1.5
Non-Established Reliability	3.0
Commercial or Unknown	10.0

Table 2.3.1. Quality Factors for Capacitors as a Function of Quality Levels

The environmental factor, π_E, is an attribute of the environment. The table from MIL-HDBK-217F for capacitors is shown in Table 2.3.2. Consideration of the reliability of this board under harsh conditions as characterized by the military designation A_{UC} will be discussed in Section 3.

Designation	Meaning	π_Q
G_B	Ground, benign	1.0
G_F	Ground, Fixed	10.0
G_M	Ground, Mobile	20.0
N_S	Naval, Sheltered	7.0
N_U	Naval, Unsheltered	15.0
A_{IC}	Airborne, Inhabited, Cargo	12.0
A_{IF}	Airborne, Inhabited, Fighter	15.0
A_{UC}	**Airborne, Uninhabited, Cargo**	**25.0**
A_{UF}	Airborne, Uninhabited, Fighter	30.0
A_{RW}	Airborne, Rotary, Winged	40.0
S_F	Space Flight	0.5
M_F	Missile, Flight	20.0
M_L	Missile, launch	50.0
C_L	Cannon, Launch	570

Table 2.3.2. Environmental Factors for Capacitors as a Function of Environment

2.4. Low Frequency Diodes

From MIL-HDBK-217F, Section 6.1, the hazard rate for low frequency diodes is specified as the following:

$$\lambda_p = \lambda_b * \pi_T * \pi_S * \pi_C * \pi_Q * \pi_E \quad (2.4.1)$$

where:
λ_p = the overall hazard rate.
λ_b = the base hazard rate
π_T = the temperature factor
π_S = the stress factor
π_C = the contact construction factor
π_Q = the quality factor
π_E = the environment factor (2.4.2)

There are several different types of low frequency diodes defined in the handbook. The types that are included in this category are: general purpose analog, switching, fast recovery, power rectifier, transient suppressor, current regulator, voltage regulator, and voltage reference. Each type tends to have the failure factors shown above, although the values may differ from type to type. In this design, there are two types of diodes used: ***general purpose (GP), and voltage regulator (VR).*** For the general purpose diode, the base failure rate is specified as 3.8 failures per 1E9 hours. For the voltage regulator diode, the base failure rate is 2.0 failures per 1E9 hours.

2.4.1. Temperature Factor for General Purpose Diodes

The aging of diodes is accelerated with increasing temperature, compared to operation at a reference temperature. The temperature factor, π_T, modifies the base rate as shown in equation (2.4.1). It is a function of the junction temperature, T_j, which is given by:

$$T_j = T_a + (R_{th} * \mathrm{P}) \quad (2.4.3)$$

Where:
T_j = Junction temperature
T_a = Ambient temperature
R_{th} = Thermal resistance between junction & ambient
P = Power dissipation (2.4.4)

Once the junction temperature is known, the temperature factor, π_T, can be found. For the general purpose diode, the first set of the temperature tables is used. The value of π_T is modeled by the equation:

$$\pi_T = e^{\left(-3091*\left(\frac{1}{T_j+273} - \frac{1}{T_a+273}\right)\right)} \quad (2.4.5)$$

where the temperatures are in Celsius. A plot of the temperature factor as a function of the junction temperature for a general purpose diode is shown in Fig. 2.4.1.

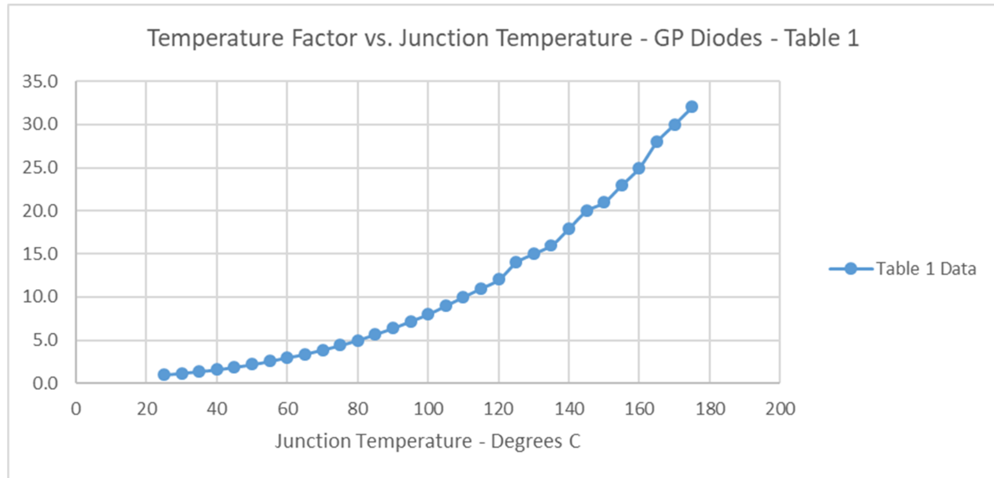

Fig. 2.4.1. Temperature Factor vs. Temperature for General Purpose Diodes (Referenced to 25 Deg. C Ambient)

2.4.2. Temperature Factor for Voltage Regulator Diodes

For the voltage regulator diode, the second set of the temperature tables is used. The value of π_T is modeled by the equation:

$$\pi_T = e^{\left(-1925 * \left(\frac{1}{T_j+273} - \frac{1}{T_a+273}\right)\right)} \tag{2.4.6}$$

where the temperatures are in Celsius. A plot of the temperature factor as a function of the junction temperature for a voltage regulator diode is given in Fig. 2.4.2.

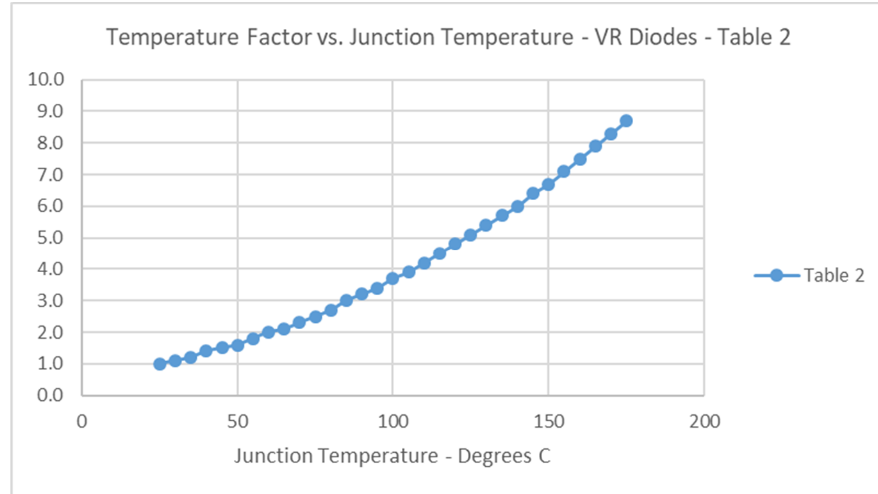

Fig. 2.4.2. Temperature Factor vs. Temperature for Voltage Regulator Diodes (Referenced to 25 Deg. C Ambient)

2.4.3. Stress, Contact Construction, Quality, and Environmental Factors

Voltage stress can occur in diodes under reverse bias conditions. The acceleration factor for stress, π_S, also modifies that base rate as shown in equation (2.2.1). For the voltage regulator diode, the stress factor is specified to be 1.0, voltage stress is not a factor for these devices. For all low frequency diodes, the stress is modeled by:

$$\pi_S = 0.054 \text{ , for } 0 \leq V_S \leq 0.3 \qquad (2.4.7)$$

$$\pi_S = (0.54) * e^{(2.43 * S)} \text{ , for } 0.3 < V_S \leq 1, \qquad (2.4..8)$$

where $V_S = \dfrac{Actual\ Reverse\ Voltage}{Max\ Reverse\ Voltage\ Rating}$.

A plot of the stress factor is shown in Fig. 2.4.3.

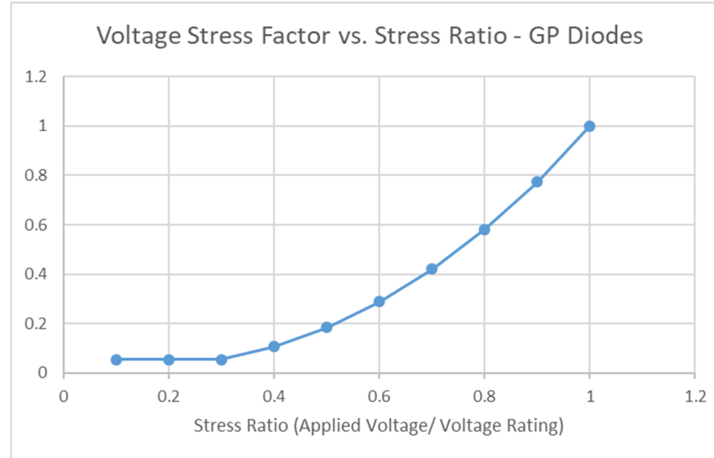

Fig. 2.4.3. Stress Factor vs. Stress Ratio for Low Frequency Diodes under Reverse Bias

The quality factor, π_Q, is an attribute of the quality level in manufacturing from the vendor. The table from MIL-HDBK-217F for low frequency diodes is shown in Table 2.4.1. Unless specifically called out in the Bill of Materials, it will be assumed that the quality level is "JAN."

Designation	π_Q
JANTXV	0.7
JANTX	1.0
JAN	2.4
Lower	5.5
Plastic	8.0

Table 2.4.1. Quality Factors for Low Frequency Diodes as a Function of Quality Levels

The environmental factor, π_E, is an attribute of the environment. The table from MIL-HDBK-217F for diodes is shown in Table 2.4.2. Consideration of the reliability of this board under harsh conditions as characterized by the military designation A_{UC} will be discussed in Section 3.

Designation	**Meaning**	π_Q
G_B	Ground, benign	1.0
G_F	Ground, Fixed	6.0
G_M	Ground, Mobile	9.0
N_S	Naval, Sheltered	9.0
N_U	Naval, Unsheltered	19.0
A_{IC}	Airborne, Inhabited, Cargo	13.0
A_{IF}	Airborne, Inhabited, Fighter	29.0
A_{UC}	**Airborne, Uninhabited, Cargo**	**20.0**
A_{UF}	Airborne, Uninhabited, Fighter	43.0
A_{RW}	Airborne, Rotary, Winged	24.0
S_F	Space Flight	0.5
M_F	Missile, Flight	14.0
M_L	Missile, launch	32.0
C_L	Cannon, Launch	320

Table 2.4.2. Environmental Factors for Low Frequency Diodes as a Function of Environment

2.5. Low-Frequency, Silicon MOSFETS

There are several different types of Field Effect Transistors (FETs), including N-channel, P-channel, enhancement mode, depletion mode, power, JFETs, GaAsSFETs, etc. They differ in construction depending on the application, such as small-signal, switching, or power. FETS can come as discrete, or as part of a larger integrated circuit. Also, FETs are fabricated in many different technologies and feature sizes. The MIL-HDBK-217F has chosen to divide FETs into three main categories: low-frequency silicon MOSFETS (less than or equal to 400 MHz); high frequency silicon MOSFETs, and GaAsFETs. JFETs are included in the low-frequency silicon MOSFETs. Integrated circuits are considered separately. In this design, only low-frequency silicon MOSFETs are used, designated as ***MOS, LF***.

From MIL-HDBK-217F, Section 6.4, the hazard rate for low-frequency, silicon MOSFETs is given as the following:

$$\lambda_p = \lambda_b * \pi_T * \pi_A * \pi_Q * \pi_E \qquad (2.5.1)$$

where:
λ_p = the overall hazard rate.
λ_b = the base hazard rate
π_T = the temperature factor
π_A = the application factor
π_Q = the quality factor
π_E = the environment factor (2.5.2)

The base hazard rate, λ_b, is the hazard rate of a part under normal operation. For the low-frequency MOSFETs, the base rate is specified as 12.0 failures per 1E9 hours of operation.

The aging of MOSFETs is accelerated with increasing temperature, compared to operation at a reference temperature. The temperature factor, π_T, modifies the base rate as shown in equation (2.5.1). It is a function of the junction temperature, T_j, which is given by:

$$T_j = T_a + (R_{th} * \mathrm{P}) \qquad (2.5.3)$$

Where:
T_j = Junction temperature
T_a = Ambient temperature
R_{th} = Thermal resistance between junction & ambient
P = Power dissipation (2.5.4)

Once the junction temperature is known, the temperature factor, π_T, can be found. For the MOSFET, the value of π_T is modeled by the equation:

$$\pi_T = e^{\left(-1925 * \left(\frac{1}{T_j+273} - \frac{1}{T_a+273}\right)\right)} \qquad (2.5.5)$$

where the temperatures are in Celsius. A plot of the temperature factor as a function of the junction temperature for the low-frequency MOSFET is shown in Fig. 2.5.1.

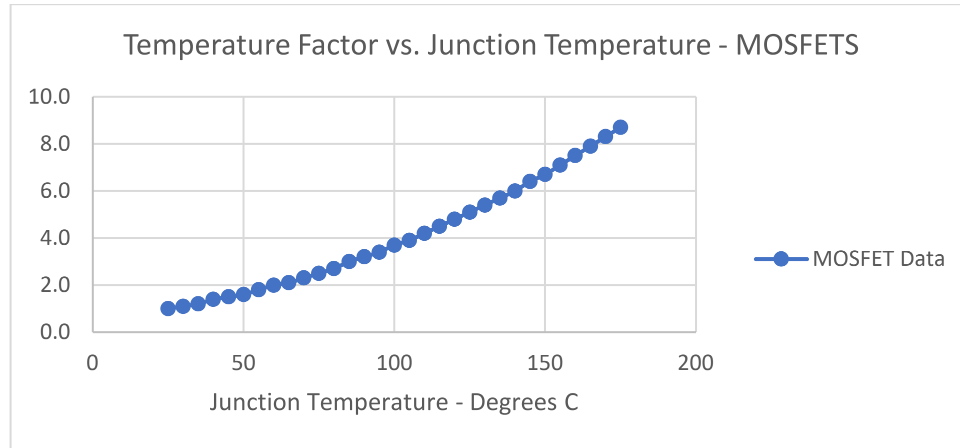

Fig. 2.5.1. Temperature Factor vs. Temperature for the Low-frequency MOSFET (Referenced to 25 Deg. C Ambient)

The application factor, π_A, accounts for stress on the device that is application-dependent. The handbook divides into three categories: linear, switching, and power. The application factor table from MIL-HDBK-217F for low-frequency silicon MOSFETs is shown in Table 2.5.1. For this design, the application is linear, so the value for π_A will be taken to be 1.5.

Application	π_A
Linear	1.5
Small Signal Switching	0.7
Power, 2W≤ P < 5W	2.0
Power, 5W≤ P < 50W	4.0
Power, 50W≤ P < 250W	8.0
Power, P ≥ 250W	10

Table 2.5.1. Quality Factors for MOSFETS as a Function of Application

The quality factor, π_Q, is an attribute of the quality level in manufacturing from the vendor. The table from MIL-HDBK-217F for MOSFETs is shown in Table 2.5.2. Unless specifically called out in the Bill of Materials, it will be assumed that the quality level is JAN.

Designation	π_Q
JANTXV	0.5
JANTX	1.0
JAN	2.0
Lower	5.0

Table 2.5.2. Quality Factors for MOSFETS as a Function of Quality Levels

The environmental factor, π_E, is an attribute of the environment. The table from MIL-HDBK-217F for MOSFETs is shown in Table 2.5.3. Consideration of the reliability of this board under harsh conditions as characterized by the military designation A_{UC} will be discussed in the analysis section.

Designation	**Meaning**	π_Q
G_B	Ground, benign	1.0
G_F	Ground, Fixed	6.0
G_M	Ground, Mobile	9.0
N_S	Naval, Sheltered	9.0
N_U	Naval, Unsheltered	19.0
A_{IC}	Airborne, Inhabited, Cargo	13.0
A_{IF}	Airborne, Inhabited, Fighter	29.0
A_{UC}	**Airborne, Uninhabited, Cargo**	**20.0**
A_{UF}	Airborne, Uninhabited, Fighter	43.0
A_{RW}	Airborne, Rotary, Winged	24.0
S_F	Space Flight	0.5
M_F	Missile, Flight	14.0
M_L	Missile, launch	32.0
C_L	Cannon, Launch	320

Table 2.5.3. Environmental Factors for MOSFETS as a Function of Environment

2.6. Low-Frequency Bipolar Transistors

There are three main types of junction transistors: bipolar junction transistors (BJT), unijunction, and heterojunction. For bipolar junction transistors, there are two main topologies: NPN and PNP. The types differ in fabrication and construction details depending the application, including small signal, high frequency, or power. Different fabrication technologies can be used, including silicon, germanium, and gallium arsenide, and can have different feature sizes. The MIL-HDBK-217F has chosen to divide junction transistors into three main categories: low-frequency silicon bipolar (less than or equal to 200 MHz); low-noise, high-frequency silicon bipolar; high-frequency power bipolar, and unijunction. In this design, only ***low-frequency silicon bipolar transistors*** are used, designated as ***BJT, LF***.

From MIL-HDBK-217F, Section 6.3, the hazard rate for low-frequency (< 200 MHz) silicon bipolar transistors is specified as the following:

$$\lambda_p = \lambda_b * \pi_T * \pi_A * \pi_R * \pi_S * \pi_Q * \pi_E \qquad (2.6.1)$$

where:
λ_p = the overall hazard rate.
λ_b = the base hazard rate
π_T = the temperature factor
π_A = the application factor
π_R = the power rating factor
π_S = the voltage stress factor
π_Q = the quality factor
π_E = the environment factor (2.6.2)

The base hazard rate, λ_b, is the hazard rate of a part under normal operation. For the low-frequency bipolar transistors, the base rate is specified as 0.74 failures per 1E9 hours of operation. It is the same for NPN and PNP devices.

The aging of BJTs is accelerated with increasing temperature, compared to operation at a reference temperature. The temperature factor, π_T, modifies the base rate as shown in equation (2.6.1). It is a function of the junction temperature, T_j, which is given by:

$$T_j = T_a + (R_{th} * \mathrm{P}) \qquad (2.6.3)$$

Where:
T_j = Junction temperature
T_a = Ambient temperature
R_{th} = Thermal resistance between junction & ambient
P = Power dissipation (2.6.4)

Once the junction temperature is known, the temperature factor, π_T, can be found. For the BJT, the value of π_T is modeled by the equation:

$$\pi_T = e^{\left(-2114*\left(\frac{1}{T_j+273}-\frac{1}{T_a+273}\right)\right)} \tag{2.6.5}$$

where the temperatures are in Celsius. A plot of the temperature factor as a function of the junction temperature for the low-frequency bipolar transistor is shown in Fig. 2.6.1.

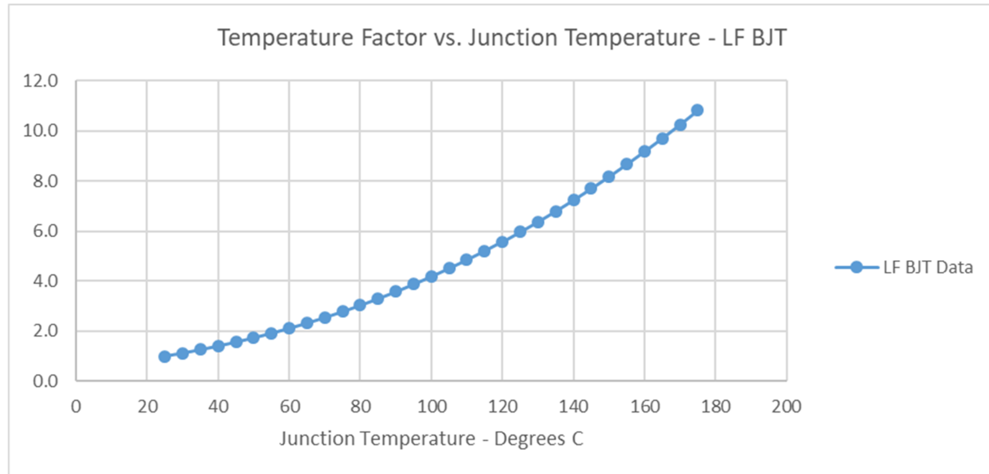

Fig. 2.6.1. Temperature Factor vs. Junction Temperature for the Low-frequency MOSFET (Referenced to 25 Deg. C Ambient)

The application factor, π_A, accounts for stress on the device that is application-dependent. The handbook divides into two categories: linear and switching. The application factor table from MIL-HDBK-217F for low-frequency bipolar transistors is shown in Table 2.6.1. For this design, the application is linear, so the value for π_A will be taken to be 1.5.

Application	π_A
Linear	1.5
Switching	0.7

Table 2.6.1. Quality Factors for LF BJTs as a Function of Application

Power dissipation in a transistor creates heat, and therefore contributes to age acceleration in a similar way as temperature. The acceleration factor for power rating, π_R, modifies the base rate as shown in equation (2.6.1). The handbook defines this factor as a function of the power rating only, with increasing values as the power rating increases. For the LF BJT, the relationship is modeled by:

$$\pi_R = 0.43 \text{ for } P_R \leq 0.1\text{Watt} \tag{2.6.6}$$

$$\pi_R = (Power\ Rating)^{0.37} \text{ for } P_R > 0.1\text{Watt} \tag{2.6.7}$$

A plot of the power rating factor as a function of operating temperature is shown in Fig. 2.6.2.

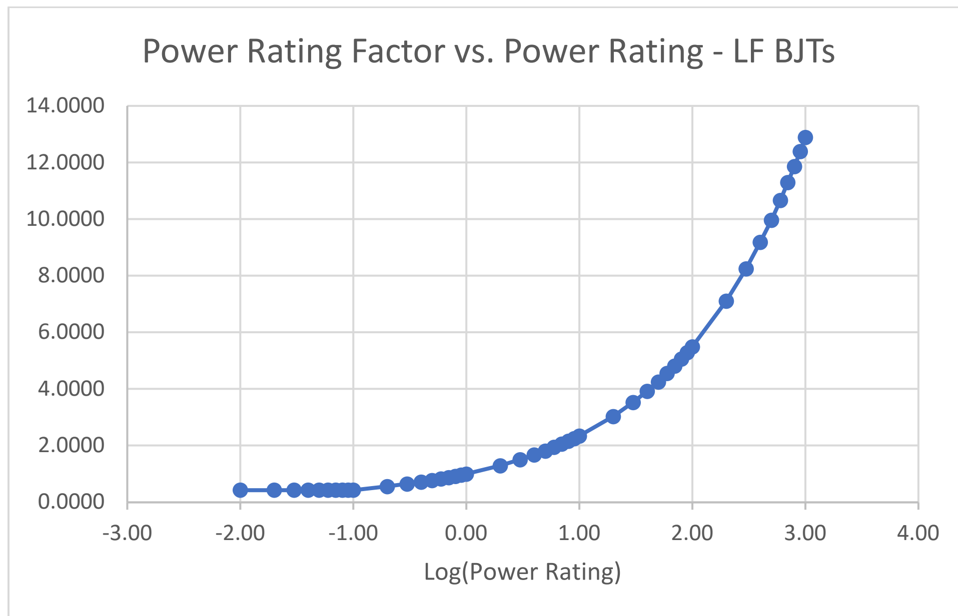

Fig. 2.6.2. Power Factor vs. Power Rating for LF BJTs

The applied voltage to a transistor also creates stress, which can lead to early failure. The acceleration factor for voltage stress, π_S, also modifies that base rate as shown in equation (2.6.1). The stress is a function of the applied voltage compared to the voltage rating. For the low-frequency BJT, the relationship is modeled by:

$$\pi_S = 0.045 * e^{(3.1 * V_S)}, \text{ where } V_S = \frac{V_{CE}}{V_{CEO}} \tag{2.6.8}$$

A plot of the stress factor as a function of the ratio V_S for a LF BJT is shown in Fig. 2.6.3.

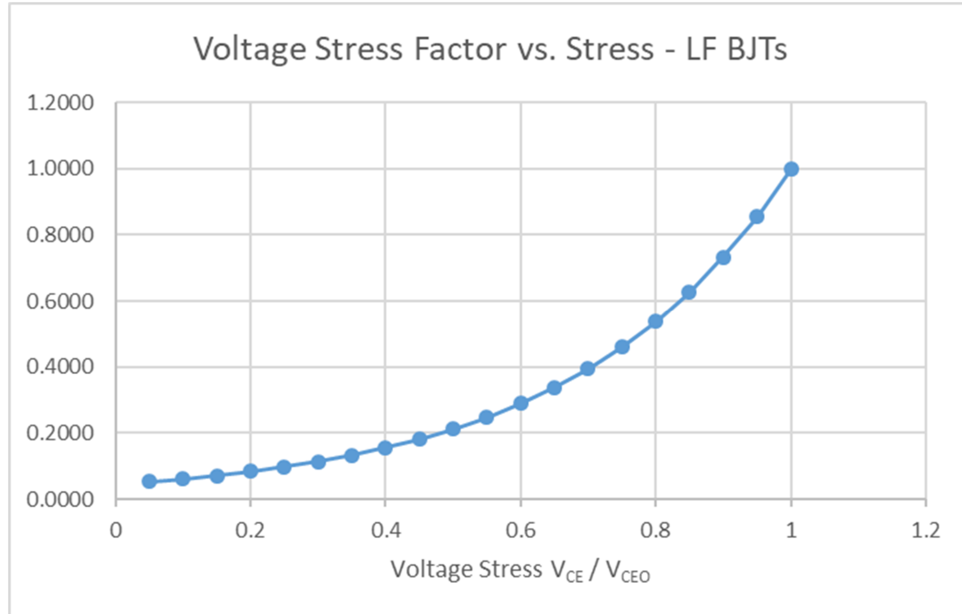

Fig. 2.6.3. Voltage Stress Factor vs. Stress Ratio for LF BJTs

The quality factor π_Q is an attribute of the quality level in manufacturing from the vendor. The table from MIL-HDBK-217F for BJTs is shown in Table 2.6.2. Unless specifically called out in the Bill of Materials, it will be assumed that the quality level is "JAN."

Designation	π_Q
JANTXV	0.7
JANTX	1.0
JAN	2.4
Lower	5.5
Plastic	8.0

Table 2.6.2. Quality Factors for LF BJTs as a Function of Quality Levels

The environmental factor, π_E, is an attribute of the environment. The table from MIL-HDBK-217F for BJTs is shown in Table 2.6.3. Consideration of the reliability of this board under harsh conditions as characterized by the military designation A_{UC} will be discussed in the analysis section.

Designation	**Meaning**	π_Q
G_B	Ground, benign	1.0
G_F	Ground, Fixed	6.0
G_M	Ground, Mobile	9.0
N_S	Naval, Sheltered	9.0
N_U	Naval, Unsheltered	19.0
A_{IC}	Airborne, Inhabited, Cargo	13.0
A_{IF}	Airborne, Inhabited, Fighter	29.0
A_{UC}	**Airborne, Uninhabited, Cargo**	**20.0**
A_{UF}	Airborne, Uninhabited, Fighter	43.0
A_{RW}	Airborne, Rotary, Winged	24.0
S_F	Space Flight	0.5
M_F	Missile, Flight	14.0
M_L	Missile, launch	32.0
C_L	Cannon, Launch	320

Table 2.6.3. Environmental Factors for LF BJTs as a Function of Environment

2.7. Linear Integrated Circuits

Section 5 of MIL-HDBK-217F covers the reliability of all types of integrated circuits. The hazard rate of linear integrated circuits, denoted as ***IC, LIN*** is defined in Section 5.1 as:

$$\lambda_p = (C_1 * \pi_T + C2 * \pi_E) * \pi_Q * \pi_L \quad (2.7.1)$$

where:
λ_p = the overall hazard rate.
C_1 = the die complexity failure rate
π_T = the temperature factor
C_2 = the package failure rate
π_E = the environmental factor
π_Q = the quality factor
π_L = the learning factor (2.7.2)

Factors C_2, π_T, π_E, π_Q, and π_L are defined in sections 5.8 – 5.11. Note that there is no base hazard rate defined for this category.

2.7.1. Temperature Factor for Linear ICs

The temperature factor includes the die complexity factor, C_1, which accounts for increasing failure rate with increasing complexity. Generally, complexity is defined as being a function of the number of transistors in a device. This is shown in Table 2.7.1. The handbook specifies the same table for both bipolar and CMOS ICs, and makes no distinction on feature size. In general, unless the IC design is custom, it is very difficult to ascertain how many devices are in an IC design. For the purposes of this analysis, the guidance shown in the righthand column of Table 2.7.1, developed by the author based upon will be used.

No. Transistors	C1	Example Devices (Annotated)
1 to 100	0.010	Voltage References
101 to 300	0.020	Op Amps
301 to 1000	0.040	DACs
1001 to 10,000	0.060	ADCs

Table 2.7.1. Die Complexity Factors as a Function of the Number of Transistors

The temperature factor, π_T, modifies the base rate as shown in equation (2.7.1). It is a function of the junction temperature, T_j, which is given by:

$$T_j = T_a + (R_{th} * \mathrm{P}) \tag{2.7.3}$$

Where: T_j = Junction temperature
T_a = Ambient temperature
R_{th} = Thermal resistance between junction & ambient
P = Power dissipation (2.7.4)

Once the junction temperature is known, the temperature factor can be found. It is modeled by the equation:

$$\pi_T = 0.1 * e^{\left(\frac{-E_a}{8.617 * 10^{-5}} * \left(\frac{1}{T_j + 273} - \frac{1}{T_a + 273}\right)\right)} \tag{2.7.5}$$

where the temperatures are in Celsius. E_a is the activation energy, which for linear ICs is taken to be 0.65. A plot of the temperature factor as a function of the junction temperature for a linear IC is shown in Fig. 2.7.1.

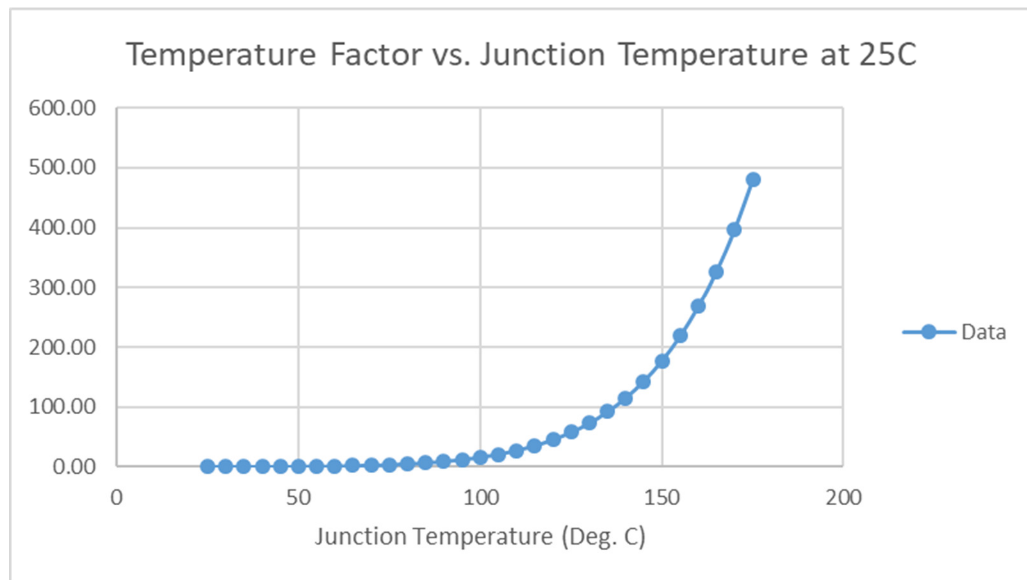

Fig. 2.7.1. Temperature Factor vs. Junction Temperature for Linear ICs
(Referenced to 25 Deg. C Ambient)

2.7.2. Environmental Factor for Linear ICs

The environmental factor includes the package failure rate factor, C_2, which is a function of the number of pins in a package, and also the package construction. This is described in section 5.9 of the handbook. Package types considered include hermetic DIPs and SMTs, cans, and DIPs with glass seals, and non-hermetic DIPs and SMTs. Generally, the factors grow larger with package type, respectively. For this analysis, all of the linear ICs are non-hermetic SMT. The relationship of the factor C2 as a function of the number of pins in the package for the non-hermetic SMT package is modeled by the equation:

$$C_2 = 3.6 * 10^{-4} * (N_p)^{1.08} \tag{2.7.6}$$

where Np is the number of pins. A plot of this relationship is shown in Fig. 2.7.2.

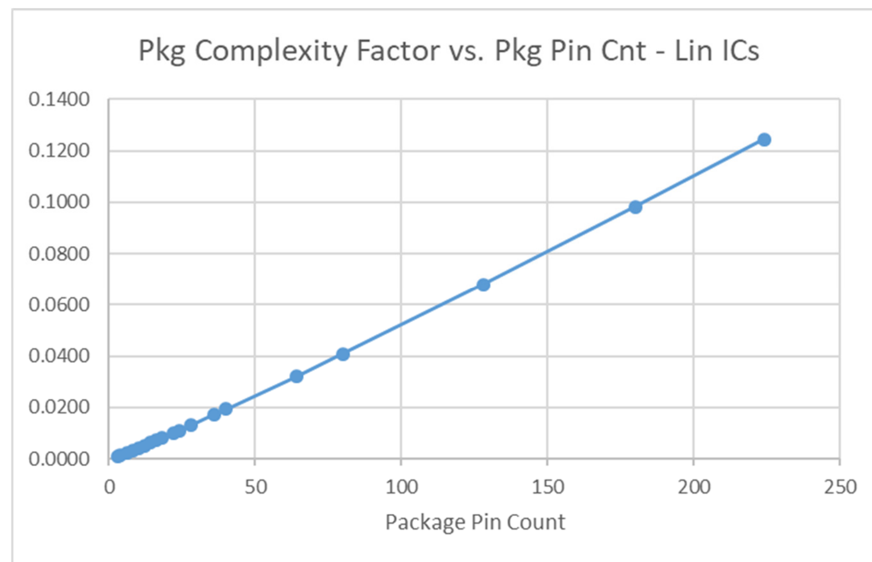

Fig. 2.7.2. Package Complexity Factor C2 vs. Package Pin Count

The environmental factor, π_E, for linear ICs is defined in Section 5.10 of the handbook. The table is shown in Table 2.7.2. Consideration of the reliability of this board under harsh conditions as characterized by the military designation A_{UC} will be discussed in the analysis section.

Designation	Meaning	π_Q
G_B	Ground, benign	0.5
G_F	Ground, Fixed	2.0
G_M	Ground, Mobile	4.0
N_S	Naval, Sheltered	4.0
N_U	Naval, Unsheltered	6.0
A_{IC}	Airborne, Inhabited, Cargo	4.0
A_{IF}	Airborne, Inhabited, Fighter	5.0
A_{UC}	**Airborne, Uninhabited, Cargo**	**5.0**
A_{UF}	Airborne, Uninhabited, Fighter	8.0
A_{RW}	Airborne, Rotary, Winged	8.0
S_F	Space Flight	0.5
M_F	Missile, Flight	5.0
M_L	Missile, launch	12.0
C_L	Cannon, Launch	220.0

Table 2.7.2. Environmental Factors for Linear ICs as a Function of Environment

2.7.3. Quality and Learning Factors for Linear ICs

The handbook specifies a detailed description for determining the quality factor, π_Q, as a function of different levels of testing in Section 5.10. For this project, none of the ICs have undergone pre-testing or burn-in. Thus, the default value for commercial or unknown screening levels will be used:

$$\pi_Q = 10 \tag{2.7.7}$$

The handbook defines a learning factor, π_L, which takes into account the number of years that a part has been in production. The general idea is that for complex integrated circuits, there may be bugs in the design that are evident early in the production, but become identified and are addressed as time goes on so that later production cycles have a lower probability of having problems. After a couple of years, the handbook projects that all potential bugs have been addressed. The model as specified in Section 5.10 is given as:

$$\pi_L = 0.01 * e^{(5.35-(0.35*Y))} \text{ , for } 0 \leq Y < 2 \quad (2.7.8)$$

$$\pi_L = 1 \text{ for } Y \geq 2 \quad (2.7.9)$$

A plot of the learning factor as a function of production years is shown in Fig. 2.7.3.

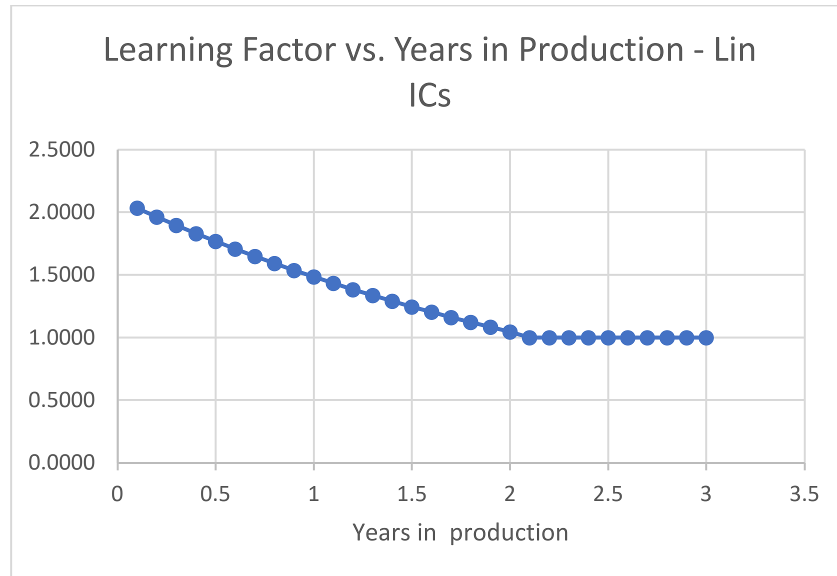

Fig. 2.7.3. Learning Factor vs. Number of Years in production for Linear ICs

2.8. Connectors

From MIL-HDBK-217F, Section 15.1, the hazard rate for a mated pair of connectors is specified as the following:

$$\lambda_p = \lambda_b * \pi_T * \pi_K * \pi_Q * \pi_E \quad (2.8.1)$$

where:
λ_p = the overall hazard rate
λ_b = the base hazard rate
π_T = the temperature factor
π_K = the mating/un-mating factor
π_Q = the quality factor
π_E = the environment factor (2.8.2)

There are many different types of connectors identified in the handbook, including: circular/cylindrical, card edge (PCB), hexagonal, rack and panel, rectangular, RF coaxial, telephone, power, and triaxial. Each type tends to have the acceleration factors shown above, although the values may differ from type to type. For this board, there two types of connectors used: a ***Rectangular Connector, RC,*** and mating pins for the the SiPM connection. There is no type defined in the handbook for the mating pins, so it will be assumed that they are similar in reliability to ***Power Connectors, PC***, since they are robust and large gauge.

The base hazard rate, λ_b, is the hazard rate of a part under nominal operation. For the type RC connector, the base rate is specified as 46 failures per 1E9 hours of operation. For the type PC connector, the base rate is specified as 7 failures per 1E9 hours of operation.

The aging of connectors is accelerated with increasing temperature, compared to operation at a reference temperature. In this context, aging is synonymous with failure rate. The temperature factor, π_T, modifies the base rate as shown in equation (2.8.1). The value of π_T is modeled by the following relationship:

$$\pi_T = e^{\left(\frac{-0.14}{8.617* 10^{-5}} * \left(\frac{1}{T_0+273} - \frac{1}{T_{REF}+273}\right)\right)} \quad (2.8.3)$$

where T_0 is the contact temperature, and T_{REF} is a reference temperature. The contact temperature has a provision to include self-heating due to current flow, having a general form:

$$T_0 = T_a + \Delta_T = T_a + [\, K * (I)^{1.85} \,] \quad (2.2.4)$$

where Δ_T is the insert temperature, T_a is the ambient temperature, I is the current in Amperes flowing through the connector, and K is a factor that is dependent upon the gauge of the contacts. The reference temperature is usually taken to be room temperature (25 C.) The value of K varies from 0.1 for 12 gauge contacts, to 3.256 for 32 gauge contacts. This

relationship is the same for all connector types. Since the current flowing through the connectors is significantly less than 1 amp, the difference between the contact temperature and the ambient temperature is of order ~a few degrees, and will be ignored since it is small. A plot of the temperature factor as a function of operating temperature for connectors is shown in Fig. 2.8.1.

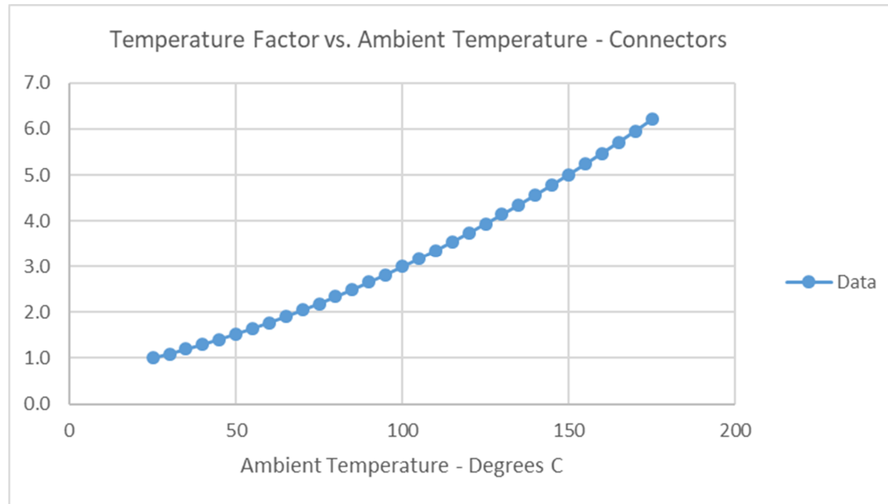

Fig. 2.8.1. Temperature Factor vs. Temperature for Connectors
Plot is for low currents, and neglects any self-heating.

Mating and un-mating a connector pair creates stress on the connector contacts, as well as in the connections of the pins and sockets of the connector to the wires or cables. The acceleration factor for mating/un-mating, π_K, modifies the base rate as shown in equation (2.8.1), and is a function of the frequency of the interconnects, as shown in Table 2.8.1. A cycle includes both connect and interconnect. The values are the same for all connector types. In normal operation, the plugging and unplugging of this board will be done rarely, so the low-frequency value will be assumed.

Mating/Un-mating Cycles (per 1000 hours)	π_K
0 to 0.05	1.0
0.05 to 0.5	1.5
0.5 to 5	2.0
5 to 50	3.0
> 50	4.0

Table 2.8.1. Mating/Un-Mating Factors for Connectors as a Function of Interconnect Frequency.

The quality factor, π_Q, is an attribute of the quality level in manufacturing from the vendor. The table from MIL-HDBK-217F for connectors is shown in Table 2.8.2. Unless specifically called out in the Bill of Materials, it will be assumed that the quality level is “Lower.”

Designation	π_Q
Mil-Spec	1
Lower	2

Table 2.8.2. Quality Factors for Connectors as a Function of Quality Levels

The environmental factor, π_E, is an attribute of the environment. The table from MIL-HDBK-217F for connectors is shown in Table 2.8.3. As discussed earlier, this analysis will use the “A_{UC}, Airborne, Uninhabited Cargo” for consideration of harsh conditions in HEP experiments that may accelerate failure. This will be discussed in the Section 3.

Designation	**Meaning**	π_E
G_B	Ground, benign	1.0
G_F	Ground, Fixed	1.0
G_M	Ground, Mobile	8.0
N_S	Naval, Sheltered	5.0
N_U	Naval, Unsheltered	13.0
A_{IC}	Airborne, Inhabited, Cargo	3.0
A_{IF}	Airborne, Inhabited, Fighter	5.0
A_{UC}	**Airborne, Uninhabited, Cargo**	**8.0**
A_{UF}	Airborne, Uninhabited, Fighter	12.0
A_{RW}	Airborne, Rotary, Winged	19.0
S_F	Space Flight	0.5
M_F	Missile, Flight	10.0
M_L	Missile, launch	27.1
C_L	Cannon, Launch	490

Table 2.8.3. Environmental Factors for Connectors as a Function of Environment

3. Analysis Results

3.1. Analysis Results 1 – No Harsh Environment Factors

The parts used on the board were identified and categorized according to the methodology in MIL-HDBK-217F, as described in Section 2. The base hazard rates for each part were defined. The various acceleration factors for each part were calculated, based upon the expected operating conditions. For this stage of analysis, the environmental factors π_E for all components were set to 1.

The result of this analysis is shown in Table 3.1.1. The hazard rates for all components were summed to give the overall hazard rate for the board, as described in equation (2.1.4). This is shown at the top of Table 3.1.1.

The overall hazard rate for the board, λ_{BD}, is found to be:

$$\lambda_{BD} = 519\ Failures\ per\ 1E9\ Hours \tag{3.1.1}$$

This gives the Mean Time to Failure (MTTF) as:

$$MTTF = \frac{1E9}{\lambda_{BD}} = 1.92E6\ \text{Hours} \tag{3.1.2}$$

MIL-HDBK-217F
Electronic Board Reliability Analysis
G. Drake, Mar. 12, 2020, V2.00

Project:	Mu2e Calorimeter Front End Board
Version:	V2
Designer:	G. Corradi
Date:	March 12, 2020
# Boards:	2696

Part Information from Bill of Material

Board Reliability Calculation Results

Harsh:	OFF	λ_{NET}:	519.5382
Ambient T:	12	MTTF:	1.9248E+06

Item	Qnty/Bd	Reference	Part	Nominal FITS	Reliability Weighting	Weighted FITS (Calc)	Total per Board
1	1	C1	100n	2.0000	1.3160	2.6320	2.6320
2	1	C2	100n	2.0000	1.3262	2.6523	2.6523
3	1	C3	100n	2.0000	1.3262	2.6523	2.6523
4	1	C6	100n	2.0000	1.3160	2.6320	2.6320
5	1	C7	100n	2.0000	1.3096	2.6192	2.6192
6	1	C8	100n	2.0000	1.3108	2.6217	2.6217
7	1	C14	100n	2.0000	1.3122	2.6244	2.6244
8	1	C17	100n	2.0000	1.3262	2.6523	2.6523
9	1	C19	100n	2.0000	1.3262	2.6523	2.6523
10	1	C52	100n	2.0000	1.3262	2.6523	2.6523
11	1	C53	100n	2.0000	1.3095	2.6190	2.6190
12	1	C56	100n	2.0000	1.3119	2.6238	2.6238
13	1	C63	100n	2.0000	1.3096	2.6192	2.6192
14	1	C4	10n	2.0000	1.0779	2.1559	2.1559
15	1	C12	10n	2.0000	1.0664	2.1327	2.1327
16	1	C62	10n	2.0000	1.0661	2.1322	2.1322
17	1	C5	1u	2.0000	1.6111	3.2221	3.2221
18	1	C9	1u	2.0000	1.6111	3.2221	3.2221
19	1	C61	1u	2.0000	1.6112	3.2224	3.2224
20	1	C10	47p	2.0000	0.6571	1.3141	1.3141
21	1	C13	4p7	2.0000	0.5342	1.0685	1.0685
22	1	C24	100n	2.0000	4.4136	8.8271	8.8271
23	1	C25	100n	2.0000	1.3344	2.6687	2.6687
24	1	C29	100n	2.0000	1.3344	2.6687	2.6687
25	1	C36	100n	2.0000	1.3103	2.6206	2.6206
26	1	C39	100n	2.0000	1.3096	2.6193	2.6193
27	1	C26	22p	2.0000	1.9619	3.9238	3.9238
28	1	C27	100p	2.0000	2.9160	5.8320	5.8320
29	1	C28	10n	2.0000	4.9017	9.8034	9.8034
30	1	C30	1n2	2.0000	0.8657	1.7314	1.7314
31	1	C31	1n	2.0000	0.8657	1.7314	1.7314
32	1	C32	10n	2.0000	1.0693	2.1387	2.1387
33	1	C38	10n	2.0000	1.0645	2.1289	2.1289
34	1	C44	10n	2.0000	1.0846	2.1692	2.1692
35	1	C68	10n	2.0000	1.0693	2.1387	2.1387
36	1	C72	10n	2.0000	1.0650	2.1301	2.1301
37	1	C74	10n	2.0000	1.0680	2.1360	2.1360
38	1	C78	10n	2.0000	1.0647	2.1295	2.1295
39	1	C80	10n	2.0000	1.0693	2.1387	2.1387
40	1	C81	10n	2.0000	1.0644	2.1288	2.1288
41	1	C46	12p	2.0000	0.5813	1.1627	1.1627
42	1	C47	12p	2.0000	0.5813	1.1627	1.1627
43	1	C70	12p	2.0000	0.5813	1.1627	1.1627
44	1	C76	12p	2.0000	0.5813	1.1627	1.1627
45	1	C77	12p	2.0000	0.5813	1.1627	1.1627
46	1	C51	22p	2.0000	0.6137	1.2273	1.2273
47	1	C54	47p	2.0000	0.6573	1.3146	1.3146
48	1	C55	10n	2.0000	1.2564	2.5128	2.5128
49	1	C64	10u	2.0000	2.0866	4.1731	4.1731
50	1	C65	10u	2.0000	2.0866	4.1731	4.1731
51	1	C66	10u	2.0000	2.0866	4.1731	4.1731
52	1	C67	10u	2.0000	2.0866	4.1731	4.1731
53	1	C69	1u	2.0000	1.6185	3.2370	3.2370
54	1	C71	1u	2.0000	1.6120	3.2240	3.2240
55	1	C73	1u	2.0000	1.6165	3.2330	3.2330
56	1	C75	1u	2.0000	1.6165	3.2330	3.2330
57	1	C79	1u	2.0000	1.6165	3.2330	3.2330
58	1	D1	CMAD6001	3.8000	0.1296	0.4925	0.4925
59	1	D3	CMAD6001	3.8000	0.1296	0.4925	0.4925
60	1	D4	CMAD6001	3.8000	0.1296	0.4925	0.4925
61	1	D5	CMAD6001	3.8000	0.1296	0.4925	0.4925
62	1	D6	CMAD6001	3.8000	0.1296	0.4925	0.4925

Table 3.1.1a. Calorimeter Front End Board parts List with Calculated FITS Values, Nominal Environment (Partial, 1 of 3)

MIL-HDBK-217F Electronic Board Reliability Analysis					Board Reliability Calculation Results		
G. Drake, Mar. 12, 2020, V2.00							
Project:	Mu2e Calorimeter Front End Board			Harsh:	OFF	λNET:	519.5382
Version:	V2			Ambient T:	12	MTTF:	1.9248E+06
Designer:	G. Corradi						
Date:	March 12, 2020		Part Information from Bill of Material				
# Boards:	2696						

Item	Qnty/Bd	Reference	Part	Nominal FITS	Reliability Weighting	Weighted FITS (Calc)	Total per Board
64	4	J1	SIPM_MU2e	7.0000	1.5596	10.9175	43.6701
65	1	J2	HSE	46.0000	1.5596	71.7438	71.7438
66	1	J3	J_GAIN	46.0000	1.5596	71.7438	71.7438
67	1	M1	AO3162	12.0000	3.8624	46.3490	46.3490
68	1	M2	BSS126	12.0000	3.7735	45.2820	45.2820
69	1	M3	AO3162	12.0000	3.8624	46.3490	46.3490
70	1	Q1	MMBT5771	0.7400	0.1090	0.0807	0.0807
71	1	Q2	MMBT5771	0.7400	0.1218	0.0902	0.0902
72	1	Q6	MMBT5771	0.7400	0.1218	0.0902	0.0902
73	1	Q3	MMBT3904	0.7400	0.5183	0.3835	0.3835
74	1	Q4	MMBT3904	0.7400	0.1226	0.0907	0.0907
75	1	R1	100R	3.7000	0.0510	0.1886	0.1886
76	1	R59	100R	3.7000	0.0510	0.1886	0.1886
77	1	R2	1k	3.7000	0.0207	0.0767	0.0767
78	1	R10	1k	3.7000	0.0207	0.0767	0.0767
79	1	R11	1k	3.7000	0.0207	0.0767	0.0767
80	1	R13	1k	3.7000	0.0207	0.0767	0.0767
81	1	R16	1k	3.7000	0.0207	0.0767	0.0767
82	1	R19	1k	3.7000	0.0207	0.0767	0.0767
83	1	R21	1k	3.7000	0.0207	0.0767	0.0767
84	1	R61	1k	3.7000	0.0034	0.0127	0.0127
85	1	R3	460R	3.7000	0.3182	1.1774	1.1774
86	1	R4	4k7	3.7000	0.1768	0.6540	0.6540
87	1	R5	22k	3.7000	0.1216	0.4499	0.4499
88	1	R24	22k	3.7000	0.1004	0.3715	0.3715
89	1	R81	22k	3.7000	0.1004	0.3715	0.3715
90	1	R6	50R	3.7000	0.0018	0.0068	0.0068
91	1	R14	50R	3.7000	0.0669	0.2476	0.2476
92	1	R83	50R	3.7000	0.0669	0.2476	0.2476
93	1	R84	50R	3.7000	0.0669	0.2476	0.2476
94	1	R7	2k	3.7000	0.2544	0.9414	0.9414
95	1	R82	2k	3.7000	0.2544	0.9414	0.9414
96	1	R8	220R	3.7000	0.0315	0.1164	0.1164
97	1	R9	220R	3.7000	0.0315	0.1164	0.1164
98	1	R15	220R	3.7000	0.1797	0.6648	0.6648
99	1	R12	68R	3.7000	0.0593	0.2194	0.2194
100	1	R17	10R	3.7000	0.1271	0.4704	0.4704
101	1	R18	1k6	3.7000	0.0101	0.0372	0.0372
102	1	R20	56k	3.7000	0.0720	0.2663	0.2663
103	1	R23	330R	3.7000	0.0018	0.0068	0.0068
104	1	R60	330R	3.7000	0.0320	0.1183	0.1183
105	1	R26	56R	3.7000	0.3444	1.2744	1.2744
106	1	R34	330R	3.7000	0.1514	0.5600	0.5600
107	1	R35	4K7	3.7000	0.0113	0.0420	0.0420
108	1	R36	1K	3.7000	0.0018	0.0068	0.0068
109	1	R37	3Meg	3.7000	0.3557	1.3159	1.3159
110	1	R38	15K	3.7000	0.1034	0.3827	0.3827
111	1	R39	38K3	3.7000	0.1073	0.3971	0.3971
112	1	R40	1K	3.7000	0.0207	0.0767	0.0767
113	1	R106	1K	3.7000	0.0207	0.0767	0.0767
114	1	R41	100R	3.7000	0.0510	0.1886	0.1886
115	1	R42	220R	3.7000	0.7567	2.7999	2.7999
116	1	R43	22K	3.7000	0.0062	0.0230	0.0230
117	1	R44	10K	3.7000	0.0084	0.0313	0.0313
118	1	R45	270K	3.7000	0.0023	0.0086	0.0086
119	1	R46	1K2	3.7000	0.0193	0.0715	0.0715
120	1	R47	10K	3.7000	0.0084	0.0313	0.0313
121	1	R51	2R2	3.7000	0.2441	0.9032	0.9032
122	1	R55	2R2	3.7000	0.2370	0.8771	0.8771

Table 3.1.1b. Calorimeter Front End Board parts List with Calculated FITS Values, Nominal Environment (Partial, 2 of 3)

MIL-HDBK-217F Electronic Board Reliability Analysis				Board Reliability Calculation Results			
G. Drake, Mar. 12, 2020, V2.00							
Project:	Mu2e Calorimeter Front End Board			Harsh:	OFF	λ_{NET}:	519.5382
Version:	V2			Ambient T:	12	MTTF:	1.9248E+06
Designer:	G. Corradi						
Date:	March 12, 2020		Part Information from Bill of Material				
# Boards:	2696						
Item	**Qnty/Bd**	**Reference**	**Part**	**Nominal FITS**	**Reliability Weighting**	**Weighted FITS (Calc)**	**Total per Board**
123	1	R99	2R2	3.7000	0.2370	0.8771	0.8771
124	1	R54	5K23	3.7000	0.1367	0.5059	0.5059
125	1	R56	100R	3.7000	0.0509	0.1885	0.1885
126	1	R105	100R	3.7000	0.0509	0.1885	0.1885
127	1	R57	10R	3.7000	0.1263	0.4673	0.4673
128	1	R107	10R	3.7000	0.1263	0.4673	0.4673
129	1	R58	120R	3.7000	0.1460	0.5402	0.5402
130	1	R62	2k2	3.7000	0.0128	0.0474	0.0474
131	1	R63	2k2	3.7000	0.0128	0.0474	0.0474
132	1	R85	22R	3.7000	0.0075	0.0276	0.0276
133	1	R86	22R	3.7000	0.0075	0.0276	0.0276
134	1	R87	PT1000	3.7000	0.1181	0.4370	0.4370
135	1	R88	806R	3.7000	0.0226	0.0835	0.0835
136	1	R90	806R	3.7000	0.0226	0.0835	0.0835
137	1	R89	2K55	3.7000	0.0144	0.0533	0.0533
138	1	R91	3k9	3.7000	0.0122	0.0451	0.0451
139	1	R92	33R	3.7000	0.0788	0.2917	0.2917
140	1	R94	33R	3.7000	0.0788	0.2917	0.2917
141	1	R96	33R	3.7000	0.0788	0.2917	0.2917
142	1	R100	33R	3.7000	0.0788	0.2917	0.2917
143	1	R101	33R	3.7000	0.0788	0.2917	0.2917
144	1	R93	11K	3.7000	0.0018	0.0068	0.0068
145	1	R95	10K	3.7000	0.1051	0.3890	0.3890
146	1	R97	10K	3.7000	0.1051	0.3890	0.3890
147	1	R104	10K	3.7000	0.0880	0.3256	0.3256
148	1	R98	1K	3.7000	0.0731	0.2704	0.2704
149	1	R102	4K22	3.7000	0.2118	0.7835	0.7835
150	1	R103	4K22	3.7000	0.1246	0.4611	0.4611
151	1	U1	AD8014ARTZ	1.0000	0.0005	0.0005	0.0005
152	1	U3	AD8014ARTZ	1.0000	0.0006	0.0006	0.0006
153	1	U2	AD8099ARD	1.0000	0.0004	0.0004	0.0004
154	1	U7	OPA180	1.0000	0.0005	0.0005	0.0005
155	1	U8	LMP7707	1.0000	0.0005	0.0005	0.0005
156	1	U9	LMP7707	1.0000	0.0005	0.0005	0.0005
157	1	U10	LMP7707	1.0000	0.0004	0.0004	0.0004
158	1	U15	AD8038AKSZ	1.0000	0.0006	0.0006	0.0006
159	1	U16	TL1963_ADJ	1.0000	2.4337	2.4337	2.4337
160	1	U17	TL1963_ADJ	1.0000	0.0134	0.0134	0.0134
161	1	U18	DAC121S101	1.0000	0.0010	0.0010	0.0010
162	1	U19	ADC128S102	1.0000	0.0048	0.0048	0.0048
163	1	JUMP1		0.0000	0.0000	0.0000	0.0000
	Total failure Rate (per 1E9 hours):						519.5382
		Calculated MTTF:					1.9248E+06
		# Failures in 1st Year:					9.80
	Probability of Failure in 1st Year:						0.36%
		# Failures in 5 Years:					48.64
	Probability of Failure in 5 Years:						1.80%

Table 3.1.1c. Calorimeter Front End Board parts List with Calculated FITS Values, Nominal Environment (Partial, 3 of 3)

The probability of failure at time t_i is given by the CDF:

$$Probability\ of\ Failure(t_i) = F(t_i) = 1 - e^{(-\lambda_{BD} * 1E-9 * t_i)} \quad (3.1.3)$$

For a system consisting of N boards, with no repairs being conducted, the expected cumulative number of failures at time t_i is given by:

$$\#\ Failures(t_i) = N * F(t_i) = N * [1 - e^{(-\lambda_{BD} * 1E-9 * t_i)}] \quad (3.1.4)$$

Assuming that the Mu2e Calorimeter readout system has 2,696 Front End Boards in the full readout system, and assuming 80% up-time each year (with the power to the electronics turned off during the down-time), with no repairs performed, the associated probabilities and expected number of failures in the system are summarized in Table 3.1.2.

Year	**Probability of Failure**	**Predicted Number of Failures**
1	0.36%	9.80
2	0.73%	19.56
3	1.09%	29.29
4	1.45%	38.98
5	1.80%	48.64

Table 3.1.2. Predicted Probability of Failure and Numbers of Failures as a Function of Time, Nominal Environment

3.2. Analysis Results 2 – With Harsh Environment Factors

As discussed in in Section 1.3, the methodology of MIL-HDBK-217F provides for each electronic component to include an environmental factor. For the analysis described in Section 3.1, the environmental factors were set to 1. In the following, the same analysis was performed, but with the environmental factors for the different components set to the values corresponding with environment *A_{UC}, Airborne, Uninhabited Cargo*, as described in Section 2. The result of this analysis is shown in Table 3.2.1. As before, the resulting hazard rates were summed to give the overall hazard rate for the board, as given by equation (2.1.4). This is shown at the top of Table 3.2.1.

The overall hazard rate λ_{BD_E} with environmental factors included is given by:

$$\lambda_{BD_E} = 9{,}182\ Failures\ per\ 1E9\ Hours \qquad (3.2.1)$$

This gives the Mean Time to Failure for the A_{UC} environment, denoted as $MTTF_E$ to be:

$$MTTF_E = \frac{1E9\ Hours}{\lambda_{BD_E}} = 1.09E5\ \text{Hours} \qquad (3.2.2)$$

The MTTF of the board is reduced by a factor of 17.6 in this environment.

As in Section 3.1, the probability of failure and the expected number of failures at time t_i can be calculated.

Again assuming that the Mu2e Calorimeter readout system has 2,696 Front End Boards in the full readout system, and assuming 80% up-time per year (with the power to the electronics turned off during the down-time), with no repairs performed, the associated probabilities and expected number of failures are summarized in Table 3.2.2.

Year	Probability of Failure	Predicted Number of Failures
1	7.50%	202.25
2	14.44%	389.34
3	20.86%	562.38
4	26.80%	722.45
5	32.29%	870.50

Table 3.2.2. Predicted Probability of Failure and Numbers of Failures as a Function of Time, Harsh Environment

MIL-HDBK-217F Electronic Board Reliability Analysis G. Drake, Mar. 12, 2020, V2.00	
Project:	Mu2e Calorimeter Front End Board
Version:	V2
Designer:	G. Corradi
Date:	March 12, 2020
# Boards:	2696

Part Information from Bill of Material

Board Reliability Calculation Results			
Harsh:	ON	λ_{NET}:	9182.7787
Ambient T:	12	MTTF:	1.0890E+05

Item	Qnty/Bd	Reference	Part	Nominal FITS	Reliability Weighting	Weighted FITS (Calc)	Total per Board
1	1	C1	100n	2.0000	32.8998	65.7996	65.7996
2	1	C2	100n	2.0000	33.1539	66.3078	66.3078
3	1	C3	100n	2.0000	33.1539	66.3078	66.3078
4	1	C6	100n	2.0000	32.8998	65.7996	65.7996
5	1	C7	100n	2.0000	32.7401	65.4802	65.4802
6	1	C8	100n	2.0000	32.7707	65.5415	65.5415
7	1	C14	100n	2.0000	32.8045	65.6091	65.6091
8	1	C17	100n	2.0000	33.1539	66.3078	66.3078
9	1	C19	100n	2.0000	33.1539	66.3078	66.3078
10	1	C52	100n	2.0000	33.1539	66.3078	66.3078
11	1	C53	100n	2.0000	32.7380	65.4761	65.4761
12	1	C56	100n	2.0000	32.7979	65.5959	65.5959
13	1	C63	100n	2.0000	32.7401	65.4802	65.4802
14	1	C4	10n	2.0000	26.9485	53.8970	53.8970
15	1	C12	10n	2.0000	26.6592	53.3183	53.3183
16	1	C62	10n	2.0000	26.6527	53.3054	53.3054
17	1	C5	1u	2.0000	40.2765	80.5531	80.5531
18	1	C9	1u	2.0000	40.2765	80.5531	80.5531
19	1	C61	1u	2.0000	40.2794	80.5589	80.5589
20	1	C10	47p	2.0000	16.4264	32.8528	32.8528
21	1	C13	4p7	2.0000	13.3558	26.7116	26.7116
22	1	C24	100n	2.0000	110.3392	220.6784	220.6784
23	1	C25	100n	2.0000	33.3588	66.7176	66.7176
24	1	C29	100n	2.0000	33.3588	66.7176	66.7176
25	1	C36	100n	2.0000	32.7569	65.5139	65.5139
26	1	C39	100n	2.0000	32.7407	65.4813	65.4813
27	1	C26	22p	2.0000	49.0470	98.0941	98.0941
28	1	C27	100p	2.0000	72.9004	145.8007	145.8007
29	1	C28	10n	2.0000	122.5421	245.0842	245.0842
30	1	C30	1n2	2.0000	21.6423	43.2846	43.2846
31	1	C31	1n	2.0000	21.6423	43.2846	43.2846
32	1	C32	10n	2.0000	26.7336	53.4673	53.4673
33	1	C38	10n	2.0000	26.6114	53.2229	53.2229
34	1	C44	10n	2.0000	27.1151	54.2301	54.2301
35	1	C68	10n	2.0000	26.7336	53.4673	53.4673
36	1	C72	10n	2.0000	26.6258	53.2517	53.2517
37	1	C74	10n	2.0000	26.7003	53.4005	53.4005
38	1	C78	10n	2.0000	26.6183	53.2367	53.2367
39	1	C80	10n	2.0000	26.7336	53.4673	53.4673
40	1	C81	10n	2.0000	26.6106	53.2211	53.2211
41	1	C46	12p	2.0000	14.5332	29.0664	29.0664
42	1	C47	12p	2.0000	14.5332	29.0664	29.0664
43	1	C70	12p	2.0000	14.5332	29.0664	29.0664
44	1	C76	12p	2.0000	14.5332	29.0664	29.0664
45	1	C77	12p	2.0000	14.5332	29.0664	29.0664
46	1	C51	22p	2.0000	15.3417	30.6834	30.6834
47	1	C54	47p	2.0000	16.4328	32.8656	32.8656
48	1	C55	10n	2.0000	31.4100	62.8199	62.8199
49	1	C64	10u	2.0000	52.1640	104.3280	104.3280
50	1	C65	10u	2.0000	52.1640	104.3280	104.3280
51	1	C66	10u	2.0000	52.1640	104.3280	104.3280
52	1	C67	10u	2.0000	52.1640	104.3280	104.3280
53	1	C69	1u	2.0000	40.4630	80.9260	80.9260
54	1	C71	1u	2.0000	40.2998	80.5997	80.5997
55	1	C73	1u	2.0000	40.4125	80.8249	80.8249
56	1	C75	1u	2.0000	40.4125	80.8249	80.8249
57	1	C79	1u	2.0000	40.4125	80.8249	80.8249
58	1	D1	CMAD6001	3.8000	2.5920	9.8496	9.8496
59	1	D3	CMAD6001	3.8000	2.5920	9.8496	9.8496
60	1	D4	CMAD6001	3.8000	2.5920	9.8496	9.8496
61	1	D5	CMAD6001	3.8000	2.5920	9.8496	9.8496
62	1	D6	CMAD6001	3.8000	2.5920	9.8496	9.8496
63	1	D2	BZX84C12	2.0000	48.0000	96.0000	96.0000

Table 3.2.1a. Calorimeter Front End Board parts List with Calculated FITS Values, Harsh Environment (Partial, 1 of 3)

MIL-HDBK-217F Electronic Board Reliability Analysis G. Drake, Mar. 12, 2020, V2.00				Board Reliability Calculation Results			
Project:	Mu2e Calorimeter Front End Board			Harsh:	ON	λ_{NET}:	9182.7787
Version:	V2			Ambient T:	12	MTTF:	1.0890E+05
Designer:	G. Corradi						
Date:	March 12, 2020		Part Information from Bill of Material				
# Boards:	2696						

Item	Qnty/Bd	Reference	Part	Nominal FITS	Reliability Weighting	Weighted FITS (Calc)	Total per Board
64	4	J1	SIPM_MU2e	7.0000	12.4772	87.3402	349.3609
65	1	J2	HSE	46.0000	12.4772	573.9501	573.9501
66	1	J3	J_GAIN	46.0000	12.4772	573.9501	573.9501
67	1	M1	AO3162	12.0000	77.2483	926.9790	926.9790
68	1	M2	BSS126	12.0000	75.4700	905.6398	905.6398
69	1	M3	AO3162	12.0000	77.2483	926.9790	926.9790
70	1	Q1	MMBT5771	0.7400	2.1803	1.6134	1.6134
71	1	Q2	MMBT5771	0.7400	2.4365	1.8030	1.8030
72	1	Q6	MMBT5771	0.7400	2.4365	1.8030	1.8030
73	1	Q3	MMBT3904	0.7400	10.3651	7.6701	7.6701
74	1	Q4	MMBT3904	0.7400	2.4521	1.8145	1.8145
75	1	R1	100R	3.7000	1.5805	5.8477	5.8477
76	1	R59	100R	3.7000	1.5805	5.8477	5.8477
77	1	R2	1k	3.7000	0.6428	2.3785	2.3785
78	1	R10	1k	3.7000	0.6428	2.3785	2.3785
79	1	R11	1k	3.7000	0.6428	2.3785	2.3785
80	1	R13	1k	3.7000	0.6428	2.3785	2.3785
81	1	R16	1k	3.7000	0.6428	2.3785	2.3785
82	1	R19	1k	3.7000	0.6428	2.3785	2.3785
83	1	R21	1k	3.7000	0.6428	2.3785	2.3785
84	1	R61	1k	3.7000	0.1067	0.3947	0.3947
85	1	R3	460R	3.7000	9.8645	36.4986	36.4986
86	1	R4	4k7	3.7000	5.4798	20.2752	20.2752
87	1	R5	22k	3.7000	3.7691	13.9455	13.9455
88	1	R24	22k	3.7000	3.1123	11.5154	11.5154
89	1	R81	22k	3.7000	3.1123	11.5154	11.5154
90	1	R6	50R	3.7000	0.0573	0.2119	0.2119
91	1	R14	50R	3.7000	2.0746	7.6762	7.6762
92	1	R83	50R	3.7000	2.0746	7.6762	7.6762
93	1	R84	50R	3.7000	2.0746	7.6762	7.6762
94	1	R7	2k	3.7000	7.8873	29.1829	29.1829
95	1	R82	2k	3.7000	7.8873	29.1829	29.1829
96	1	R8	220R	3.7000	0.9752	3.6084	3.6084
97	1	R9	220R	3.7000	0.9752	3.6084	3.6084
98	1	R15	220R	3.7000	5.5698	20.6081	20.6081
99	1	R12	68R	3.7000	1.8385	6.8024	6.8024
100	1	R17	10R	3.7000	3.9410	14.5817	14.5817
101	1	R18	1k6	3.7000	0.3116	1.1530	1.1530
102	1	R20	56k	3.7000	2.2310	8.2546	8.2546
103	1	R23	330R	3.7000	0.0573	0.2119	0.2119
104	1	R60	330R	3.7000	0.9909	3.6664	3.6664
105	1	R26	56R	3.7000	10.6776	39.5071	39.5071
106	1	R34	330R	3.7000	4.6921	17.3609	17.3609
107	1	R35	4K7	3.7000	0.3515	1.3005	1.3005
108	1	R36	1K	3.7000	0.0573	0.2119	0.2119
109	1	R37	3Meg	3.7000	11.0254	40.7941	40.7941
110	1	R38	15K	3.7000	3.2067	11.8647	11.8647
111	1	R39	38K3	3.7000	3.3273	12.3111	12.3111
112	1	R40	1K	3.7000	0.6428	2.3785	2.3785
113	1	R106	1K	3.7000	0.6428	2.3785	2.3785
114	1	R41	100R	3.7000	1.5805	5.8477	5.8477
115	1	R42	220R	3.7000	23.4583	86.7958	86.7958
116	1	R43	22K	3.7000	0.1925	0.7123	0.7123
117	1	R44	10K	3.7000	0.2618	0.9688	0.9688
118	1	R45	270K	3.7000	0.0724	0.2679	0.2679
119	1	R46	1K2	3.7000	0.5987	2.2152	2.2152
120	1	R47	10K	3.7000	0.2618	0.9688	0.9688
121	1	R51	2R2	3.7000	7.5674	27.9995	27.9995
122	1	R55	2R2	3.7000	7.3484	27.1892	27.1892

Table 3.2.1b. Calorimeter Front End Board parts List with Calculated FITS Values, Harsh Environment (Partial, 2 of 3)

MIL-HDBK-217F Electronic Board Reliability Analysis			**Board Reliability Calculation Results**	
G. Drake, Mar. 12, 2020, V2.00				
Project:	Mu2e Calorimeter Front End Board	Harsh: ON	λ_{NET}:	9182.7787
Version:	V2	Ambient T: 12	MTTF:	1.0890E+05
Designer:	G. Corradi			
Date:	March 12, 2020	**Part Information from Bill of Material**		
# Boards:	2696			

Item	Qnty/Bd	Reference	Part	Nominal FITS	Reliability Weighting	Weighted FITS (Calc)	Total per Board
123	1	R99	2R2	3.7000	7.3484	27.1892	27.1892
124	1	R54	5K23	3.7000	4.2390	15.6843	15.6843
125	1	R56	100R	3.7000	1.5794	5.8439	5.8439
126	1	R105	100R	3.7000	1.5794	5.8439	5.8439
127	1	R57	10R	3.7000	3.9156	14.4878	14.4878
128	1	R107	10R	3.7000	3.9156	14.4878	14.4878
129	1	R58	120R	3.7000	4.5262	16.7471	16.7471
130	1	R62	2k2	3.7000	0.3971	1.4693	1.4693
131	1	R63	2k2	3.7000	0.3971	1.4693	1.4693
132	1	R85	22R	3.7000	0.2313	0.8556	0.8556
133	1	R86	22R	3.7000	0.2313	0.8556	0.8556
134	1	R87	PT1000	3.7000	3.6617	13.5482	13.5482
135	1	R88	806R	3.7000	0.6993	2.5873	2.5873
136	1	R90	806R	3.7000	0.6993	2.5873	2.5873
137	1	R89	2K55	3.7000	0.4462	1.6508	1.6508
138	1	R91	3k9	3.7000	0.3780	1.3987	1.3987
139	1	R92	33R	3.7000	2.4440	9.0428	9.0428
140	1	R94	33R	3.7000	2.4440	9.0428	9.0428
141	1	R96	33R	3.7000	2.4440	9.0428	9.0428
142	1	R100	33R	3.7000	2.4440	9.0428	9.0428
143	1	R101	33R	3.7000	2.4440	9.0428	9.0428
144	1	R93	11K	3.7000	0.0573	0.2119	0.2119
145	1	R95	10K	3.7000	3.2595	12.0603	12.0603
146	1	R97	10K	3.7000	3.2595	12.0603	12.0603
147	1	R104	10K	3.7000	2.7281	10.0940	10.0940
148	1	R98	1K	3.7000	2.2653	8.3814	8.3814
149	1	R102	4K22	3.7000	6.5648	24.2899	24.2899
150	1	R103	4K22	3.7000	3.8635	14.2950	14.2950
151	1	U1	AD8014ARTZ	1.0000	0.0024	0.0024	0.0024
152	1	U3	AD8014ARTZ	1.0000	0.0032	0.0032	0.0032
153	1	U2	AD8099ARD	1.0000	0.0022	0.0022	0.0022
154	1	U7	OPA180	1.0000	0.0024	0.0024	0.0024
155	1	U8	LMP7707	1.0000	0.0024	0.0024	0.0024
156	1	U9	LMP7707	1.0000	0.0024	0.0024	0.0024
157	1	U10	LMP7707	1.0000	0.0021	0.0021	0.0021
158	1	U15	AD8038AKSZ	1.0000	0.0028	0.0028	0.0028
159	1	U16	TL1963_ADJ	1.0000	12.1685	12.1685	12.1685
160	1	U17	TL1963_ADJ	1.0000	0.0670	0.0670	0.0670
161	1	U18	DAC121S101	1.0000	0.0050	0.0050	0.0050
162	1	U19	ADC128S102	1.0000	0.0239	0.0239	0.0239
163	1	JUMP1		0.0000	0.0000	0.0000	0.0000
	Total failure Rate (per 1E9 hours):						9182.7787
		Calculated MTTF:					1.0890E+05
		# Failures in 1st Year:					168.03
	Probability of Failure in 1st Year:						6.23%
		# Failures in 5 Years:					741.75
	Probability of Failure in 5 Years:						27.51%

Table 3.2.1c. Calorimeter Front End Board parts List with Calculated FITS Values, Harsh Environment (Partial, 3 of 3)

3.3. Discussion

With the environment factors set to 1, the MTTF was found to be 1.92E6 hours. The resulting probability of failure was found to be 0.36% in the first year. The reliability requirements for the Calorimeter, as specified in [35], state that the overall failure rate should be "at the percent level" per year [24]. This includes all electronics in the readout chain, plus the silicon photo-multipliers that comprise the active detector. Based upon this analysis, the predicted failure rate is within the stated requirements, approximately 1/3 of the allocation per year, which falls within the specification, with margin.

One advantage that the Calorimeter Front End Board electronics has is the active cooling system that will be in place, providing an operating environment estimated to have a temperature of 12 C. The normal reference temperature for this analysis is 25 C. As described throughout the document, higher ambient temperatures accelerate the lifetime of electronics. It is also true that lowering the ambient temperature will decelerate aging. This can be seen in Table 3.3.1. The cooler environment for this system provides an improvement of about 27% in the hazard rate, MTTF, and probability of failure. This also translates to an improvement in failure rate, with approximately 25% fewer boards predicted to fail in the first year.

Reliability vs. Temp.	25C	12C
Hazard Rate (per 1E9 Hrs)	710	519
MTTF	1.41E6	1.92E6
Prob. Failure 1st Yr	0.50%	0.36%

Table 3.3.1. Comparison of Reliability Performance
at Cooler Operating Temperature vs. Room Temperature

The analysis can be used to identify the parts that have the poorest reliability. The parts having the highest predicted failure rates for the board are shown in Table 3.3.2. The table is expressed in FIT values (failures per 1E9 hours.) Topping the list are the connectors. These have a high base hazard rate, as prescribed from the handbook, although the acceleration factors are modest. The next highest category of failures comes from the FETs, which also have a relatively large base hazard rate, as prescribed by the handbook.. It is worth noting that in the early days of FET fabrication, the reliability was not as good as it is today, so these values may not be truly representative of modern-day FET performance. High voltage capacitors C24 and C28 round out the list. C28 is a bypass capacitor on the 230V coming into the board for biasing the SiPMs. Likewise, C24 is a bypass capacitor on the output side of the bias regulator, which nominally operates at 200V. Both capacitors are rated for 250V. The fact that these capacitors operate so close to the rating is the primary contribution to the high value of the weighted FIT.

Reference	Part	Base FITS	Acc. Factors	Weighted FITS
J2	Card edge connector	46.0000	1.5596	71.7438
J3	3-pin Jumper	46.0000	1.5596	71.7438
M1	AO3162 FET	12.0000	3.8624	46.3490
M2	BSS126 FET	12.0000	3.7735	45.2820
M3	AO3162 FET	12.0000	3.8624	46.3490
J1	SiPM connector	7.0000	1.5596	10.9175
C28	10 nF capacitor	2.0000	4.9017	9.8034
C24	100 nF capacitor	2.0000	4.4136	8.8271

Table 3.3.2. Parts on the Board having the Highest Predicted Failure Rates

As described in Section 3.2, the MTTF decreases by a factor of 17.6 when the environment factors for harsh condition A_{UC} are incorporated in the calculations. This is significant, and if taken literally, would imply that the reliability of the board would miss the performance goal.

The consideration of the effect on the MTTF under harsh environmental conditions was introduced earlier. The handbook defines "A_{UC}, Airborne Uninhabited Cargo." as, *"Environmentally uncontrolled areas which cannot be inhabited by an aircrew during flight. Environmental extremes of pressure, temperature and shock may be severe. Examples include uninhabited areas of long mission aircraft."* There are some similarities with this definition to the Mu2e experiment. Certainly, the front-end electronics will be inaccessible during the running of the experiment, where access is expected approximately once per year for maintenance. The experiment will have wide variation in air pressure/vacuum. Temperature swings will be present, although likely not to the level experienced in uninhabited aircraft. There should not be much mechanical vibration or shock in the Mu2e detector, although the detector train will move, albeit with much smaller forces and velocity. However, a significant environmental factor for the Mu2e front-end electronics is radiation damage, which is not mentioned in the definition of A_{UC}, even though there is a radiation effect in aircraft. The thinning of the atmosphere results in a higher flux of cosmic rays, resulting in a higher radiation dose, albeit small, compared to ground-based operation. Even so, the most extreme dose and fluence levels in aircraft are orders of magnitude smaller than in Mu2e. So, there are similarities between the two environments, but differences as well. Again, given the uncertainties in the definition of associated environmental acceleration factors for the different types of electronic components, consideration of the A_{UC} environment provides a sense of how the MTTF is affected by harsh environmental conditions. That said, the results from the inclusion of the environmental acceleration factors should be regarded as illustrative only, with uncertain expectation that it will match realistic operating conditions concerning reliability. The exercise does serve though to underscore the importance of understanding the radiation tolerance of the electronic components in a front-end design.

3.4. Interpretation of this Analysis

As stated above, military handbook MIL-HDBK-217F was developed to be a reference, providing a methodology for calculating the reliability of electronic boards. It is inherently an estimation tool. To make this intent clear, the first sentence of the handbook states, *"This handbook is for guidance only and shall not be cited as a requirement."* It continues, *"The handbook is intended to be used as a tool to increase the reliability of the equipment being designed."* It is in this spirit that the analysis and results presented in this document are to be interpreted.

The handbook is not without caveats, limitations, and other issues, some of which are identified below.

- The handbook tends to generalize reliability aspects across broad ranges of manufacturers, manufacturing processes for a given type of component, and differences that can occur in manufacturing lots or batches. The methodology in the handbook was developed from the collective experience of the developers, which included reliability measurements on certain components, as well as general operating experience over some range of projects and applications. Much of the background is referenced in mil-spec documents. As such, the analysis incorporates general trends, but does not represent the reliability of the actual parts used.

- The handbook is quite dated. The first edition was released in 1961, around the advent of the marketing of transistors. The original basis for the handbook was experience with vacuum tube electronics. There have been several releases since that first version, attempting to include parts and developments in technology as they evolved. The latest version, MIL-HDBK-217F, was released in 1991. Since this time, there have obviously been additional major advances in integrated circuit technology nodes (fabrication feature sizes.) For example, in 1991, the CMOS 0.35 um technology node began production. Today the smallest technology node in production is 5 nm, a factor of 70 in feature size, or 1400 in area, which matches the predictions of Moore's Law [23-24]. New IC fabrication companies have come and gone in this time. The 1991 handbook makes virtually no reference to technology nodes. In another example, the majority of electronic components manufactured today are surface mount, in a variety of sizes, packages, and materials, but in the 1991 handbook, surface mount parts tend to be lumped into single categories, although some discrimination is provided for power ratings. Many important differences in surface mount components and packages that are known today to affect reliability have been neglected. While it appears that the Dept. of Defense will not be issuing any more updates to the handbook, the VITA Standards Organization (VSO) [25] has produced updates [26], which some reliability analyses have been incorporating. These updates from VITA have not been included in this analysis.

- The handbook methods are based upon elementary reliability concepts, which do not take into account newer developments in reliability analysis. Some of these can be found in [27-30]. In addition, a recent thrust has been in the study of "physics of failure" [31]. The analysis described herein is based entirely on the methodology set forth in the handbook, and does not include any of these modern aspects to reliability theory. An overview of the foundation for this analysis is provided in the Appendix.

As a result, the methodology in this handbook might appropriately be regarded as a tool for evaluating design and parts choices in a relative way rather than predicting the reliability performance form an absolute perspective. Despite these limitations, the handbook is widely used in the design and vetting of electronic systems used in military and aerospace applications, where a premium is placed upon high-reliability design and operation due in part to personnel safety, but also in consideration of the situation where accessibility is limited, making it difficult or impossible to service the electronics when it fails. In high-risk applications such as aerospace, the component testing regimen often incorporates aspects of the handbook as specifications for qualifying parts for use. For electronics systems where reliability is an important aspect of performance, the need for an evaluation framework like this is evident. Indeed, the handbook has also found extensive use in commercial electrical systems where reliability is an important part of the performance goals. Reliability is certainly important for on-detector electronics in HEP experiments that have limited access and "harsh" environmental conditions. The analysis described herein can thus be viewed in the context of standard reliability calculation techniques used in the broad electronics community, but with the caveats and limitations described above.

4. Appendix I – Overview of Reliability Analysis Methodology

The following overview comes from [32]:

In general, there are three categories of failures in electronic systems, and correspond to three periods of lifetime:

1. Early failure, also known as the Infant Mortality period. This type of failure happens early in the lifetime of a component, and is usually caused by manufacturing defects.
2. Useful lifetime, also known as the period of constant failure rate. In this period, failures are random, but occur with an overall constant rate.
3. End of life, also known as the Wear-Out period.

Taken together, these periods comprise the "bathtub curve," as shown in Fig. 4.1.1 [36]. Generally speaking, this note is concerned with calculating the (constant) failure rate for the useful lifetime period.

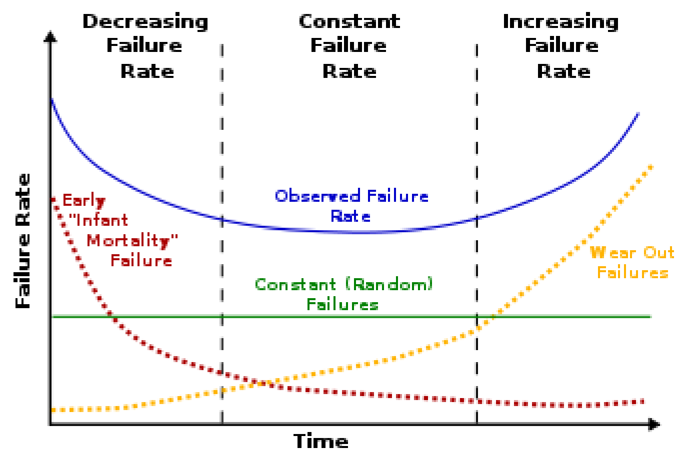

Fig. 4.1.1. Bathtub Curve, showing the three types of failures and their associated periods. (Courtesy of Wikipedia [26].)

In general, failures of electronic components and systems during their useful lifetime tend to have an exponential form [22-23]. A plot of the cumulative number of failures as a function of time, represented as a fraction of the total number of a given component type, typically looks like that in Fig. 4.1.2, and has the form:

$$F(t) = 1 - e^{-\lambda t}, \quad 0 \leq t \leq \infty \tag{4.1}$$

where λ is a constant.

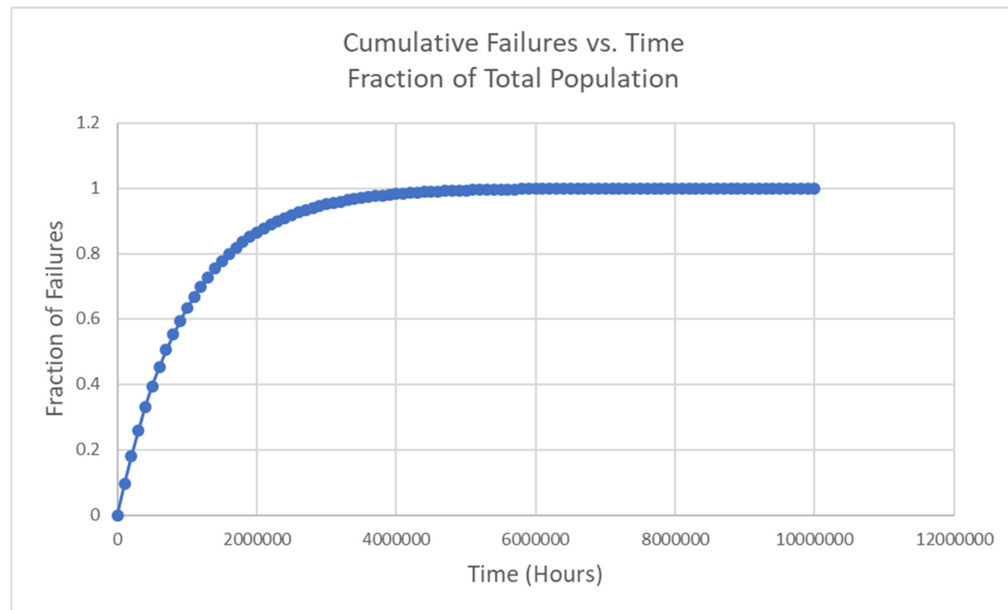

Fig. 4.1.2. Typical distribution of the cumulative failures of a given type of electronic component as a function of time, expressed as a fraction of the total population.

The quantity F(t) is called the Cumulative Distribution Function (CDF). The CDF can be interpreted as:

1. F(t) is the probability that a random component of a specific type and value in a system fails by time t; or
2. F(t) is the fraction of all like components in a system fail by time t.

Note that while the point at which F(t) = 1 effectively represents the failure of all components of a particular type in the entire system, this is distinctly different from the "wear out" failure rate shown in the bathtub curve of Fig. 4.1.1. Wear out comes from fatigue from use, whereas the failures in the useful lifetime is considered to be random events related to imperfection in the manufacturing process. Typically, parts wear out much sooner than the random failures would deplete the population.

It is useful to consider the probability of a failure occurring as a function of time. The *Probability Density Functions* (PDF) is defined as:

$$f(t) = \frac{d}{dt} F(t) = \lambda * e^{-\lambda t}, \quad 0 \leq t \leq \infty \tag{4.2}$$

where λ is a constant, which will be discussed shortly. A plot f(t) is shown in Fig. 4.1.3, for the case where λ = 1E6. The quantity f(t) dt represents the fraction of failure times in interval dt.

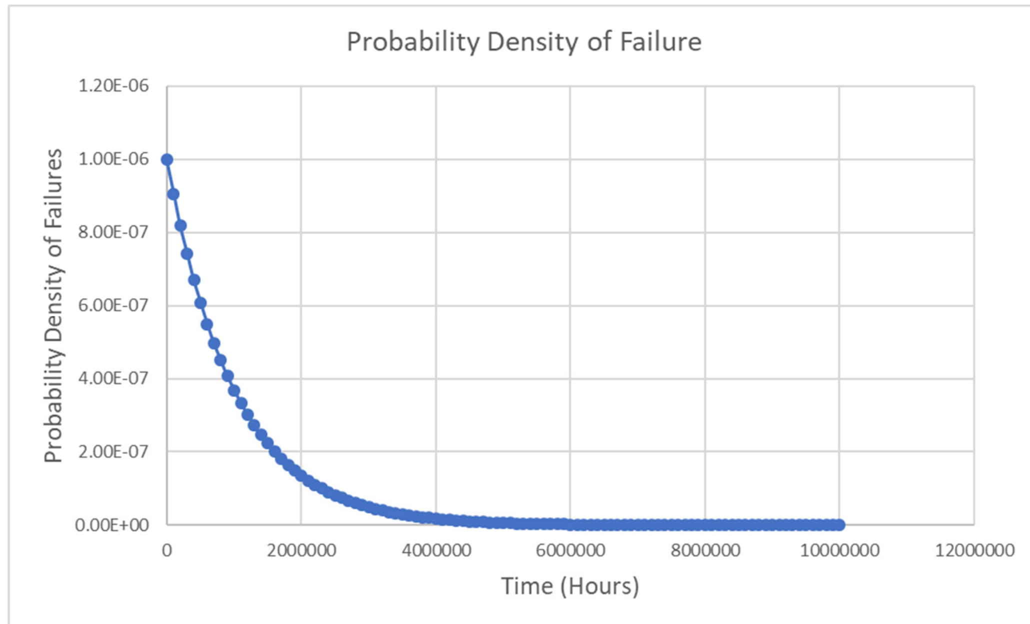

Fig. 4.1.3. Plot of a PDF having an exponential distribution

The Reliability function (also called the Survival function), is defined as:

$$R(t) = 1 - F(t) \tag{4.3}$$

The Reliability function can be interpreted as:

1. R(t) is the probability that a random component of a specific type and value in a system will still be operating after t hours; or
2. R(t) is the fraction of all like components in a system that will still be operating after t hours.

At a given time τ, some number of failures will have occurred in the system. The probability of failure in the next $\Delta\tau$ of time is expressed as a conditional probability, the probability of failure in the next $\Delta\tau$ of time given that number of components that have survived to time τ:

$$P(Fail\ in\ next\ \Delta\tau \mid survive\ to\ time\ \tau) = \frac{F(\tau+\Delta\tau)-F(\tau)}{R(\tau)} \tag{4.4}$$

Of interest in reliability analysis is the rate of failure, also known as the hazard rate or instantaneous failure rate. This is denoted as h(t), and is defined as:

$$h(t) = \lim_{\tau\to 0} \frac{1}{\Delta\tau} \frac{F(\tau+\Delta\tau)-F(\tau)}{R(\tau)} = \frac{f(t)}{R(t)} \tag{4.4}$$

For the case where f(t) is an exponential as represented in (4.2), the hazard rate reduces to:

$$h(t) = \lambda \tag{4.5}$$

The units of λ are in "number of failures per unit time," which is a failure rate. Electronic component manufacturers often express failure rates in terms of the number of failures in 1E9 hours, which is called "failures in time" or FITs.

In the general case, h(t) can vary as a function of time. Of interest is the *Average Failure Rate*, or AFR. Over a time period $t_2 - t_1$, this is defined as:

$$AFR(t_2 - t_1) = \frac{\int_{t_1}^{t_2} h(t)dt}{t_2 - t_1} \tag{4.6}$$

Again, for the case where f(t) has an exponential form as shown in (4.2), the AFR is:

$$AFR(t_2 - t_1) = \lambda \tag{4.7}$$

Thus, assuming an exponential form of the Cumulative Distribution Function for the failures of electronic components, the FITs value will be an indicator of the average failure rate of the components in the system.

Of interest in reliability analysis is the *Mean Time to Failure*, of MTTF. This is related to the hazard function as:

$$MTTF = \frac{1}{\lambda} \tag{4.8}$$

Note that MTTF is for the case where components fail in a system and are not replaced (immediately). This would be the situation for a detector in which access to perform repairs is infrequent. This should not be confused with the term *Mean Time Between Failures*, or MTBF, in which components are replaced as they fail. These terms are often used interchangeably, although their meaning is different.

The goal of this analysis is to calculate the value of the hazard function for an entire printed circuit board. A printed circuit board typically has many components on it,

each having their own hazard function. The probabilities of failure (or survival) of the different components must be combined in order to get the overall probability of failure (or survival) for the entire board. For two events, A and B, the probability of them occurring simultaneously (intersection of event spaces) is given by conditional probability:

$$P(A \mid B) = \frac{P(A \cap B)}{P(B)} \tag{4.9}$$

Rearranging:

$$P(A \cap B) = P(B) * P(A \mid B) \tag{4.10}$$

If the events are independent, then:

$$P(A \mid B) = P(A) \tag{4.11}$$

Then:

$$P(A \cap B) = P(B) * P(A) \tag{4.12}$$

For a simple printed circuit board that has two different components on it, A and B, having probabilities of survival P(A) and P(B) respectively, the probability of them both surviving as a function of time t is obtained by multiplying the two probabilities together to get the overall probability. This assumes that their failures are independent of each other, that the failure of one does not cause the failure of the other. For simple reliability calculations, this is what is generally assumed. If component A have a hazard rate of λ_A, and component B have a hazard rate λ_B, then the combined probability for *survival* as a function of time t is given by:

$$R_{NET}(t) = e^{-\lambda_A t} * e^{-\lambda_B t} = e^{-[(\lambda_A + \lambda_B) * t]} \tag{4.12}$$

Extrapolating to a printed circuit board containing M components, each with hazard rates λ_1, λ_2, …λ_M respectively, the hazard rates are added together to give an overall hazard rate for the board λ_{BD}:

$$\lambda_{BD} = \sum_{i=1}^{M} \lambda_i \tag{4.13}$$

Once the overall hazard rate for a board is known, the probability of having a board failure as a function of time is given by Cumulative Distribution Function:

$$Probabality\ of\ Failure = F(t) = (1 - e^{-(\lambda_{BD} * t)}) \tag{4.14}$$

For a system having N identical boards, the CDF can be used to calculate the number of expected failures of boards in the system:

$$\# \, Failures \; at \; time \; t_1 = N * F(t_1) = N * (1 - e^{-(\lambda_{BD} * t_1)}) \tag{4.15}$$

For any given component on a board, there may be several factors that contribute to the hazard rate. Examples include temperature, mechanical or electrical stress, overall quality of the part, the environment, etc. One could model this as individual hazards or failure mechanisms. Assuming that the failure mechanisms are independent, the overall survival probability would be given by the product of the individual probabilities for each failure mechanism, i.e., the net probability that all independent failure mechanisms will not occur at time t. Rather than doing this, the approach used in MIL-HDBK-217F is to define a base hazard rate, λ_b, and then define multiplicative factors that are functions of the particular failure mechanism. The resulting hazard rate, λ_p, has the form,

$$\lambda_p = \lambda_b * \pi_1 * \pi_2 * \ldots * \pi_K \text{ , for K failure mechanisms} \tag{4.16}$$

Handbook MIL-HDBK-217F describes the different failure mechanisms, and provides guidance on how to calculate the π_i factors for each type of component.

5. References

[1] "Reliability Prediction of Electronic Equipment," *MIL-HDBK-217F*, Washington, DC 20301: Department of Defense, December 1991.

[2] R. Ray, et al., "Mu2e Technical Design Report," Mu2e Internal Report, DocDB 4299, Mar. 11, 2015.

[3] N. Atanov, et al., "The Calorimeter Final Technical Design Report," Mu2e Internal Report, DocDB 8429, Dec. 28, 2016.

[4] L. Lucchesi, "Test of the Calorimeter Front End Unit," Mu2e Internal Report, DocDB 14556, Nov. 28, 2017.

[5] G. Corradi, et al., "Technical description of the Calorimeter FEE Boards," Mu2e Internal Note, DocDB 29910, Nov. 18, 2019.

[6] G. Corradi, et al., "Technical Specification of Calorimeter FEE Boards and Cables," Mu2e Internal Note, DocDB29817, Nov. 18, 2019.

[7] G. Corradi, et al., "Summary of FEE Rad Test," Mu2e Internal Note, DocDB 24486, Nov. 15, 2019.

[8] G. Corradi, et al., "Temperature Trend in Calorimeter FEE Boards," Mu2e Internal Note, DocDB 29814, Nov. 11, 2019.

[9] G. Corradi, et al., "Design of the Calorimeter FEE and Mezzanine Boards," Mu2e Internal Note, DocDB 27589, Jul. 17, 2019.

[10] G. Corradi, et al., "Neutron and TID Test of Calorimeter FEE," Mu2e Internal Note, DocDB 22903, Dec. 11, 2018.

[11] G. Corradi, et al., "Mu2e Calorimeter Development Electronics FEE Review," Mu2e Internal Note, DocDB 14634, Dec. 4, 2017.

[12] G. Corradi, et al., "CD2 EMC Front End Electronics," Mu2e Internal Note, DocDB 4686, Oct. 11, 2014.

[13] F. Abe et. al., "The CDF Detector: An Overview," *Nucl. Instrum. Meth.*, vol. A271, 1988, pp. 387-403.

[14] Bin Lu, Luke W. Mo, Thomas A. Nunamaker, "The Cockcroft-Walton photomultiplier tube base and the Ethernet high voltage controller," *Nuc. Inst. Meth. A,* Vol. 313, Issues 1–2, 1992, pp. 135-141, ISSN 0168-9002, https://doi.org/10.1016/0168-9002(92)90089-M.

[15] A. Byon-Wagner, K. Byrum, J.W. Dawson, G. Drake, C. Drennan, G.W. Foster, W.N. Haberichter, J. Hoff, S. Kuhlmann, M.A. Lindgren, L.J. Nodulman, J. Proudfoot, J.L. Schlereth, and J.Y. Wu, "The Shower Maximum Front-End Electronics for the CDF Upgrade," *IEEE Trans .Nucl. Sci.*, vol. 49, 2002, pp. 2567-2573.

[16] S. Fourletov, "Straw tube tracking detector (STT) for ZEUS," *Nuc. Inst. Meth. A,* Vol. 535, Issues 1–2, 2004, pp. 191-196, ISSN 0168-9002, https://doi.org/10.1016/j.nima.2004.07.212.

[17] T. Cundiff, J. W. Dawson, L. Dalmonte, G. Drake, T. Fitzpatrick, W. Haberichter, D. Huffman, W. Luebke, C. Nelson, D. Reyna, J. L. Schlereth, P. Shanahan, J. L. Thron, and M. Watson, "The MINOS Near Detector Front End Electronics," *IEEE Trans. Nucl. Sci.*, vol. 53, 2006, pp. 1347-1355.

[18] H. P. Beck, M. Abolins, et al., "Performance of the Final Event Builder for the ATLAS Experiment," *IEEE Trans. Nucl. Sci.*, vol. 55, 2006, pp. 177-181. Presented at the 15th IEEE 2007 NPSS Real Time Conference, Batavia, IL, Apr. 29-May 4, 2007.

[19] F. Tang, et al., "Design of the Front-End Readout Electronics for the ATLAS Tile Calorimeter at the LHC," *IEEE Trans. Nucl. Sci.*, vol. 60, 2013, pp 1255-1259.

[20] G. Drake, et al., "Design of a New Switching Power Supply for the ATLAS TileCal Front-End Electronics," *J. of Inst.*, vol. 8, 2013, article C02032.

[21] D. L. Adams, et al., "Photon Detector System Timing Performance in the DUNE 35-Ton Prototype Liquid Argon Time Projection Chamber," *J. of Inst.*, vol. 13, 2018, article P06022.

[22] G. Drake, "Radiation Tolerance requirements for the Mu2e Front End Electronics," Mu2e Internal Note, DocDB 11288, June, 21, 2017.

[23] "Technology Node – Wiki Chip," https://en.wikichip.org/wiki/technology_node

[24] "Moore's Law," https://en.wikipedia.org/wiki/Moore%27s_law

[25] VITA Standards Organization, https://www.vita.com/.

[26] "VITA 51.1 - Reliability Prediction MIL-HDBK-217 Subsidiary Specification," 13th Edition, 2008, with Reaffirmation Notice , 2018.

[27] A. Mosleh, Y.H. Chang, "Model-Based Human Reliability Analysis: Prospects and Requirements," *Reliability Engineering & System Safety*, vol. 83, num. 2, 2004, pp. 241-253, ISSN 0951-8320, https://doi.org/10.1016/j.ress.2003.09.014.

[28] H.-Z. Huang, "Reliability Analysis Method in the Presence of Fuzziness Attached to Operating Time, *Microelectronics Reliability*, Volume 35, Issue 12, 1995, pp. 1483-1487, ISSN 0026-2714, https://doi.org/10.1016/0026-2714(94)00173-L.

[29] G. Levitin, “Computational Intelligence in Reliability Engineering: Evolutionary Techniques in Reliability Analysis and Optimization,” Volume 39 of Studies in Computational Intelligence,” Springer Science & Business Media, 2006, ISBN 3540373675, 9783540373674, 398 p.

[30] Jiang, C., Lu, G.Y., Han, X. et al., “A New Reliability Analysis Method for Uncertain Structures with Random and Interval Variables,” *Int J Mech Mater Des*, vol. 8, 2012, pp. 169–182, https://doi.org/10.1007/s10999-012-9184-8

[31] M. Pecht and A. Dasgupta, "Physics-of-Failure: An Approach to Reliable Product Development," *IEEE 1995 International Integrated Reliability Workshop*, Final Report, Lake Tahoe, CA, USA, 1995, pp. 1-4.

[32] P. Tobias, D. Trindade, “Applied Reliability,” Van Nostrad, 1986, ISBN 0-442-28310-5.

[33] MENDENHALL, W. & HADER, R. J. (1958), "Estimation of parameters of mixed exponentially distributed failure time distributions from censored life test data", Biometrika, 45, 1958.

[34] Ansell, J., & Phillips, M. (1989), “Practical Problems in the Statistical Analysis of Reliability Data,” Journal of the Royal Statistical Society. Series C (Applied Statistics), 38(2), 205-247. doi:10.2307/2348057

[35] S. Giovannella, S. Miscetti, “ Mu2e Calorimeter Operational Requirements,” Mu2e Internal Note, DocDB 22786, V7, Feb. 11, 2020.

[36] D. Smith, “Reliability, Maintainability and Risk - Practical Methods for Engineers,” Elsevier, 9th Ed., 2017, ISBN 978-0-08-102010-4.

Nuclear Inst. and Methods in Physics Research, A 988 (2021) 164874

Contents lists available at ScienceDirect

Nuclear Inst. and Methods in Physics Research, A

journal homepage: www.elsevier.com/locate/nima

Assessment of operational availability for the PIP-II Superconducting Radio Frequency linear accelerator facility

Arun Saini [a,*], Ram Prakash [a,b,c], Joseph D. Kellenberger [a]

[a] Fermi National Accelerator Laboratory, Batavia IL 60510, USA
[b] Raja Ramanna Centre for Advanced Technology, Indore 452013, India
[c] Homi Bhabha National Institute, Anushaktinagar, Mumbai 400094, India

ARTICLE INFO

Keywords:
SRF accelerator facility
Operational availability
Down-time

ABSTRACT

Operational availability is a critical performance measure for an accelerator facility in modern time. A high availability enables the facility to serve a wide range of users simultaneously. Consequently, besides pure accelerator physics considerations, newly proposed accelerator facilities account for the availability and reliability aspects in the design phases. It allows incorporation of appropriate mitigation strategies for the most vulnerable systems in the machine and therefore, minimizes unscheduled interruptions during the operation. This paper lays out a methodology for the availability assessment of the complete particle accelerator facility and presents an initial assessment of the availability of the newly proposed Proton Improvement Plan-II (PIP-II) accelerator facility at Fermilab. The paper describes a comprehensive reliability model of the PIP-II facility that comprises not only 800 MeV linear accelerator (linac) system but also essential utility systems in the form of cryogenic, water, power and air systems. The paper details estimations of the availability of the PIP-II facility for two operational modes i.e. the nominal operational mode featuring 800 MeV beam and critical operational mode involving operation with the lowest objective beam energy of 600 MeV.

1. Introduction

Availability analyses have been a standard protocol in industries where the operational costs are taken into account at design level of a new product. However, practice of the reliability engineering in research infrastructures, that are usually driven by a fixed construction cost, is relatively new. The late introduction of the reliability engineering in the particle accelerator design is mainly due to a very complex nature of the machine. Every particle accelerator is unique in the design and operation. Thus, input data required for such analyses are usually limited and specific to a given system. This adds uncertainty against realization of the reliability engineering aspect in the accelerator design. However, this trend has been changing lately and the modern accelerator facilities are anticipating importance of the reliability engineering in the accelerator design.

Most of newly proposed accelerator facilities around the world such as Linac Coherent Light Source-II (LCLS-II) [1], European Spallation Source (ESS) [2], Indian Spallation Neutron Source (ISNS) [3], China Accelerator Driven System (CADS) [4], etc. are based on the Superconducting Radio Frequency (SRF) technology. Recent advancements in the SRF technology make its usage more practical and cost effective for large accelerator facilities as well as for the commercial applications. The SRF technology brings in multiple advantages to an accelerator facility. It enables not only a high duty beam operation but also facilitates a high accelerating gradient in the cavities. With all numerous benefits, the SRF technology also brings in an adverse feature in terms of the additional complex systems (cryostat, cryo-plant, cryogen distribution etc.) needed for its implementation to an accelerator facility. Furthermore, repair or replacement of a malfunctioned superconducting component is both expensive and time consuming. Restoring a nominal accelerator operation after an interruption also takes time. This in turn, reduces overall availability of an accelerator. Consequently, modern SRF accelerator facilities are sighting importance of the availability and reliability analyses [5–8] to reduce operational cost of the unreliable accelerators. To assure a reliable operation with the minimal unscheduled interruptions, the reliability engineering aspects need to be considered from the design phases of the SRF accelerators. Performing the availability analysis at various stages of the design enables identification of critical components with a higher probability of failure as well as prediction of the unscheduled down time during operations. This in turn, may allow developing a mitigation strategy for critical components, appropriate allocation of redundancy and, resources for spare and replacement parts.

In the past, the availability analysis for the particle accelerators was often carried out either for certain sub-systems of the machine

* Corresponding author.
E-mail addresses: asaini@fnal.gov (A. Saini), rprakash@rrcat.gov.in (R. Prakash).

https://doi.org/10.1016/j.nima.2020.164874
Received 14 April 2020; Received in revised form 16 November 2020; Accepted 16 November 2020
Available online 19 November 2020
0168-9002/© 2020 Elsevier B.V. All rights reserved.

Table 1
Design specifications for operational beam parameters of the PIP-II linac.

Parameter	Magnitude	Units
Final beam energy	800	MeV
Beam pulse repetition rate	20	Hz
Beam pulse length	0.55	ms
Average CW beam current	2	mA
Final ε_z	<0.4	mm-mrad
Final ε_t	≤0.3	mm-mrad

ε_z normalized RMS longitudinal emittance; ε_t normalized RMS transverse emittance.

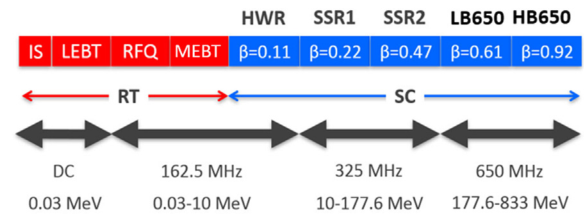

Fig. 1. Block diagram representation of the PIP-II Linac. Red coloured blocks represent the warm sections (RT) whereas the blue blocks represent superconducting sections (SC) operating at 2 K. Normalized design velocity (β) of the cavity in each section is also shown. (For interpretation of the references to colour in this figure legend, the reader is referred to the web version of this article.)

Table 2
Optics elements and transition energy in each section of the PIP-II SRF linac.

Section	CM	Cav/Mag per CM	Operating Frequency	Energy (MeV)
HWR	1	8/8	162.5 MHz	2.1–10
SSR1	2	8/4	325 MHz	10–32
SSR2	7	5/3	325 MHz	32–177
LB	9	4/1[a]	650 MHz	177–516
HB	4	6/1[a]	650 MHz	516–833

[a]Normal conducting quadrupole doublet.

(e.g. cryo-plant, RF system etc.) or considering a simple form of the major beamline elements [9–13]. For this reason, the paper lays out a methodology for the availability assessment of the complete particle accelerator facility. It describes a comprehensive reliability model for the availability assessment of the Proton Improvement Plan-II (PIP-II) SRF accelerator facility [14] that includes not only the accelerator components but also essential utility systems in terms of the water, air, cryogenic and power systems. Furthermore, the model implements the accelerator components in their detail composition that implies an accelerator component is described with its essential auxiliary systems. For an instance, an accelerator cavity in the model is implemented with its power coupler, frequency tuner and RF power source. Thereafter, the paper discusses studies for the PIP-II facility that lead to finding of the most critical section determining the unavailability budget of the PIP-II facility. Lastly, the paper converses the input data sensitivity analysis assessing impact of a spread in the reliability input data on the model prediction and, validation of the model methodology using a reference model of the existing operational accelerator facility.

The paper is organized in seven sections. Section 2 provides an overview of the PIP-II SRF linear accelerator whereas Section 3 introduces key definitions and concepts of the availability analysis for an accelerator system. Section 4 discusses preparation of the PIP-II accelerator facility model and describes components selection criteria, operational modes and the high-level functional block diagram of the facility. Section 5 converses results of the availability analyses while Section 6 presents a sensitivity analysis and the model benchmarking with an operational accelerating facility. The paper concludes with a summary in Section 7.

2. PIP-II SRF linac accelerator facility

Fermilab is planning to perform a systematic upgrade to its existing accelerator complex to support a world leading neutrino program. A comprehensive roadmap named "Proton Improvement Plan (PIP)" has been established. The second stage of the Proton Improvement Plan comprises construction of a new superconducting linear accelerator (linac) capable of accelerating a 2 mA H^- ion beam up to 800 MeV in a continuous wave (CW) regime. However, the initial operational goal is to deliver a 1.1% duty factor pulsed beam to the existing Booster synchrotron [15]. The PIP-II accelerator facility aims at the operational availability of 90% over a fiscal year [16]. Table 1 summarizes the most relevant operational beam parameters of the PIP-II linac.

A schematic of the SRF linac's architecture is shown in Fig. 1. It is composed of a warm front-end and an SRF accelerating section. The warm front-end comprises an H^- ion source (IS) capable of delivering a 15 mA, 30 keV, DC or pulsed beam, a 2 m long Low Energy Beam Transport (LEBT) line [17], a 162.5 MHz, CW Radio Frequency Quadrupole (RFQ) [18] that accelerates the beam to 2.1 MeV and a 13 m long Medium Energy Beam Transport (MEBT) line [19] that includes variety of diagnostic devices and a chopper system capable of generating an arbitrary bunch pattern before the beam is injected into the SRF section.

The MEBT is followed by the SRF linac that uses five families of SRF cavities to accelerate the beam up to 800 MeV. Based on these families, the linac is segmented into five SRF sections named as, Half Wave Resonator (HWR) [20], Single Spoke Resonator (SSR) 1 & 2 [21,22], and Low Beta (LB650) and High Beta (HB650) [23]. Table 2 highlights configuration of each section and includes details of a number of cryomodules (CM), focusing magnets and cavities as well as operating frequency of cavities and their accelerating ranges. Note that, superconducting solenoid magnets are used in the HWR, SSR1 and SSR2 sections whereas normal conducting (NC) quadrupole magnets arranged in doublet configuration are utilized in the LB650 and HB650 sections for the transverse beam focusing.

The linac optics has been carefully designed to deliver a high-quality beam at the Booster entrance. Fig. 2 shows the accelerating voltage and output energy at each cavity along the linac for the baselined optics. Detailed description of the linac architecture and its optics design has been presented elsewhere [24].

3. Availability formalism for accelerators

There are many good text books [25,26] dedicated to the reliability engineering theory. For the comprehension of this article, this section introduces necessary theory and, discusses how it is applicable in the framework of accelerators.

The failure rate (λ) of a component through its life span usually follows a bath-tub distribution as shown in Fig. 3. Initial portion of the bath-tub curve is called the burn-in period that consists of a high failure rate due to the infant mortality. Similar behaviour is observed at the end of the curve due to deterioration of components. This period is defined as the wearing-out period. Between these two regions, a system has a useful life period which consists of a relatively lower and constant failure rate. Assuming, accelerators also follow the bath-curve analogy. The burn-in period is then referred to the commissioning period when the accelerators are being actively tuned and tested to deliver operational parameters. A wear-out period for the accelerators is the period when an upgrade or replacement is needed to maintain its operational performance. In this paper, the main emphasis is on the useful period of an accelerator which can be interpreted as its nominal operational period. In subsequent sections, the availability model is solved using the assumption of a constant failure rate of components. Note that, the assumption not only justifies the bath-tub analogy but also permits solving the model analytically which otherwise becomes too cumbersome to solve analytically for the large systems.

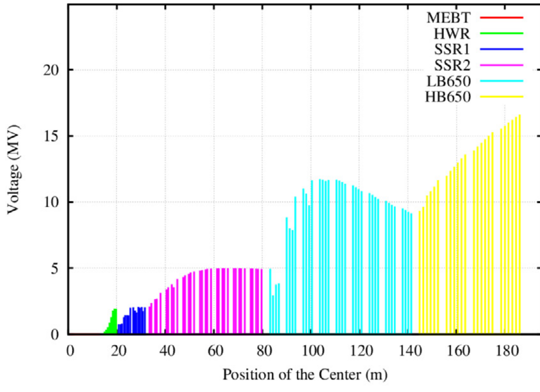

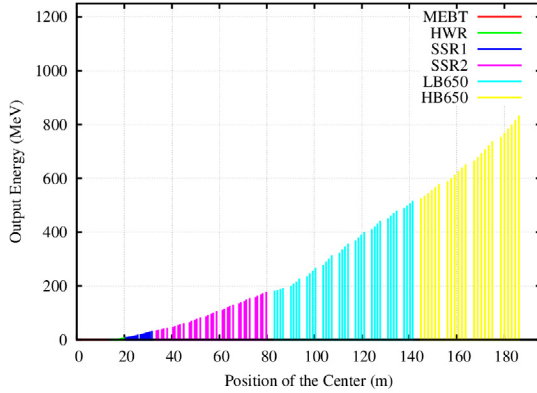

Fig. 2. (a) Accelerating voltage and (b) output energy along the PIP-II linac for the nominal optics. Note that, the bunching cavities in MEBT operates at -90^0 synchronous phase and therefore provides no acceleration. (For interpretation of the references to colour in this figure legend, the reader is referred to the web version of this article.)

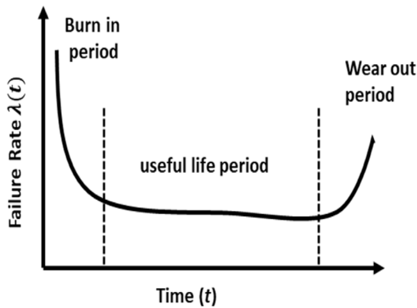

Fig. 3. Evolution of the characteristic failure rate function of a system over a length of time.

The cumulative experience with existing operating accelerator facilities suggests a gradual degradation in performance of the accelerator components over a period of time. For instance, surface contaminations of the SRF cavities may reduce the maximum available accelerating gradient. These gradual degradations in the operational performance over time are called parametric drift failures in the reliability engineering. Adding a safety margin in the operational parameters and using new advances in the accelerator technology, such as plasma processing of the SRF cavities [27], and allowing others to address the parametric failures in the accelerators at some extent. Thus, in this article, it is assumed that a component has only two states of operation either a nominal working state or a failed state.

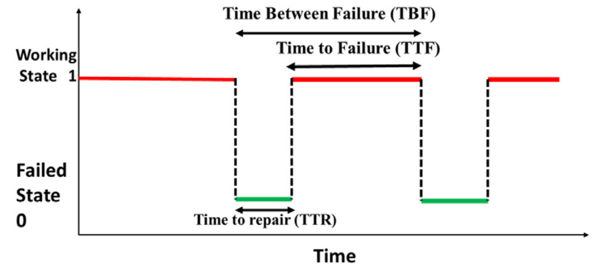

Fig. 4. Evolution of operating states of a binary system with time.

3.1. General formalism

Fig. 4 illustrates a system which has only two operating states i.e. working state and failed state. The length of time for which the system keeps a working state is called Time to Failure (TTF) whereas the time taken to repair the system after a failure is termed as Time to Repair (TTR). The time between successive failed states is quantified as Time Between Failure (TBF). These times are collectively called the characteristic times of a system. In a n-component system there are several ways a system might fail and be repaired. Thus, it is more appropriate to determine the characteristics times from mean of respective distributions.

The Mean Time Between Failure (MTBF) is then expressed as:

$$MTBF = MTTF + MTTR; \tag{1}$$

where Mean Time To Fail (MTTF) is the statistical average of operating time and Mean Time To Repair (MTTR) is the statistical average of the repair time for a system. In case of a constant failure rate (λ), MTTF for a non-repairable system can be written as:

$$MTTF = \frac{1}{\lambda}. \tag{2}$$

The reliability of an accelerator is defined as the probability that it does not fail in a given mission time whereas the availability (A) is proportion of its "up time" to the total operational time over a defined operation period. It can be quantified as:

$$A = \frac{MTTF}{MTTF + MTTR}. \tag{3}$$

One can conclude from their definitions that the mean time between the failure and the failure rate are measures of the reliability. To obtain a high reliability and availability, an accelerator must avoid repetitive failures and long down time after a failure occurrence. Thus, decreasing the mean time to repair is one of the main design considerations. Common strategies to minimize MTTR include frequent monitoring of accelerator-systems to identify probable issues before failure occurrence; proper distribution of diagnostic devices to minimize diagnostic time, appropriate allocation of spares to reduce logistics and minimizing the replacement time; establishing a dedicated team of experts to perform quick repairs, etc. It is clear that improvement in MTTR is achieved at the expense of an increase in overall cost of the facility. A balance must be obtained between objective MTTR and the resulting cost.

The foremost step in estimation of the availability of an accelerator is to obtain availabilities of individual components using their MTTF and MTTR input data. Then, the next step involves acquiring information of the component functional roles in the accelerator-system. This system-component functional relationship is often expressed in the form of a Reliability Block Diagram (RBD) where each component is represented in the form of a block. Fig. 5 shows the most common system-component functional relationship. In this example, the components are connected in a series (failure of a component leads to a failure of the overall system, similar to the logical AND gate analogy) and in parallel arrangements (failure of a component will not lead to

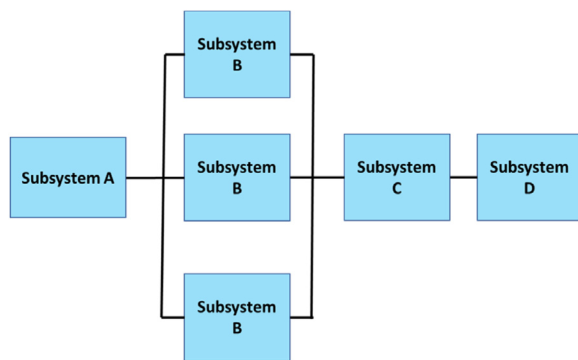

Fig. 5. A reliability block diagram representing common system-component functional relationship in a complex system.

a failure of the overall system until all parallel connected components get failed, similar to the logical OR gate analogy). Note that series and parallel connections are a limiting case of the "k out of n" system where the availability of a system with n identical components is obtained as following:

$$A(t)_{sys(r\leq k)} = \sum_{r=0}^{k} \frac{n!}{r!\,(n-r)!} A(t)^{n-r} (1 - A\,(t))^{r} \tag{4}$$

where r is number of failures, k is maximum allowable failures and $A(t)$ is the availability of the component at time t. When k=0, all components are connected in series while for $k = n - 1$, all components are connected in parallel.

In an accelerator, a variety of component-system functional relationships such as series, parallel, standby, redundant connects etc., might exist simultaneously. A list of formulae for the system availability and reliability with such configurations has been presented in the Appendix A.1.

4. Availability assessment model for PIP-II

A comprehensive availability assessment model of the PIP-II accelerator facility in form of the high-level functional block diagram is developed to compute its availability. This section details preparation of the model and delineates assumptions and guidelines used to build the model.

4.1. Component selection

It is evident that an accelerator comprises numerous components and dependent systems. Many of these components need additional auxiliary elements to execute their nominal function. For instance, an accelerating cavity assembly in the beamline is comprised of several auxiliary elements such as, power coupler to feed RF power; a mechanical tuner to tune its resonant frequency etc. This in turn, adds another layer of elements in the model. Consequently, the model of an accelerator facility becomes very large and cumbersome. In order to resolve this issue, a component-selection criterion was applied to the PIP-II model. A component features any of following characteristics is included in its detailed composition as practically permissible while preparing the model of the PIP-II facility.

- Components having moving parts such as vacuum pumps, cavity tuners etc.
- Components operating in pulsed mode such as high voltage switches, kicker system in the MEBT etc.
- Components that are involved in thermal cycling processes *e.g.* heat exchangers for low conductivity water (LCW).
- Components containing a high stored energy, *e.g.* RF cavities and magnets etc.
- Components involved in the high current operations *e.g.* modulators.
- A larger set of commercial components as they might not be designed for high reliability.

Note that, components exhibiting above characteristics are relatively more vulnerable to failures and therefore, drive the overall availability of the PIP-II facility.

4.2. Model assumptions

The model uses the following assumptions to compute the availability of the PIP-II facility:

- As also mentioned earlier, each component in the model possesses only binary states of the operation i.e. either operating nominally or failed. The component can migrate any state independent of its history of the operation.
- A component exhibits a constant failure rate during its operation.
- Each component fails at a random time with an exponential distribution determined by its MTBF. Two simultaneous failures are prohibited in the model. Those uncorrelated component failures are then represented by the Markov chains [26] and solved analytically to evaluate the system availability.
- When a component fails, it leads to the system failure (unless fault-tolerances are specified) resulting in an unscheduled accelerator shut-down. A temporary component failure such as one resulting from quenching of an SRF cavity or magnet is not treated as a failure in the model.
- The model assumes components meet their design specifications and the system is maintained to its best operable condition. Thus, the model does not incorporate manufacturing errors, human errors and environmental errors. Additionally, implications of the drift failures or degradation in performance of components are not included in the model.
- The model implements only corrective maintenance. It implies the fault detection time, logistic time at various stages of repair, tuning etc. are excluded. As soon as a failure is detected, the maintenance process is launched. After a repair, the component is treated "as good as new". Thus, resulting availability of the system is called inherent availability. Note that, the availability in this paper is always attributed to the inherent availability.
- The model is further simplified with the assumption that the facility transits from a no-beam state after a failure to the nominal beam state as soon as a repair is completed.
- A mission time of about a year, equivalent to eight thousand operational hours, is assumed for the availability analysis of the PIP-II accelerator facility.

4.3. Operational modes

A system can require to operate in different modes. These operational modes define the system-component functional relationship and therefore, a failure pattern of the system. Consequently, the system operational availability may vary from one operational mode to another. Thus, it is essential to establish operational modes of a system before estimating its availability. In this article, the availability of the PIP-II accelerator facility is evaluated for two operational modes named as the nominal operational mode and critical operational mode.

4.3.1. Nominal operational mode

In the nominal operational mode, the PIP-II facility delivers 800 MeV beam to the Booster synchrotron with the design specifications listed in Table 1. Note that, the baseline configuration of the SRF linac has been designed to accelerate the beam up to 833 MeV. This additional energy provides a safety margin to achieve the nominal

operational mode. It has been shown elsewhere [28,29] that the SRF linac optical design is sufficiently robust to tolerate a failure of optical element in each SRF section without conceding the design specifications. Consequently, the nominal operational mode can be achieved in two ways. The first nominal operational scenario, termed as no-failure-permit in this paper, involves all optical elements are operating with their design parameters. In this configuration, any component failure will produce a complete system failure. The second scenario is named as the fail-tolerance operation that permits a faulty/malfunctioned accelerating cavity in each SRF section (HWR, SSR1, SSR2, LB650 and HB650). It implies that the facility would keep operating even after a failure of the SRF cavity in each section. Note that, a repair or replacement of an element in cryogenic environment requires relatively a longer time in comparison to repair of a normal-conducting element. Consequently, the fault-tolerances in the availability estimate have been included only in SRF sections. This choice for the analysis does not infer the fault-tolerance capability of the normal-conducting sections and, allows a conservative estimate of the availability. It is worth to mention that a conservative assessment is beneficial at the design phase where a number of factors (human errors and environmental impacts) are relatively less known.

4.3.2. *Critical operational mode*

The lowest permissible beam energy out of the linac, at which the PIP-II facility could sustain an operation, is specified to be 600 MeV. This energy is called the critical threshold energy below which Booster synchrotron operation becomes incompatible due to excessive beam losses. Availability assessment of the PIP-II facility is also performed for this mode where the linac delivers 600 MeV beam with same rest of specifications as listed in Table 1.

5. Availabilty assessment for PIP-II facility

5.1. *Input data*

The reliability input data, MTTF and MTTR, for components are acquired from various sources including educated guess from the subject experts, operational experience with similar components at Fermilab as well as existing accelerator facilities, and from prototype tests. The beam commissioning of the PIP-II front-end at the Proton Improvement Plan-II Injector Test (PIP2IT) facility [30] also provided a useful information about operational reliability of the PIP-II components such as ion-source, magnet power supplies etc. A few components were commercially available and therefore, corresponding data were readily available. In addition, a few references [5–13] were also used to obtain data that were unavailable otherwise.

Fig. 6 shows most vulnerable components in the PIP-II accelerator facility model. It can be noticed from Fig. 6 that components in the ion source assembly possess the minimum MTTF that are followed by the compressor in the air utility system. Fig. 7 shows the most robust and reliable components of the PIP-II facility model that have longest MTTF. Note that, a high MTTF implies less frequent failures of the component.

It can be noticed from Fig. 8 that the high voltage transformer in the electrical power grid and the SRF cavities acquire longest MTTR in the model. Based on previous experience at Fermilab, experts suggest that a repair/replacement of such transformer could take up to full two weeks. Considering an eight-hours work shift per day, the repair time is then estimated to more than 1000 h (24 × 3x14 >1000 h). Because of this, the PIP-II facility envisions two power lines. Electric-power loads is swiftly shifted from one line to another in case of a failure. A repair is then performed in parallel without a long interruption. Also note that, repair of an SRF cavity may need warming of the cryomodule from a cryogenic temperature to the room temperature, taking cryomodule out from the accelerator tunnel and then, dismantle it to replace/repair the faulty cavity. It could result in a long unscheduled down time spanning over several months. To minimize this time at the PIP-II facility, the

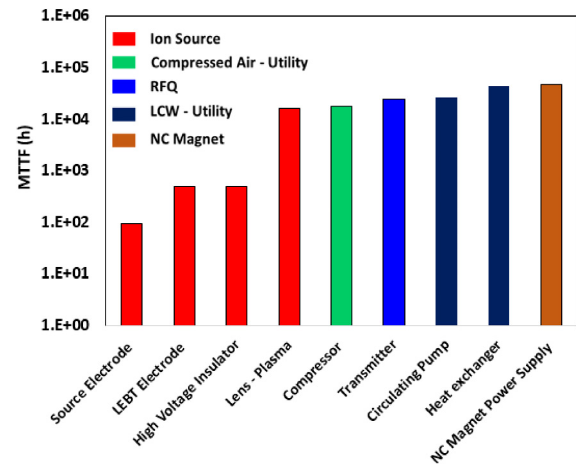

Fig. 6. Components with the minimum MTTFs in the PIP-II model. The colour of the bar represents the component's association with respective assembly or section. For instance, red coloured bar shows the MTTF of components in the ion-source assembly. (For interpretation of the references to colour in this figure legend, the reader is referred to the web version of this article.)

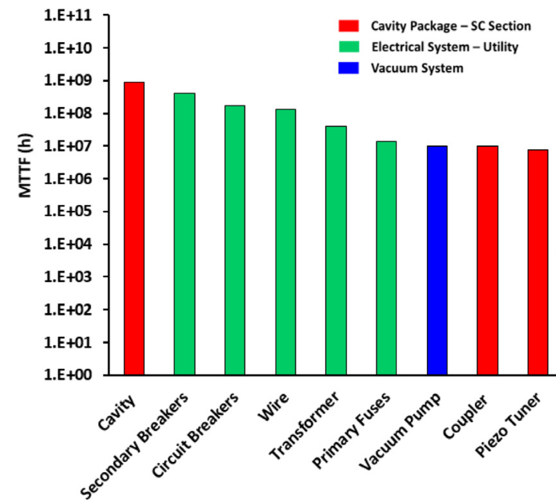

Fig. 7. Components with the maximum MTTF in the PIP-II facility model. The colour of the bar represents the component's association with respective assembly or section. For instance, red coloured bars represent components in a superconducting (SC) cavity assembly. (For interpretation of the references to colour in this figure legend, the reader is referred to the web version of this article.)

mitigation strategy involves replacing the faulty cryomodule with a fully-functional spare cryomodule. Then, repair of the faulty-element in the cryomodule is carried out in parallel without affecting the accelerator operational time. This strategy restricts the repair time of a superconducting element to only about a month.

5.2. *High-level functional diagram for the PIP-II facility*

As a next step for the availability assessment, a high-level functional block diagram model of the PIP-II facility was developed. The facility, as shown in Fig. 9, was modelled in two main parts: Utility systems and linac systems.

5.2.1. *Utilities systems*

A utility system in the model indicates a central facility of the core supply essential to operate an accelerator such as a cryo-plant to supply the cryogen for the SRF cavities. The model incorporates four utility systems that are subsequently discussed in detail.

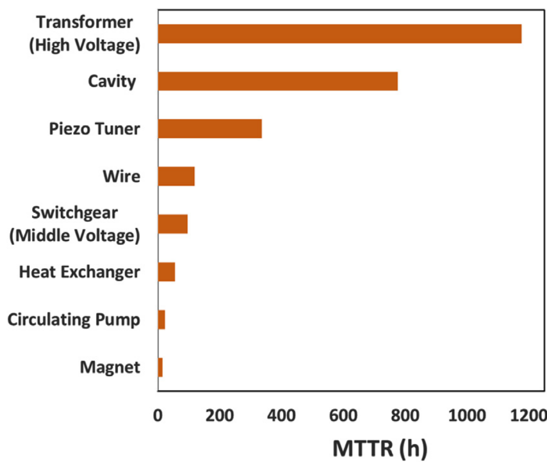

Fig. 8. Components with the longest MTTR in the PIP-II facility model.

• *Electrical-Power System:* The PIP-II accelerator facility envisions two electrical-power substations where one of the substations is available in the standby mode. In an event of failure, the power-load is swiftly shifted to the standby substation. The model includes major electrical components such as transformers, switchgears, fuses, circuit breakers and cables. The most vulnerable component in the electrical system is the Vacuum Circuit Breaker (VCB) which exhibits a higher failure rate. Because of this, four out of every eight VCBs are redundant in the electrical system. Note that, the model does not incorporate the power generating system but only the supply system.
• *Cryo-plant System:* A cryo-plant supplies the cryogen necessary to maintain cryogenic temperature of the superconducting cavities. The main components of the cryo-plant included in the model are the cold compressors, turbines, expanders, warm compressors and, associated control systems. The warm compressors are the most susceptible to failures among the cryo-plant components.
• *Low Conductivity Water (LCW) System:* It delivers water to maintain the operating temperature of normal conducting water-cooled elements such as the RFQ. The LCW system includes circulating pumps, heat exchangers, gauges, transducers, flow meters and, valves. Among those components, the circulating pumps are more often involved in the failures. Consequently, the LCW system of the PIP-II facility includes a redundant unit per three circulating pumps.
• *Compressed Air System:* The air system supplies compressed air for cooling of the radiation-cooled components, actuation and control of pneumatic valves etc. Two main components of the air-system are the compressor, and dryer. Each of them has a redundant unit in the model.

5.2.2. Linac system

The model includes a detailed description of the accelerator system. Along with the SRF linac (described in Section-II), details of the Beam Transfer Line (BTL) [31] were also included in the model. The BTL line is used to transport the beam from the end of the SRF linac to the Booster entrance. It is about 350 m long and mainly composed of normal conducting quadrupole and dipole magnets.

As shown in Fig. 9, the utility systems are connected to the linac in a series configuration. It implies failure of any functional blocks will shut-down the complete facility. After establishing the component-system functional relationship, the PIP-II accelerator facility model was incorporated in a Python-based program. The program has been developed at Fermilab to automate the availability assessment. It not only computes availability of the complete facility but also for the individual section and component. This feature facilitates finding the most vulnerable section determining overall availability of the facility.

Table 3
Components and their functions in the respective packages in the HWR cryomodule.

Component	Function
Cavity package	
Cavity	Acceleration, longitudinal beam focusing
Tuner	Tune cavity resonant frequency
Power coupler	Feeding RF power to cavity
Interlock sensors and electronics	Sensors and electronics
Low Level RF	RF control and instrumentation
Solid state Amplifier (SSA)	RF power source
RF control package: SSA control and timing	
SSA controls	RF controls to SSA
SSA timing	Timing to the SSA
Magnet assembly package: Solenoid magnets assembly	
Magnet power supply	Power supply to solenoids
Magnet	Transverse focusing of the beam.
Magnet instrumentation	Control system
Steering assembly package	
Steering Magnet	Beam Trajectory Correction
Steering Power Supply	Magnet power supply
Vacuum system package	
Vacuum Valves	Maintain vacuum
Vacuum. Pump	Creating vacuum in the beamline
Vacuum pump power supply	Powering the vacuum pump
Local cryogenic system package	
Local cryogenic system	Cryogenic distribution, cryostat structure and control

5.3. Case study of availability assessment for HWR section

In order to illustrate how the availability assessment is performed, this section discusses a detailed case study for the HWR section and describes the methodology applied to evaluate the availability of the complete PIP-II facility.

The HWR section is the first SRF section in the PIP-II linac. As shown in Table 2, it consists of one cryomodule that comprises eight solenoid magnets and same number of HWR cavities. Each solenoid magnet includes the steering magnets to correct the beam trajectories in horizontal and vertical planes. Those beamline elements further need auxiliary components to execute their nominal operation. Thus, it is more appropriate to describe an essential element in terms of the package including all supporting components. The cryomodule model is then represented using six packages: cavity, RF control, magnet assembly, steerer assembly, vacuum system and local cryogenic system packages. Table 3 lists major components and their functions in respective packages for the HWR cryomodule.

Availability assessment for the HWR cryomodule is performed for two operational modes: no-failure-permit and a cavity-fail-tolerance. In a no-failure-permit mode, failure of any component leads to failure of the complete HWR cryomodule whereas in, a cavity-fail-tolerance mode, the cryomodule keeps operating even after failure of one out of any eight SRF cavities. Fig. 10 illustrates the functional block diagrams of the HWR cryomodule describing logical connections among element packages for two operational modes. In the no-failure-permit mode, all elements packages are connected in the series configuration (Fig. 10(a)). In a cavity-fail-tolerance mode (Fig. 10(b)), all element packages are connected in series with the cavity packages that are configured in seven out of eight arrangement.

After establishing the functional diagram for the HWR cryomodule, next step involves computing availability of individual component in an element package using input data of MTTF and MTTR in Eq. (3). Table 4 shows availabilities of components in the cavity and magnet

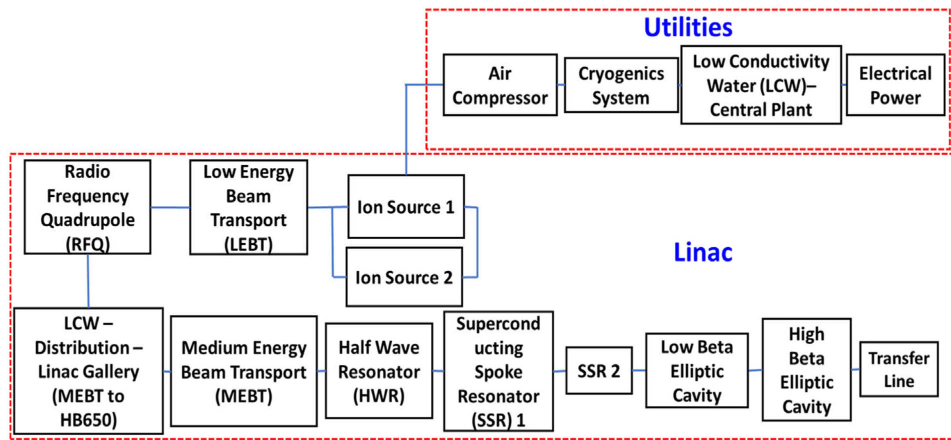

Fig. 9. High level functional diagram for the PIP-II accelerator facility.

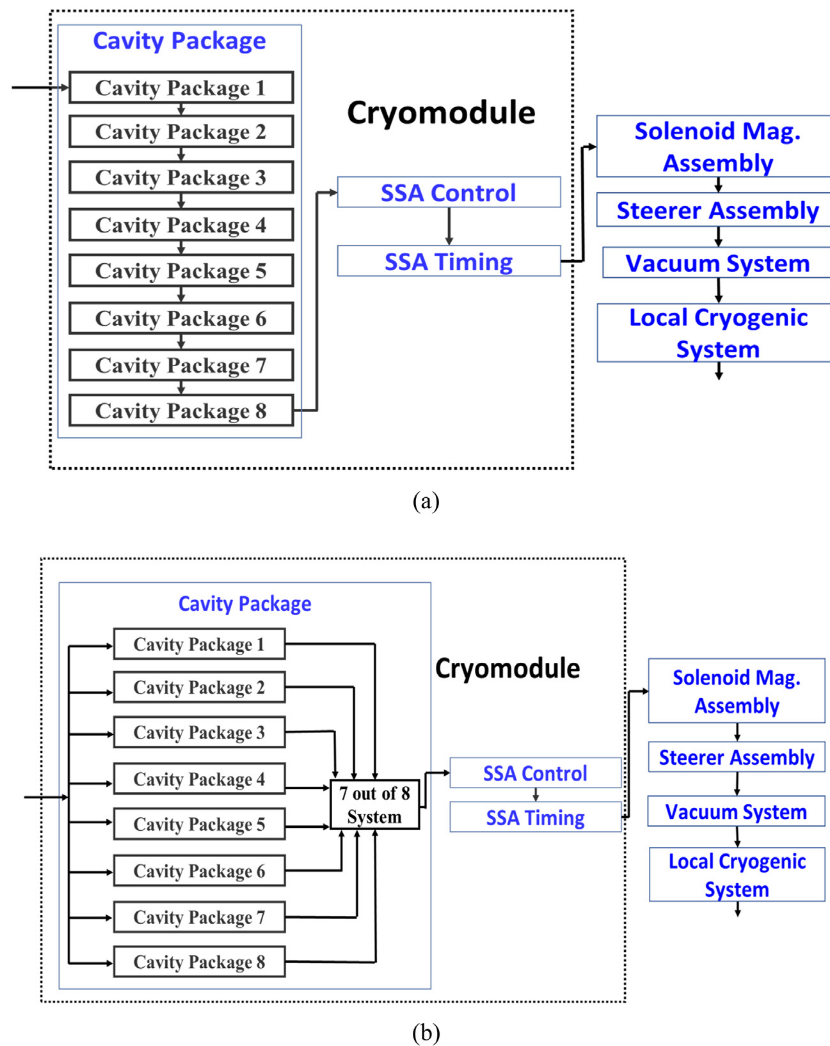

Fig. 10. Functional block diagram for the HWR cryomodule for two operational modes :(a) no-failure-permit and (b) a cavity-fail-tolerance.

packages. Then, using the knowledge of components logical connections in an element package, availability of the package is evaluated. Since components are connected in series configuration in the packages, availability of a package is obtained using equation:

$$A_p = \prod_{i=1}^{N} A_i \tag{5}$$

where A_p is the element package availability, A_i is the availability of ith component in the package and N is total number of components in a package. Similarly, failure rate of the $\lambda_p = \sum_{i=1}^{N} \lambda_i$ element package is computed as:

$$\lambda_p = \sum_{i=1}^{N} \lambda_i \tag{6}$$

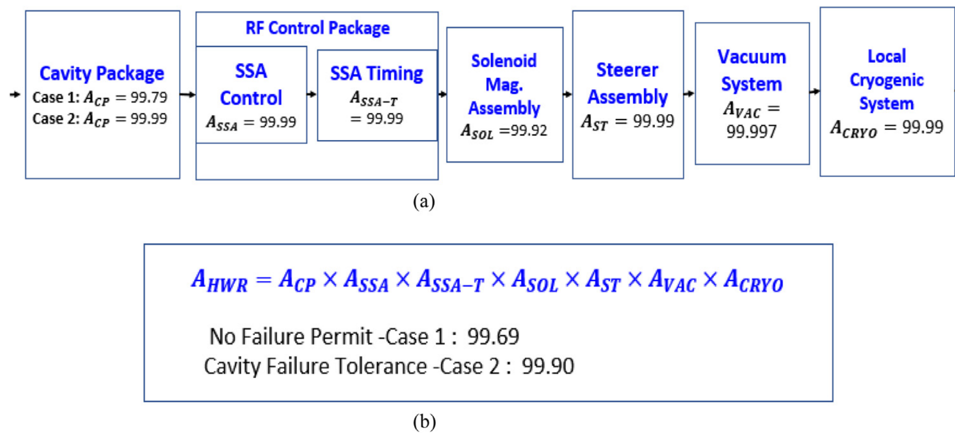

Fig. 11. HWR cryomodule is modelled using six essential element packages that are connected in a series configuration with the cavity package. (a) Combined availability of each essential package and (b) availability of the full HWR cryomodule for two operational modes i.e. no-failure-permit (Case 1) and a cavity-fail-tolerance (Case 2).

where λ_p is the failure rate of an element package and, λ_i is the failure rate of individual components connected in a series configuration. As shown in Table 4, the failure rate of the cavity and magnet packages are 3.45E−05 and 1.2E−05 per hour respectively. Thereafter, the combined availability (A_{cp}) and Mean Time Between Failure $MTBF_{CP}$ of the packages are obtained after accounting for total number of the respective package and logical arrangement among them in the HWR cryomodule. It can be noticed from Table 4 that the combined availability of the cavity package in the HWR cryomodule was computed to be 99.79% for the no-failure-permit mode and 99.99% for a cavity-fail-tolerance mode. The combined availability of the solenoid magnet assembly package was obtained to be 99.989%. Similarly, combined availabilities of the rest of the packages in the HWR cryomodule were computed. Fig. 11(a) shows the combined availability of all element package in the HWR cryomodule. Note that, without a fail tolerance, the cavity package offers the least combined availability. Since all element packages are connected in a series configuration with the cavity package (as shown in Fig. 10), availability of the full HWR cryomodule is simply obtained from the product of their combined availabilities as depicted in Fig. 11(b). Resulting availability of the HWR cryomodule was obtained to be 99.69% for the no-failure-permit mode that increases to 99.90% for a cavity-fail-tolerance mode.

To benchmark this calculation, availability assessment of the HWR cryomodule for the no-failure-permit mode was performed using a trial version of commercially available Monte-Carlo simulation package BlockSim [32]. The results were in good agreements with our estimation as shown in Appendix A.2.

5.4. Availability assessment of the PIP-II facility for nominal operational mode

Availability of the full PIP-II facility for the nominal operational mode was modelled using the same methodology applied to the HWR section. Note that, as discussed earlier in Section 4.3.1, there are two variants of the nominal operational mode i.e. no-failure-permit and fail-tolerance mode. In subsequent availability assessment, the fail-tolerance mode includes failure of an accelerating cavity in every SRF section.

The availability results show that an ion source offers the least availability of 89.08%. It is mainly because of the fact that the ion source requires the filament replacement for every three hundred hours of operation. Consequently, it creates a bottleneck on availability of the complete facility. To improve the ion source availability and therefore, for the complete facility, an additional ion source is installed in the standby configuration. In this arrangement, an ion source is always available for operation while others get repaired. This in turn, improves the ion source availability to 98.67%. Table 5 lists availability of each

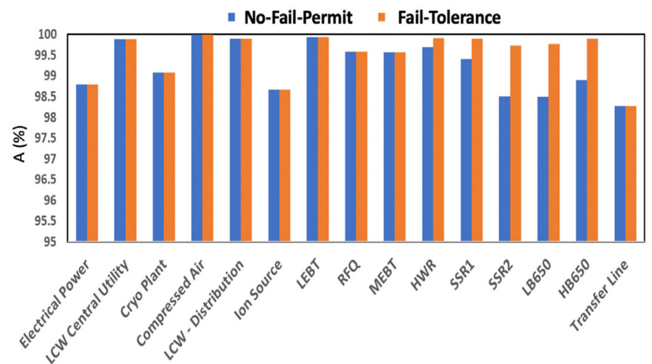

Fig. 12. Availability of each section of the PIP-II facility for two variants of the nominal operational modes i.e. no-failure-permit mode (blue) and fail-tolerance mode (orange). Note that the fail-tolerance was applied only to the SRF section. (For interpretation of the references to colour in this figure legend, the reader is referred to the web version of this article.)

sectional block (shown in Fig. 9) of the PIP-II facility model for both nominal operational modes. In addition, it highlights the least available components/system-units in the respective sections. It is apparent from Table 5 that the transfer line possesses the least availability among all sections. Note that, the transfer line is about two times longer than the SRF linac and, mainly composed of conventional normal conducting quadrupole and dipole magnets. The power supplies of the magnets exhibit a relatively higher failure rate with MTTF of ∼4E+04 h that brings down the availability of the section.

Fig. 12 shows a comparison of availabilities obtained from two nominal operating modes. It is evident from Fig. 12 that availabilities of the SRF sections substantially improve in the fail-tolerance mode.

To make it more suggestive for practical purposes, the PIP-II sectional blocks are grouped into three major systems i.e. Utility, NC and SRF linac. Table 6 lists the availability and MTBF of each major system. The SRF linac exhibits the lowest availability of 95% for the no-failure-permit mode that increases to 99% after applying a cavity fail tolerance in every SRF section. Then, availability of the full PIP-II facility, computed from a product of the availability of every section, was found to be 89.2% and 93.0% for the no-failure-permit and fail-tolerance modes respectively. Again, all sections were connected in a series configuration in the PIP-II model (Fig. 9). It should also be noted that the facility exhibits a higher MTBF of 74.5 h in the fail-tolerance mode in comparison to 62.5 h of the no-failure-permit mode. The MTTR of the PIP-II facility was computed using following equation:

$$MTTR = MTBF - A * MTBF \quad (7)$$

Table 4
Availability of the cavity package and the solenoid magnet assembly package in the HWR cryomodule.

Component	MTTF (T) (h)	λ (h^{-1})	MTTR (h)	A_i (%)	$MTBF_{cp}$ (h)	A_{cp} (%)
Cavity package						
Cavity	8.76E+08	1.14E−09	776	99.999	Case 1: No-failure-permit mode	
Tuner	1.00E+06	1.00E−06	216	99.978	8 cavity packages in series	8 cavity packages in series
Coupler	1.00E+07	1.00E−07	0.5[a]	99.999		
Interlock sensors	1.00E+05	1.00E−05	1	99.999	$MTBF_{CP} = \frac{1}{8\lambda_p}$ = 3623.19	$A_{CP} = (A_p)^8$ $A_{CP} = 99.79$
Interlock electronics	1.00E+05	1.00E−05	1	99.999	Case 2: A Cavity-Fail-Tolerance	
Solid state amplifier (SSA)	2.98E+05	3.36E−06	6	99.997	7 out of 8 cavity packages	7 out of 8 cavity packages
SSA Low Level RF	1.00E+05	1.00E−05	1	99.999	$MTBF_{CP} = \frac{1}{\lambda_p}\left(\frac{1}{8}+\frac{1}{7}\right)$	$A_{CP} = (A_p)^8 + 8\times(A_p)^7\times(1-A_p)$
		$\lambda_p = \sum_i^7 \lambda_i$ $\lambda_p = 3.45E-05$		$A_p = \prod_{i=1}^7 A_i$ $A_p = 99.97$	$MTBF_{CP}$ = 763.98	$A_{CP} = 99.999$
Solenoid magnet assembly						
Magnet power supply	1.00E+06	1.00E−06	2	99.992	8 Solenoid magnet assemblies are in series	8 Solenoid magnet assemblies are in series
Magnet	1.00E+06	1.00E−06	792	99.999		
Magnet controls	1.00E+05	1.00E−05	2	99.998	$MTBF_{CP} = \frac{1}{8\lambda_p}$ =	$A_{cp} = (A_p)^8$
		$\lambda_p = \sum_i^3 \lambda_i$ $\lambda_p = 1.2E-05$		$A_p = \prod_{i=1}^3 A_i$ $A_p = 99.989$	10416.67	$A_{cp} = 0.999$

[a]It is assumed that the coupler MTTR is the time needed to restore accelerator operation after detuning the cavity. Major coupler repairs are accounted in the cavity MTTR.

Table 5
Availability of the functional blocks of the PIP-II facility for two nominal modes. The component with the least availability in respective section is also listed.

	Section	Availability (%)		Component with lowest availability in the section.	
		No-Failure-Permit mode	Fail-tolerance mode	Component name	Availability (%)
1	Electrical power system	98.79	98.79	Electric wire	99.22
2	LCW central system	99.88	99.88	Pressure gauge	99.91
3	Cryo-plant system	99.07	99.07	Warm compressors	99.82
4	Compressed air system	99.99	99.99	Compressor	99.99
5	Ion source	98.67	98.67	Individual ion source	89.08
6	LEBT	99.93	99.93	High voltage switch	99.95
7	RFQ	99.58	99.58	LCW—distribution (RFQ)	99.70
8	LCW—distribution	99.89	99.89	Circulating pump	99.91
9	MEBT	99.57	99.57	Magnet power supply chain	99.80
10	HWR	99.69	99.90	Solenoid magnet	99.91
11	SSR 1	99.40	99.90	Solenoid magnet	99.91
12	SSR 2	98.50	99.72	Solenoid magnet	99.78
13	LB 650	98.49	99.76	Quadrupole magnet package	99.85
14	HB 650	98.89	99.89	Quadrupole magnet package	99.87
15	Transfer line	98.27	98.27	LCW distribution (Transfer line)	99.09

It results in the MTTR of 6.8 and 5.2 h for the no-failure and fail-tolerance modes respectively.

The operational statistics of the existing accelerator facility corroborates that the target availability of 90% is well within reach of the modern technology. The Spallation Neutron Source (SNS) accelerator facility at Oak Ridge [33] has been reporting an availability of 90% since 2011 [34,35]. The proposed ESS facility also targets the facility availability of at least 90% over a calendar year [7]. This in turn, confirms feasibility of the PIP-II availability target. It is apparent from Table 6 that the PIP-II accelerator facility can deliver the target availability of 90% over a fiscal year in both operational modes. However, the analysis also corroborates that an additional improvement in the availability can be achieved through gaining a capability of operation

Table 6
Availability and MTBF allocation by category for two operational modes of the PIP-II linac facility.

	No-failure-permit mode		Fail-tolerance-mode	
	MTBF (h)	A (%)	MTBF (h)	A (%)
Utility system	1881.2	97.6	1881.2	97.6
NC Linac system	127.8	96.1	127.8	96.1
SRF Linac system	130.9	95.1	197.8	99.2
PIP-II facility	62.5	89.2	74.5	93

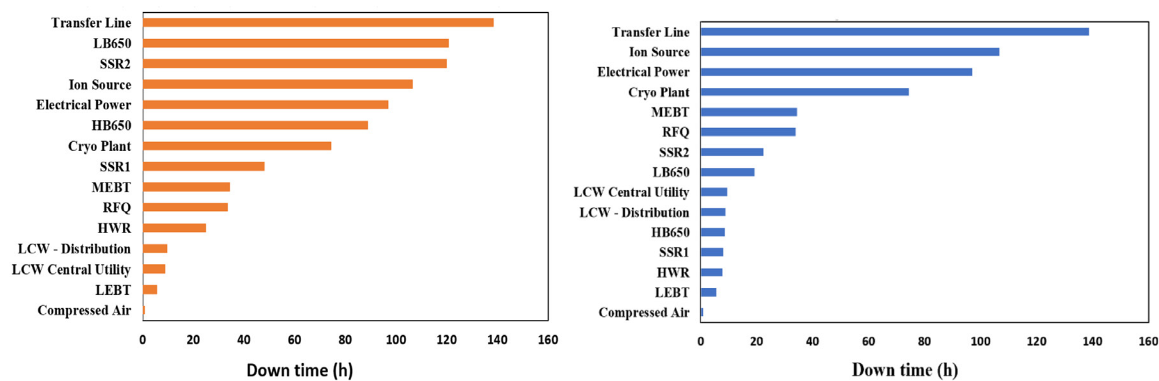

Fig. 13. Distribution of the down-time hours by sections of the PIP-II facility operating in (left) no-failure-permit and (right) fail-tolerance modes. Note that, fail-tolerance of a cavity per section was applied only to the SRF sections of the facility.

in a fail-tolerance mode. This is why the baseline design of the PIP-II linac [36] has adopted a cavity fault-tolerance in every SRF section. In addition to a local energy correction, allocation of a spare cavities per section enables optics tuning in case of malfunctioned elements which is otherwise not possible if spare cavities are located at the end of linac.

At times it is more practical to describe the unavailability in term of the down-time that can be estimated using following equation:

$$DownTime = (1 - A)\,T_{operation} \tag{8}$$

where, $T_{operation}$ is the total operational mission time. Based on the operational mission time of *8000* h (excluding scheduled maintenance), the down-time of each section of the PIP-II facility was estimated. As shown in Fig. 13, the BTL section imposes the maximum unscheduled down-time of about *138* h to the PIP-II facility. This is mainly because of the fact that the BTL is the longest section of the facility with the length of around *350* m. The second largest contributions of *120* h come from the LB650 and SSR2 SRF sections. The SRF sections enforces a collective down-time of over *400* h. However, this time shrinks to *65* h in the fail-tolerance operating mode. The second largest contribution of 106 h comes from the ion source in this mode of operation.

5.5. Availability assessment of PIP-II facility for critical operational mode

In the critical operational mode, the PIP-II facility operates to deliver the beam at 600 MeV to the Booster Synchrotron. The difference of 200 MeV from the nominal energy is modelled by turning off additional SRF cavities in the linac. These cavities are treated as the spare cavities. Since the energy gain per cavity varies substantially along the linac (Fig. 2), there are several combinations to obtain the total number of the spare cavities needed to downscale the beam energy from 800 MeV to 600 MeV. These combinations define states of the critical operational mode.

It is well known that most of the beam dynamics issues in an ion linac are associated with its low energy portion. To incorporate this fact in the availability analysis, it was assumed that there were no additional spare cavities in the HWR, SSR1 and SSR2 sections. For further simplification, it was considered that all the spare cavities were located only in one section. Thus, the critical operational mode was modelled for two cases representing all the spare cavities were located either in the LB650 or HB650 sections. Table 7 lists the number of the spare cavities in the respective sections. Note that, transit time effect [37] has been included while evaluating the total number of the spared cavities in the respective sections. Table 7 lists the availability of the PIP-II facility for two cases of the critical operational mode. It can be discerned that the facility possesses about the same availability of 93% in both cases as in the fail-tolerance nominal operational mode even after applying additional fail-tolerances in terms of the spare cavities. It is attributed to the fact that the quadrupole magnet package

Table 7
Availability of the PIP-II facility for two cases of the critical operational mode.

Section	Total number of cavities	Spare cavities	A(%)
LB650	36	11	93.35
HB650	24	15	93.34

(as shown in Table 5) is the least available unit in both LB650 and HB650 sections that determines overall availability of these sections. Consequently, additional fail-tolerances of the SRF cavities bring in only a little impact on the availabilities of these sections and therefore, on the availability of the complete facility which is primarily governed by the least available BTL and ion source sections.

6. Sensitivity analysis and benchmarking of the model

6.1. Input data sensitivity analysis

The quality of input data is the most crucial aspect of the availability analysis that needs to be assured to obtain a meaningful outcome from the analysis. On the contrary, because of the first-of-a-kind nature of every new accelerator, there are uncertainties involved with MTTF and MTTR data of the components. In order to attain an adequate level of confidence in outcome of the availability analysis, a sensitivity analysis was performed to understand the impact of a spread in the input data on the PIP-II availability.

It is evident that MTTF of a component is usually several order higher than its MTTR. In some cases (such as for the cavities), MTTF of a component could be higher from its life span. Consequently, MTTF data may possess a relatively higher uncertainty in comparison of the MTTR data especially for the large values due to a lack of the failure-rate statistics for such components. In order to analyse implication of uncertainty with the MTTF data in the PIP model, all components having MTTF above hundred years ($\sim 10^6$ h) were reduced by a scaling factor and then the facility availability was evaluated. Fig. 14 shows the availability of the PIP-II facility in the fail-tolerance mode as a function of the MTTF scaling factor. It is apparent from here that the facility reaches to its target availability even after reducing the MTTF by a factor of ten. However, the availability degraded below *80%* after MTTF were scaled down by a factor of *50*. It can easily be concluded from Fig. 15 that the SRF linac system availability is more sensitive to the fluctuations in MTTF data in comparison to the Utility and NC linac systems. Still, it attains the availability above *90%* even after applying the scaling factor of twenty-five to the MTTF data. In another approach to compute the least plausible availability of the PIP-II facility, it was assumed that the operational lifetime of the machine was thirty years. Accordingly, all the MTTFs beyond thirty years were reduced to $2.6{\times}10^5$

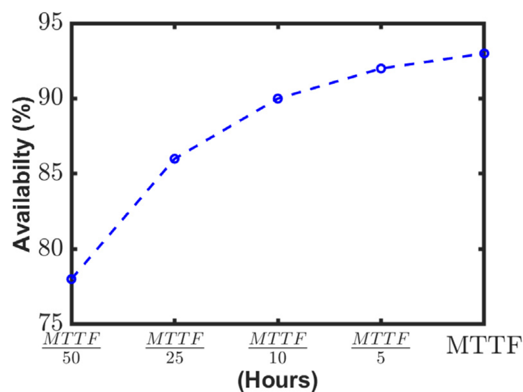

Fig. 14. Variation in availability of the total facility with the MTTF scaling factor in a fail-tolerance operational mode.

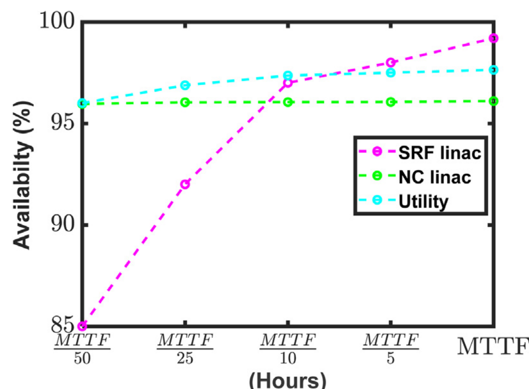

Fig. 15. Availability of each major system in the PIP-II model as a function of MTTF scaling factor in a fail-tolerance operational mode. (For interpretation of the references to colour in this figure legend, the reader is referred to the web version of this article.)

h (equivalent to thirty years) in the model. In this scenario, the facility availability was found to be *71%*. Availabilities of the utility and NC linac systems were found to be *88%* and *95%* respectively while the SRF linac system obtained the availability of *85%*.

It can be concluded from the sensitivity analysis that the PIP-II model could even tolerate a spread of *96%* to the MTTF data above $\sim 10^6$ h without substantial impact on its target availability of *90%*. Also, among all three major systems, the SRF linac system availability is affected most from the choice of the MTTF input data. However, even in a conservative estimate, the model predicted the PIP-II facility would have an up-time of *70%* of its total operational time with the SRF linac availability in high eighties.

6.2. Model benchmarking

In order to validate the methodology developed for the PIP-II availability model, a reference model of the operational SRF linac of SNS accelerator facility at Oak Ridge was developed using the same methodology. The SNS SRF linac is an ideal choice for the reference model due to a close resemblance of its configuration and operational parameters to the PIP-II, LB650 and HB650 sections. The SRF linac design information was obtained from Ref. [33–35]. It has been designed to accelerate the beam from *180* MeV to *1* GeV using two families of SRF cavities. Accordingly, the SRF linac has been segmented in two sections: Medium Beta (MB) and High Beta (HB) sections. The MB section includes eleven cryomodules where each cryomodule houses three medium beta SRF cavities. The HB section consists of twelve cryomodules and, each cryomodule is composed of four high beta SRF cavities. There are normal conducting quadrupole doublets positioned between adjacent cryomodules to provide transverse beam focusing. The SRF cavities are powered individually using klystrons. Input data (MTTF and MTTR) for klystrons and associated RF components were obtained from Ref. [10] while the PIP-II input data were applied wherever they were applicable. Then, based on their functions, components in an SRF cryomodule of the SNS linac were grouped in the element packages. Appendix A.3 provides a detailed composition and individual availabilities of each element package. Table 8 lists number of respective packages in MB and HB sections.

Table 8
Number of packages in MB and HB sections of the SNS SRF linac.

	MB	HB
Cavity package	33	48
Magnet package	22	24
Steerer package	22	24
Cryo-package	11	12
Transmitter	4	8
Modulator	3	4

Table 9
Operational availability of the SRF linac system of the SNS accelerator facility in two operational modes.

	No-failure-permit mode availability (%)	Fail-tolerance-mode availability (%)
MB section	97.2	99.4
HB section	96.1	99.3
SRF linac	93.4	98.8

The functional block diagram of the SRF linac system was prepared considering the element packages were connected to each other in a series configuration. The full SRF linac availability was then computed for the no-failure-permit and fail-tolerance operating modes. Note that, the fail-tolerance operating mode assumes one spare cavity in each section that might fail without interrupting the SRF linac operation. It can be observed from Table 9 that the model predicted the SRF linac system availability of *93%* and *99%* in the respective no-failure-permit and fail-tolerance operating modes.

The operational statistics of the SNS SRF linac has been presented in Ref. [34,35] which shows availability of the linac has been about *98%* since the fiscal year of 2011. It indicates the measured availability is in agreement with the model predicted availability especially for the fail-tolerance mode where both matches within a percentage level. An increase of five points with respect to the availability in the no-failure-permit mode may attribute to a conservative set of the reliability input data. However, it has been addressed elsewhere [35] that the design energy of 1 GeV has yet to be achieved for a nominal beam operation at the SNS accelerator facility. This is mainly because of collective effects (field-emission, multi-pacting, heating etc.) limiting the operating accelerating gradient in the SRF cavities. In this case, one can conclude that the fail-tolerance operating mode is a more representative choice to describe the SNS, SRF linac operation and therefore, the model predicted availability in this mode is in good agreement with the measured availability of the SNS linac.

The PIP-II linac baseline incorporates SNS SRF linac operational experience in its design. The PIP-II SRF cavities excludes usage of Higher Order Modes (HOMs) damper identified as roots of several associated problems (field emission, heating, etc.) limiting RF performance of the accelerating cavities in SNS linac. A detailed study presented elsewhere [38] concludes usage of HOMs dampers in SRF cavities are futile for the PIP-II SRF linac involving operation with a low average beam current of 2 mA. In addition, uncorrelated HOMs spectrums of five families of the PIP-II SRF cavities, HOMs frequency spread due to manufacturing errors and a lower HOMs impedances because of non-relativistic nature of the beam, largely preclude most of the beam

instabilities induced by HOMs. Thus, elimination of HOMs damper in PIP-II SRF cavities is a preferable choice that lowers not only overall capital cost but also allows avoiding a number of issues in SRF cavities. This in turn, could improve RF performance of the SRF cavities and hence the complete PIP-II facility .

7. Summary

The paper introduced a methodology to model the availability of the complete particle accelerator facility. A comprehensive reliability model of the proposed PIP-II accelerator facility was developed that included not only the accelerator systems but also essential supporting systems such as the central cryo-plant, electrical power systems etc. The availability assessment of the PIP-II facility reveals that the ion source is most vulnerable system with availability of only 88%. Consequently, the baseline of the PIP-II facility adopted an additional ion source configured in the standby mode. This arrangement increases the ion source availability to 98.7%. The baseline design of the PIP-II SRF linac also attributes a cavity fault-tolerance in every SRF sections that enables the facility to operate in the fail-tolerance mode. Furthermore, the PIP-II integration and operation strategy plans for a fully functional spare cryomodule always available for each SRF section in inventory to minimize a repair time of the superconducting elements and therefore, unscheduled down time of the facility.

The availability of the full PIP-II facility in nominal operational mode was found to be 89% that increased to 93% after introducing the fail-tolerance of a cavity in every SRF sections in the model. This corroborates that the baseline design of the PIP-II accelerator facility is sufficiently robust to meet the target availability in both nominal operational modes. Moreover, availability of the PIP-II facility was computed for the critical operational mode featuring the facility operation at the minimum beam energy of 600 MeV. The availability of the PIP-II facility in this mode was obtained to be 93%. An input data sensitivity analysis and the model validation using a reference model of the SNS SRF linac generate an adequate level of confidence in the PIP-II availability assessment that leads us further to initiate engineering design of the PIP-II facility.

CRediT authorship contribution statement

Arun Saini: Conceptualization, Methodology, Writing - original draft, Revising, Investigation, Data Curation, Supervision, Formal analysis, Visualization, Writing - review & editing. **Ram Prakash:** Methodology, Investigation, Formal analysis, Software. **Joseph D. Kellenberger:** Software.

Declaration of competing interest

The authors declare that they have no known competing financial interests or personal relationships that could have appeared to influence the work reported in this paper.

Acknowledgements

The authors are thankful to the large team of scientists, engineers and technical staffs who provided key input data for this study. The authors would like to express gratitude on a more personal level to A. Klebaner, A. Martinez, J. Holzbauer, D. L. Newhart and, J. E. Anderson Jr. for their constructive suggestions and discussions that helped the authors to enhance quality of the paper. The author also wishes to acknowledge efforts of L. Serio and C. Adolphsen who reviewed this work and provided their invaluable feedback. The authors are also grateful to Barbara Merrill and Dr. Priyanka Saini and Dr. Vyacheslav Yakovlev for their invaluable time to proof-read the manuscript and useful suggestions.

This manuscript has been authored by Fermi Research Alliance, LLC under Contract No. DE-AC02-07CH11359 with the U.S. Department of Energy, Office of Science, Office of High Energy Physics.

Appendix A

A.1.

For the comprehension of this article, this appendix lists standard Reliability Engineering textbook formulae. Several of those formulae were applied in this article.

For of ith component, if r_i = Reliability at any time t, a_i = Availability, λ_i = failure rate and μ_i = repair rate, then we can obtain following formulae.

1. *Series Configuration of the components in a system:*
   a. Availability of the system $A = \prod a_i$.
   b. Reliability $R = \prod r_i$.
   c. MTBF $= \frac{1}{\sum_i \lambda_i}$,
   d. Mean Time to Failure $= (1 - A) * MTBF$.
2. *Parallel Configuration of the components in a system*
   a. $1 - A = \prod (1 - a_i)$.
   b. $1 - R = \prod (1 - r_i)$.
   c. MTBF $= \frac{1}{(1-A)\sum_i \mu_i}$.
   d. Mean Time To failure $= (1 - A) * MTBF$
3. *k out of n systems:* Assume that all the components have same failure rate (λ) and repair rate (μ).
   a. $A = \sum_{i=0}^{k} \binom{n}{i} a^{n-i} (1-a)^i$ where, k is maximum number of failure allowed in a system, n is total number of components.
   b. MTBF $= \frac{1}{\lambda}\left(\frac{1}{n} + \frac{1}{n-1} + \cdots + \frac{1}{k}\right)$ for non-repairable systems.
4. *Standby (Cold):* A standby component implies that the component starts operating as soon as another component gets failed. Two components in a system have same failure rate (λ) and repair rate (μ) and one of the components is kept as standby mode, then reliability and MTBF of the system is expressed as below
   a. Reliability $R = (1 + \lambda t) e^{-\lambda t}$
   b. MTBF $= \frac{2}{\lambda} + \frac{2\mu^2}{\lambda^2(\lambda+2\mu)}$

   In general, when two components have different failure rate $\lambda_1 \& \lambda_2$ and repair rate is μ_1 and μ_2, MTBF is then express as below

   MTBF $= \frac{1}{\lambda_1} + \frac{1}{\lambda_2} + \frac{\mu_1}{\lambda_2}\left(\frac{1}{\lambda_2} - \frac{1}{\lambda_2+\mu_1+\frac{\lambda_2}{\lambda_1}\mu_2}\right)$.

A.2.

See Fig. A.1.

A.3.

See Table A.1.

Appendix B. Supplementary data

Supplementary material related to this article can be found online at https://doi.org/10.1016/j.nima.2020.164874.

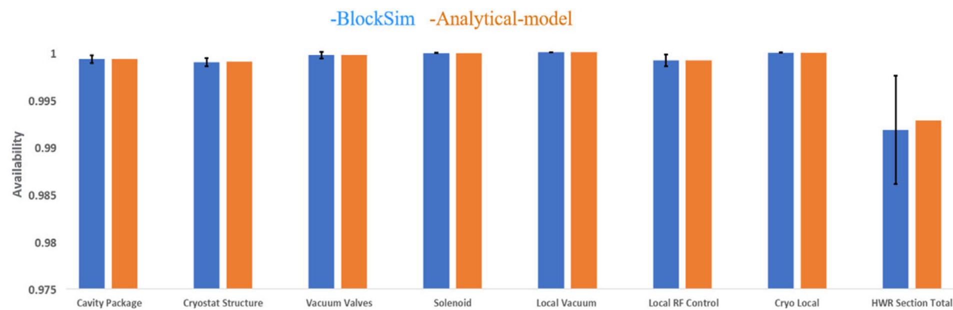

Fig. A.1. Availability of HWR cryomodule computed for no-failure-permit mode using BlockSim (blue coloured bars) and analytical model (saffron coloured bars). (For interpretation of the references to colour in this figure legend, the reader is referred to the web version of this article.)

Table A.1
A detailed view of the element packages in the SRF cryomodule of the SNS linac.

Packages	Components	MTTF	MTTR	A(%)
Magnet package	Magnet	1E+06	16	
	Power Supply	4.6E+04	2	
	Magnet Instrumentation	1E+05	2	
Magnet package availability				99.99
Cavity package	SRF cavity	8.7E+08	776	
	Tuner	1E+06	216	
	Coupler	1E+07	0.5	
	Interlock sensor	1E+05	1	
	Klystron	5E+04	4.5	
	Wave Guide	1.5E+05	3	
	Circulator	5E+04	3	
	Load	7.5E+04	3	
	LLRF	1E+05	2	
Cavity package availability				99.93
Steering magnet package	Steerer			
	Power supply	1E+06	2	
	Magnet instrumentation	1E+06	2	
	Steerer instrumentation	1E+05	2	
Steering magnet package availability				99.99
Cryo package	Vacuum valves	1E+07	8	
	Ion pump	1E+06	4	
	Ion pump power supply	1E+05	1	
	Local cryogenic distribution	5E+05	2	
Cryo-package availability				99.99
Additional components	Transmitter	2.26E+04	4	99.98
	Modulator	5.6E+03	3	99.94

References

[1] J.N. Galayda, The LCLS-II: A high-power upgrade to the LCLS, in: Proceedings of IPAC2018, Vancouver, Canada, MOYGB2, pp. 18–23.

[2] S. Peggs, et al., ESS Technical Design Report, 2013, http://inspirehep.net/record/1704813?ln=en.

[3] A. Sharma, A.R. Jana, C.B. Patidar, M.K. Pal, N. Kulkarni, P.K. Hoyal, et al., Reference physics design for 1 GeV Injector Linac and accumulator ring for Indian spallation neutron source, arXiv:1609.04518 [physics.acc-ph].

[4] Zhihui Li, Peng Cheng, Huiping Geng, Zhen Guo, Yuan He, Cai Meng, Huafu Ouyang, Shilun Pei, Biao Sun, Jilei Sun, Jingyu Tang, Fang Yan, Yao Yang, Chuang Zhang, Zheng Yang, Phys. Rev. ST Accel. Beams 16 (2013) 080101.

[5] T. Himel, J. Nelson, N. Phinney, Availability and reliability issues for ILC, in: Proceedings of PAC07, Albuquerque, New Mexico, USA, pp. 1966–1969.

[6] L. Burgazzi, P. Pierini, Reliability studies of a high-power proton accelerator for accelerator-driven system applications for nuclear waste transmutation, Reliab. Eng. Syst. Saf. 92 (2007) 449–463, http://dx.doi.org/10.1016/j.ress.2005.12.008.

[7] E. Bargalló, R. Andersson, A. Nordt, A. De Isusi, E. Pitcher, K.H. Andersen, ESS availability and reliability approach, in: Proceedings of IPAC2015, Richmond, VA, USA (2015), MOPTY045, pp. 1033–1035.

[8] J. Knaster, P. Garin, H. Matsumoto, Y. Okumura, M. Sugimoto, F. Arbeiter, P. Cara, S. Chel, A. Facco, P. Favuzza, T. Furukawa, R. Heidinger, A. Ibarra, T. Kanemura, A. Kasugai, H. Kondo, V. Massaut, J. Molla, G. Micciche, S. O'hira, K. Sakamoto, T. Yokomine, E. Wakai, Overview of the IFMIF/EVEDA project, Nucl. Fusion 57 (10) (2017) 102016, http://dx.doi.org/10.1088/1741-4326/aa6a6a.

[9] R. Andersson, A. Nordt, E. Bargalló, Machine protection systems and their impact on beam availability and accelerator reliability, in: Proceedings of IPAC2015, Richmond, VA, USA, 2015, MOPTY044, pp. 1029–1032.

[10] P. Tallerico, D. Rees, D. Anderson, An availability model for the SNS Linac RF system, in: Proceedings of PAC2001, Chicago, IL, USA, 2001, MPPH112, pp. 1035–1037.

[11] E.S. Lessner, P.N. Ostroumov, Reliability and availability in the RIA driver linac, in: Proceedings of PAC2005, Knoxville, TN, USA, 2005, FOAC005, pp. 443–445.

[12] G.W. Dodson, Accelerator systems RAM analysis, Talk in Accelerator Reliability Workshop, 2002, http://www.esrf.eu/files/live/sites/www/files/events/conferences/2002/ARW/proceedings/MONPM/Dodson.pdf.

[13] M.J. Haire, Computation of Normal Conducting and Superconducting Linear Accelerator (Linac) Availabilities, ORNL, USA, Tech. Report, ORNL/TM-2000/93, 2000, https://www.osti.gov/biblio/885853-yUWMiH/.

[14] PIP-II Conceptual Design Report, 2017, http://pip2-docdb.fnal.gov/cgi-bin/ShowDocument?docid=113.

[15] E.L. Hubbard, Booster Synchrotron Report, 1973, https://lss.fnal.gov/archive/tm/TM-0405.pdf.

[16] L. Merminga, PIP-II Global Requirements Document, FNAL, USA, PIP-II Document 1166-v8, ED0001222, 2020, https://pip2-docdb.fnal.gov/cgi-bin/RetrieveFile?docid=1166&filename=ED0001222%20PIP-II%20Global%20Requirements%20Document%20GRD.pdf&version=8.

[17] A. Shemyakin, M. Alvarez, R. Andrews, J.-P. Carneiro, A. Chen, R. D'Arcy, B. Hanna, L. Prost, V. Scarpine, C. Wiesner, PIP-II injector test's low energy beam transport: Commissioning and selected measurements, AIP Conf. Proc. 1869 (050003) (2017).

[18] S. Virostek, et al., Final design of a CW Radio Frequency Quadrupole (RFQ) for the Project X Injector Experiment (PXIE), in: Proc. NAPAC'13, Pasadena, CA, USA, 2013, WEPMA21, pp. 1025–1027.

[19] A. Saini, C.M. Baffes, A.Z. Chen, V.A. Lebedev, L. Prost, A. Shemyakin, Design of PIP-II medium energy beam transport beam, in: Proc. of IPAC 2018, Vancouver, Canada, 2018, TUPAF076, pp. 905–908.

[20] Z.A. Conway, et al., IOP Conf. Ser.: Mater. Sci. Eng. 101 (2015) 012019.
[21] M.H. Awida, et al., Development of low single-spoke resonators for the front end of the proton improvement plan-II at Fermilab, IEEE Trans. Nucl. Sci. 64 (9) (2017) 2450–2464.
[22] V. Roger, et al., Design Update of the SSR1 Cryomodule for PIP-II Project, in: Proceedings of IPAC2018, Vancouver, Canada, 2018, WEPML019, pp. 2721–2723.
[23] A. Rowe, SRF Technology for PIP-II and PIP-III, in: Proc. SRF2017, Lanzhau, China, 2017.
[24] A. Saini, Design considerations for the Fermilab PIP-II 800 MeV Superconducting Linac, in: Proc. of NA-PAC 2016, Chicago, USA, 2016, WEPOA60.
[25] D.J. Smith, Reliability, Maintainability and Risk, Elsevier Ltd, 2011, http://dx.doi.org/10.1016/C2010-0-66333-4.
[26] M. Raus, A. Hsyland, System Reliability Theory Models, Statistical Methods, and Applications, second ed., John Wiley & Sons, Inc.
[27] J. Upadhyay, D. Im, J. Peshl, M. Bašović, S. Popović, A.M. Valente-Feliciano, et al., Apparatus and method for plasma processing of SRF cavities, Nucl. Instrum. Methods Phys. Res. A 818 (2016) 76–81, http://dx.doi.org/10.1016/j.nima.2016.02.049.
[28] A. Saini, J.-F. Ostiguy, N. Solyak, V.P. Yakovlev, Studies of fault scenarios in SC CW Project-X linac, in: Proceedings of NA-PAC2013, Pasadena, California, USA, 2013, MOPMA10, pp. 318-320.
[29] A. Saini, N. Solyak, V.P. Yakovlev, S. Mishra, K. Ranjan, Study of effects of failure of beamline elements and its compensation in CW superconducting linac, in: Proceedings of IPAC2012, New Orleans, Louisiana, USA: 2012, pp. 1173–1175.
[30] P.F. Derwent, J.-P. Carniero, J. Edelen, V. Lebedev, L. Prost, A. Saini, A. Shemyakin, J. Steimel, PIP-II Injector Test: challeng-es and status, in: Proc. of LINAC'16, East Lansing, MI, USA, September 25–30, 2016, WE1A01.
[31] A. Vivoli, J. Hunt, D.E. Johnson, V. Lebedev, Transfer Line Design for PIP-II Project, in: Proceedings of IPAC2015, Richmond, VA, USA, 2015, THPF119, pp. 3989–3991.
[32] https://www.reliasoft.com/products/blocksim-system-reliability-availability-maintainability-ram-analysis-software.
[33] S. Henderson, et al., The Spallation Neutron Source Beam Commissioning and Initial Operations, ORNL, USA, Tech. Report, ORNL/TM-2015/321, 2015, https://info.ornl.gov/sites/publications/files/Pub56465.pdf.
[34] S.-H. Kim, R. Afanador, W. Blokland, M. Champion, A. Coleman, M. Crofford, et al., The status of the superconducting linac and SRF activities at the SNS, in: Proceedings of the 16th International Conference on RF superconductivity, Paris, France, September 23–27, 2013, pp. 83–88, http://accelconf.web.cern.ch/AccelConf/SRF2013/papers/mop007.PDF.
[35] S.H. Kim, et al., Overview of ten-year operation of the superconducting linear accelerator at the Spallation Neutron Source, Nucl. Instrum. Methods Phys. Res. A (ISSN: 0168-9002) 852 (2017) 20–32, http://dx.doi.org/10.1016/j.nima.2017.02.009.
[36] M. Convery, et al., The PIP-II Preliminary Design Report, PIP-II Document 2261-v33, 2020, https://pip2-docdb.fnal.gov/cgi-bin/ShowDocument?docid=2261.
[37] T.P. Wangler, RF Linear Accelerator, second ed., Wiley-VCH Verlag GmbH & Co., 2008.
[38] A. Sukhanov, A. Lunin, V. Yakovlev, M. Awida, M. Champion, C. Ginsburg, I. Gonin, C. Grimm, T. Khabiboulline, T. Nicol, Yu. Orlov, A. Saini, D. Sergatskiv, N. Solyak, A. Vostrikov, Higher order modes in project-X Linac, Nucl. Instrum. Methods Phys. Res. A 734 (part A) (2014) 9–22, http://dx.doi.org/10.1016/j.nima.2013.06.113.